NUMERICAL STUDIES OF FAST ELECTRON TRANSPORT IN LASER IRRADIATED TARGETS

by

Deryck John Bond

Imperial College

London

Thesis submitted for the degree of Doctor of Philosophy to

The University of London

July 1980

ABSTRACT

This thesis describes an investigation of fast electron transport in solid targets using, primarily, numerical simulation. The role of the electric field, which drives the thermal return current, is stressed.

Both Monte-Carlo and Multi Group methods have been employed. In the latter total energy has been used as a dependant parameter.

Simulation results which show a large inhibition of fast electron transport in targets containing a low density Gold layer are presented and a comparison is made with experimental results.

The calculation of the electric field in quasi-neutral particle simulation is discussed and a number of methods are compared.

CONTENTS

SYMBOLS

A	Vector Potential
A	Atomic Number
a_o	Bohr Radius
B	Magnetic Field
b	Impact Parameter
c	Speed of Light
E	Electric Field
E	Energy
E_D	Debye Energy
E_F	Fermi Energy
E_H	Ionization Energy of Hydrogen
e	Proton Charge
e	Electron
f	Distribution Function
h	Planck's Constant
I	Flux
I	Intensity
I	Average Ionization Energy
J	Current Density
k	Boltzmann's Constant
L	Scale Length
$\ln\Lambda$	Coulomb Logarithm
M	Mass
m_e	Electron Mass
n	Number Density
n_{crit}	Critical Density
nuc	Nuclear
P	Pressure
q	Heat Flow

R Radius

r_F Fermi Radius of Atom

s Path Length

sc Space Charge

sth Suprathermal

T Temperature

t Time

th Thermal

v velocity

v_{is} Ion Sound Speed

x Position

Z Charge

z Position

Δt Time Step

Δx Mesh Step

ε Permittivity

ε_o Permittivity of Free Space

η Resistivity

θ Angle

λ Wave Length

λ_D Debye Length

λ_{DeB} De Broglie Wave Length

λ_E Energy Loss Mean Free Path

$\lambda_{\pi/2}$ Momentum Loss Mean Free Path

μ Permeability

μ Direction Cosine

μ_o Permeability of Free Space

ν_c Collision Frequency

ν_{ie} Electron Ion Collision Frequency

ρ Density

σ Conductivity

τ Time

τ_E Energy Relaxation Time

τ_{ie} Electron Ion Collision Time

Φ Flux

ϕ Angle

ϕ Potential

Ω Angle

ω Frequency

ω_{ce} Electron Cyclotron Frequency

ω_{pe} Electron Plasma Frequency

ω Angle

Units

S.I. units are used unless otherwise stated.

CHAPTER 1

Introduction

In this chapter we introduce the concept of laser driven inertial confinement fusion. The physical processes involved in the absorption of the laser energy and in its coupling into the hydrodynamic motion of the target are discussed.

1.1 Fusion Power

The study of laser target interactions is motivated by the desire to produce power by controlled thermonuclear fusion.

The reactions which will be used in a fusion reactor are:-

$$D + T \longrightarrow {}^{4}He(3.5\ MeV) + n(14.1\ MeV) \qquad (1.1.1)$$

or

$$D + D \longrightarrow T(1\ MeV) + P(3\ MeV) \qquad (1.1.2)$$

and

$$D + D \longrightarrow {}^{3}He(0.8\ MeV) + n(2.5\ MeV) \qquad (1.1.3)$$

The ignition temperature, the temperature at which the radiation loss equals the rate at which power is produced by fusion reactions, is 4 KeV for D-T and 35 KeV for D-D.

If a reactor with efficiency of 33% is to extract more energy than is needed to heat the plasma and supply the radiation losses then the density-confinment time product ($n\tau$) must exceed

$10^{20}\ m^{-3}$ sec for DT

$10^{22}\ m^{-3}$ sec for DD

This is the Lawson Criterion (1).

1.2 Inertial Confinement

In inertial confinement fusion the confinement time, τ, is determined by the thermal velocity of the DT at ignition temperature. For a sphere of DT radius R density ρ the Lawson criterion becomes

$$\rho R > 10^3 \text{ kg m}^{-2} \qquad (1.2.1)$$

where τ has been replaced by $R / V^{th}(\text{ignition})$

The energy required for such a scheme would be in excess of 100 MJ (2) for a solid density target. This requirement on the energy which must be supplied can be vastly reduced if compression to 10^4 times solid DT density is achieved (3).

Several "drivers" have been proposed for high density I.C.F. : lasers; electron beams; and heavy and light ion beams. The relative merits of these drivers is discussed by Mead (4). In what follows only laser driven I.C.F. will be considered.

Ablation

The absorption of the laser energy causes the surface of the target to burn away (ablation). This causes the bulk of the target to be accelerated by the "rocket effect".

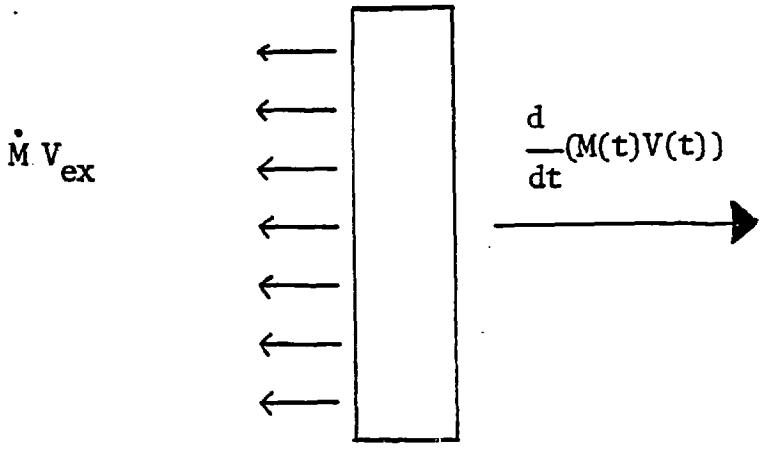

Fig.1.1 Ablative Acceleration

This problem has been studied by Bruckner and Jorna (5), using an isothermal model in plane geometry, who give the energy of the accelerated target as :-

$$\frac{\frac{1}{2} M(t)\, V(t)^2}{E_{Abs}} = \frac{\frac{1}{2} M(t)}{M_o - M(t)} \left(\ln M_o/M(t)\right)^2 \qquad (1.2.2)$$

where M_o is the initial target mass.

The maximum energy transfer is for $M_o/M(t) \simeq 5$. Thus for a given laser energy it is more efficient to burn away a large mass of material with a small exhaust velocity than to burn away a small mass of material with a large exhaust velocity. The exhaust velocity and mass ablation rate have been measured and their scaling with laser wavelength determined (6).

Compression

The maximum density ratio which may be achieved in a spherical compression with a strong shock is, for a perfect gas with γ=5/3, 33 (7). This dissapointingly low figure is a result of the increase in the entropy of the material which is to be compressed by shock heating. Kidder (8) has shown that a shock free isentropic compression minimises the work, and hence the laser power, for a given compression. Such an optimised compression requires an energy deposition rate given by :-

$$E(t) \sim 1/(t-\tau)^s \qquad (1.2.3)$$

where τ is the pulse length and $s \simeq 2$.

Fraley (9) shows that high compression may be achieved without the pulse shaping implied by (1.2.3) if the DT pellet is surrounded

by a high density shell. He also discusses the advantage of using a target with a central void. This is also discribed by Kidder (10). A conceptal high gain fusion target is described by Emmett (11).

In the remainder of this chapter some of the physical processes relevant to laser driven I.C.F. will be discussed.

1.3 Absorption and Scattering of Laser Light

There are many absorption mechanisms. Inverse Bremsstrahlung and resonance absorption, which dominate at low and high intensities respectively, will be discussed.

Inverse Bremsstrahlung

Inverse Bremsstrahlung is the absorption of a photon by an electron in the presence of an ion (ie the inverse of Bremsstrahlung radiation). It may be represented by:-

$$\hbar\omega + e^-(\text{energy } E) + A^{\pm} \longrightarrow e^-(\text{energy } E \pm \hbar\omega) + A^{\pm}$$

A simple expression for the absorption coefficient is (12)

$$K_\omega = \frac{\nu_{ei}}{c\left(1 - \frac{\omega^2}{\omega_{pe}^2}\right)} \frac{\omega_{pe}^2}{(\omega^2 + \nu_{ei}^2)} \qquad (1.3.1)$$

This assumes the heated plasma stays Maxwellian and that $v_{quiver} \ll v_{th}$. The case where the speed dependence of ν_{ei} leads to preferential heating of the cooler electrons and the formation of a sub-Maxwellian distribution is discussed by Langdon (13). It is ineffective as an absorption mechanism in high intensity irradiation of low Z targets (for $\lambda_{Las} \gtrsim 1\mu$). However for lower irradiance of high Z targets (14) and with shorter wavelenghts (15) it can be an important

absorption mechanism.

Colombant and Manheimer (16) show that ion accoustic turbulence may lead to an anomalously high collision frequency which will increase absorption.

Resonance Absorption

If EM radiation is incident on a plasma with a density gradient at an angle $\theta(\neq 0)$ it will be turned round before it reaches critical density. If there is a component of the E field in the plane of incidence an evanescent wave will excite a plasma wave at critical density. The optimum angle for resonance absorption is given (17) by

$$(2\pi L/\lambda_{Las})^{2/3} \sin^2\theta = 0.6 \qquad (1.3.3)$$

where L is the density scale length.

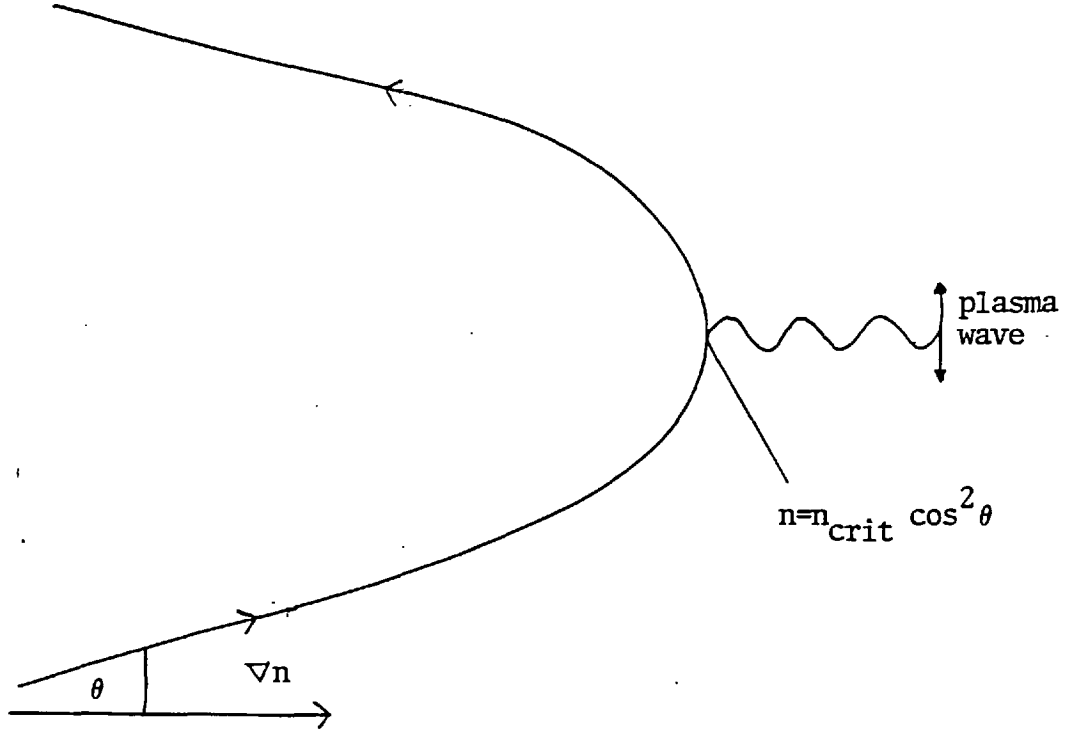

Fig.1.2 Resonance Absorption

The energy deposited in this wave is transfered to the electrons as the wave damps. 2D electromagnetic particle simulations (18,19) show that a small number of electrons are accelerated to high kinetic energies, many times the thermal energy, by this process. A feature of this process is that the suprathermal electrons so produced may be characterised by a temperature. This has been explained by considering the random nature of the resonance field (20). A steady state B field (21) or rippled critical surface (22) can lead to resonance absorption even at normal incidence.

Analysis of the angle and polarisation dependence of laser light absorption (23) at high intensities (10^{19}-10^{20} Wm^{-2}) shows resonance absorption to be the dominant absorption mechanism in these cases.

Other absorption mechanisms are: Stimulated Compton scattering (24) ; the oscillating two stream instability (25) ; the parametric decay instability (26) and the two plasmon instability (26).

The laser light may be backscattered by stimulated Raman (27) or Brillouin (28) scattering and may also be specularly reflected.

1.4 Radiation Forces

Radiation (ponderomotive) forces are the forces in a medium which are a consequence of the radiation field in that medium. They were first discussed by Landau and Lifshitz (29), and have been discussed in the context of R.F. confinement by Motz and Watson (30).

A simple model based on single particle motion in a sinusoidally varying E field (31) gives the time average non-linear force as :-

$$F_{NL} = -(1-\frac{\varepsilon}{\varepsilon_o})\nabla(\tfrac{1}{2}E^2_{rms}) \qquad (1.4.1)$$

In a more complete analysis (32) the total stress tensor, including the effect of the Maxwell stress tensor, the quiver pressure and the electron stress tensor in the oscillating electron centre of mass frame, is calculated. This gives a force :-

$$-\nabla \cdot \underline{\underline{P}}_{Total} \qquad (1.4.2)$$

where:-

$$\underline{\underline{P}}_{Total} = \tfrac{1}{2}(\varepsilon_o E^2 + \frac{1}{\mu} B^2) \underline{\underline{I}} - \varepsilon \underline{E}\,\underline{E} + \frac{1}{\mu} \underline{B}\,\underline{B} + \underline{\underline{P}}_{thermal} \qquad (1.4.3)$$

(If the quiver velocity is calculated assuming the electrons are collisionless). Equation (1.4.2) should be used in the equation for the change in total, material and radiation, momentum. Using a fluid description for the electrons the effect of collisions has been included (33).

The effect of the radiation pressure on the hydrodynamics has been extensively studied theoretically (34,35,36). A density jump at critical density has been predicted (37) and has been observed experimentally(38).

The production of magnetic fields (39,40) and the acceleration of fast ions (41) have also been discussed.

1.5 Magnetic Fields

Spontaneously-generated magnetic fields were first observed in laser-target interaction by Stamper et al (42). A brief review of the generating mechanisms will be now given.

The thermal source term, due to non parallel n_e and T_e -gradients has been extensively studied with fluid simulation codes.(43,44,45

46,47,48). The equation for the rate of change of B is given by:-

$$\frac{\partial B}{\partial t} = -\nabla\wedge E = \nabla\wedge\left[V\wedge B + \frac{1}{\mu_o}\eta\nabla\wedge B\right]$$

$$- \frac{k}{eN_e}\nabla N_e\wedge\nabla T_e - \nabla\wedge\left[\frac{\mu_o}{eN_e}\nabla\wedge B\wedge B\right]$$

$$- \frac{1}{e}\nabla\wedge(\beta\nabla T_e - \alpha b\wedge\nabla T_e) \qquad (1.5.1)$$

where the coefficients α and β , which depend on $\omega_{ce}\ \tau_{ei}$, have been derived by Braginskii (49). As Langdon (50) has pointed out, the application of equations using these coefficients to situations where the scale lengths for the magnetic field, or the source term, become comparable to r_{el} or λ_{ei} (where the coefficients are invalid), may lead to serious inaccuracies in the calculated magnetic field.

Many authors have not used the full equation (1.5.1) but have only used :-

$$\frac{\partial B}{\partial t} = \nabla\wedge\left(V_e\wedge B + \frac{\eta}{\mu_o}\nabla\wedge B\right) - \frac{k}{eN_e}\nabla N_e\wedge\nabla T_e \qquad (1.5.2)$$

This will adequately describe the evolution of the magnetic field until $\omega_{ce}\ \tau_{ie}$ becomes comparable to unity. This has been used by Craxton and Haines (45,48) to show the development of "hot spots", due to $\omega_{ce}\ \tau_{ie}$ reduction of the electron heat flux in the absorption region, and $J\wedge B$ fast ion acceleration. In this work the source term comes from the ∇n away from the target surface and the ∇T_e perpendicular to the laser axis (due to the laser spatial profile).

Tan and Laing (47) present simulations which illustrate the effect, on the source term, of including an atomic physics package. Mima et al (44) discuss the $\nabla n_e\wedge\nabla T_e$ generation of magnetic fields

in a Rayleigh-Taylor unstable plasma. The more complete equation, (1.5.1), has been used by Coulombant and Winsor (43) in their simulation. This is also used in the LASNEX laser fusion code. Comparison between code prediction and experiment have been used to investigate the role of the magnetic field in inhibiting the thermal heat flux (51).

Magnetic fields may also be created by laser light absorption (52,53). Here the laser EM fields drive eddy currents in the plasma electrons which in turn give rise to a steady state B field. This effect is most important near critical density.

Magnetic fields may also result from the suprathermal current (54,55). Some sources, such as the anisotropic part of the electron stress tensor, are beyond the scope of fluid codes.

Saturation of the magnetic field is usually due to advection, resistivity is generally ineffective. The effect of all the source mechanisms acting at the same time on the magnetic field and the resultant effect on thermal transport has been reviewed by Max(56).

Theoretical studies indicate maximum coronal B fields of the order of 10^2 Tesla. Such fields have been measured in laser-plane target interactions by Raven et al (57). The same authors were unable to detect a magnetic field ($B < 10$ Tesla) when the target was a small microballoon (radius of balloon < radius of laser focal spot) with two beam illumination.

1.6 Thermal Transport

Expressions for the classical heat flux in a thermal plasma have been derived by Spitzer (58) and Braginskii (49). These are applicable when :-

(1) Only classical collisions are important

(2) The scale length for change in temperature satisfies :-

$$\epsilon = \lambda_\varepsilon / L \ll 1 \qquad (1.6.1)$$

As pointed out by Grad (59) the expansion in ϵ used in (58,49) is asymptotic and such theories cannot be extended to give values for the heat flow at large values of ϵ.

An estimate of the maximum heat flow in a thermal plasma can be obtained as follows. Consider a perturbed Maxwellian distribution of the form:-

$$f(v,\mu) = f(v)_{\text{Maxwellian}}(1 + a(v)\mu) \qquad (1.6.2)$$

where $\mu = v.z$

The maximum value of the heat flux carried by such a distribution, subject to it being positive everywhere, is when $a(v) = 1$. This gives

$$q_{\text{free streaming}} = \frac{4}{3} n_e k T_e \left(\frac{2kT_e}{\pi m}\right)^{\frac{1}{2}} \qquad (1.6.3)$$

If the condition $J = 0$ is imposed the maximum heat flux is given for $a(v) = -1 \quad 0 < v < v_1$, $a(v) = 1 \quad v_1 < v < \infty$, where v_1 can be found numerically. This gives :-

$$q_{\text{free streaming}}\ (J=0) = q_{\text{free streaming}} \cdot 0.54$$

In the simulation of laser target interactions (60,51) a large reduction of the heat flux from its classical or free streaming value is inferred Typically a maximum value of the heat flow of $\sim 0.02 \cdot q_{\text{free streaming}}$ is inferred.

It has been suggested that this may be due to ion accoustic turbulence (61) or due to non-linear classical effects (62).

Direct measurement of the heat flux is only possible at much lower densities than those relevant to laser target studies, where ion accoustic turbulence has been identified as the flux limiting mechanism (63). However the plasma number

$$N.\lambda_D^3 = \omega_{pe}/\nu_{ie} \qquad (1.6.4)$$

is much greater in this case than it is in laser irradiated targets.

An expression for the anomalous collision frequency is given by Wesson et al (64).

$$\frac{nT_e}{0.26\ W} = \omega_{pe}/\nu_{eff} \qquad (1.6.5)$$

Where W is the energy density of electrostatic turbulence. The ratio of the classical and anomalous collision frequencies is :-

$$\frac{\nu_{eff}}{\nu_{ie}} = N\ \lambda_D^3\ \frac{0.26\ W}{nT_e} \qquad (1.6.6)$$

From which it can be seen that turbulence will not be so important for low $N\lambda_D^3$.

The $1/(1 + (\omega_{ce}\ \tau_{ie})^2)$ reduction due to magnetic fields may also reduce the heat flow (45).

1.7 Suprathermal Electrons

As we have seen, some absorption mechanisms lead to the production of electrons with an energy many times that of the thermal electrons, which constitute the bulk of the plasma .These electrons, variously called hot, fast or suprathermal electrons, play a dominant role in high intensity laser target interactions.

The mean free path of these electrons is far greater than that of the thermal electrons. They may thus deposit energy ahead of the thermal front and shock wave, so degrading the compression. Also they may lose a large proportion of their energy in the time dependant coronal electric field, this energy goes into fast ion acceleration. The acceleration of a small number of ions to very large velocities is an inefficient way to transfer momentum to the core.

Fig. 1.3 illustrates the deleterious effect of suprathermal electrons.

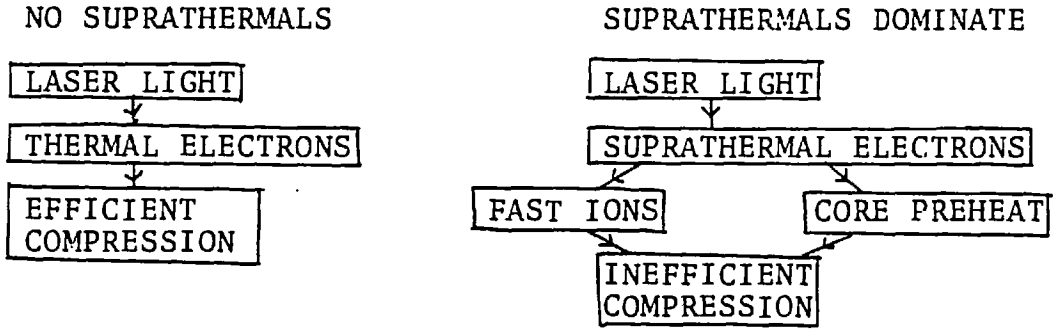

Fig.1.3

The experimental evidence for the existence of suprathermal electrons comes from : X-radiation spectra (65), the fast ion spectrum (66) and from direct measurement of target preheat (67).

The form of the source of suprathermal electrons has been investigated by comparison between experiment and code prediction (51,60). A "preheating source" has been inferred by Hares et al (67).

Relation to Target Performance

If $R_{sth}/\Delta R \gg 1$ then the specific energy deposition will be almost independent of position. The fuel is compressed as the glass "pusher" explodes inwards and outwards. The behaviour of such targets is discussed by Ahlborn and Key (68).

This type of target can produce significant thermonuclear burn (11), but high compression is not possible because the fuel is preheated by the suprathermal electrons and will be shock heated by the compression.

Quasi Ablative Targets

If $R_{sth}/\Delta R \lesssim 1$ then the specific energy deposition will be higher towards the outside of the shell.

Fig.1.4 Quasi Ablative Target

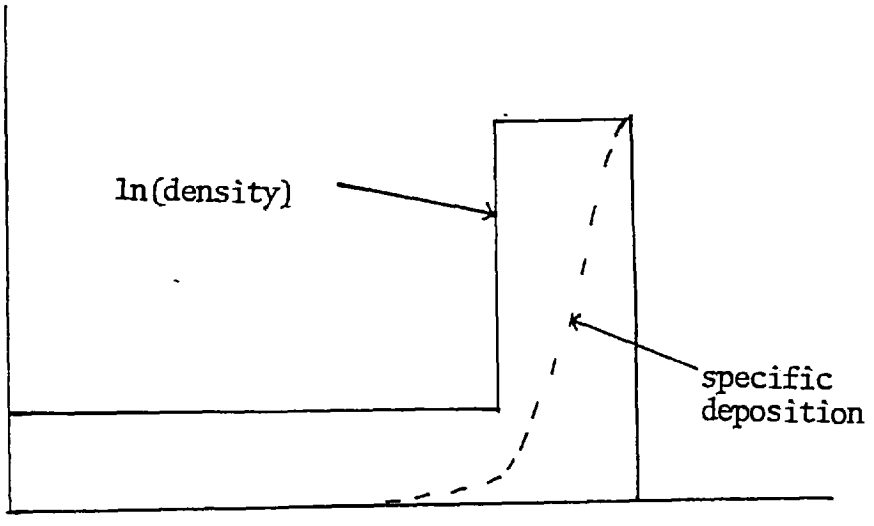

This gives rise to a pressure gradient which may accelerate the shell. This is discussed by Key (69). Experiments using glass microballoons with thick plastic coatings have been described (70,71).

1.8 Fast Ions

A feature of experiments using high intensity irradiation is that a large fraction of the absorbed energy manifests itself in a small number of fast ions (72,73).

Various mechanisms have been proposed for the production of these fast ions, including: the ponderomotive force (41), J∧B acceleration (48), the presence of suprathermal electrons (66,74) and the inhibition of the thermal energy flux (75,76). The last two will now be discussed.

The ion velocity spectrum can not be explained on the basis of a single temperature isothermal rarefaction (77). Several authors (78,79,66) have proposed that a two temperature isothermal rarefaction model may explain fast ion production and Wickens et al (66) compare experimental results of the ion spectrum and results from a slab geometry self similar solution. Fast ion spectra have also been modelled by Bruckner and co-workers (74,80) and Shvarts et al (81). The suprathermal electrons may lose energy either collisionally in the core or in the time dependent E field of the corona (essentially PdV work). If an idealised situation is considered in which the suprathermal electrons reflect off a moving, perfectly reflecting "sheath" and pass through the core between reflections then the energy losses to the ion expansion and to collisions in the core scale as:

$$\frac{\Delta E_{\text{fast ions}}}{E} \sim \frac{V_{\text{sheath}}}{V_{e_{\text{sth}}}}$$

$$\frac{\Delta E_{collisions}}{E} \sim \frac{\text{Size of core}}{\lambda_{E_{sth}}(\text{core})} \sim \frac{1}{v_{e_{sth}}^4}$$

Clearly loss to ion expansion is more important for the higher energy suprathermals.

Inhibited thermal transport increases the time a heated electron spends in the corona, before it shares its energy with the mass of the target, and so increases the energy it loses to PdV work in the corona (75). Hydrodynamic simulation codes greatly underestimate the energy transfered to fast ions if flux inhibition and suprathermal electrons are omitted.

1.9 Fluid Instabilities

If the high densities needed in I.C.F. schemes are to be achieved then it is important that fluid instabilities do not degrade the compression. The Rayleigh-Taylor instability and Convective (Bernard) instability have received much attention (82,83,84) and have been reviewed by Motz[12]. Analytic work is restricted by the idealised zero order solutions which are used. Perturbation solutions which treat all modes independently have been "piggy backed" on 1-D hydro codes (84) and full solutions of the 2-D fluid equations have been reported (83). The importance of thermal conduction and magnetic fields is still not well understood. Experimental evidence (85) suggests that fluid instabilities may degrade microballoon implosions with an aspect ratio (balloon radius/shell thickness) of greater than 10. (Targets with large aspect ratios, if stable have a higher efficiency).

1.10 Radiation Transport

The transfer of energy by radiation can play an important role in the hydrodynamic motion and energy balance of laser irradiated targets. A large fraction of the absorbed energy may be lost in X-radiation from the target (60) and hard X-radiation may preheat the core.(86).

The 3 Temperature (ion electron and radiation) approximation has been used in fluid codes (87); however this model is not valid for most cases of interest. Multi Group diffusion radiation transport has been widely used in fluid simulations (88,89) and Monte Carlo methods (87) have also been used.

S_n methods are widely used in more detailed analysis of the radiation emitted from targets, without coupling with the hydrodynamics(ie in postprocessors) (90).

Chapter 2

Introduction

In this chapter the theory of the deflection and energy loss of suprathermal electrons in a solid and a plasma is described. Simple formulae for the deflection and energy loss in a partially ionized solid are given and the relative importance of various physical processes is discussed.

Some models for suprathermal electron transport in solid targets are then introduced. These include the Monte Carlo method and the Multi Group Diffusion method which are used in chapters 4,5 and 6.

2.1 Energy Loss of Suprathermal Electrons

Collisional Energy Loss in a Solid

The stopping power of a material due to classical collisions, is defined as:-

$$(SP)_{class} = \frac{dE}{d(\rho s)})_{class} \qquad (2.1.1)$$

Where E = electron energy, ρ = material density and s = path length

For non relativistic electrons the appropriate formula is (91):-

$$-\frac{dE}{ds} = \frac{Zn_i e^4}{4\pi\epsilon_o^2 m_e v_e^2} \ln(2m_e v_e^2/I) \qquad (2.1.2)$$

Stopping powers have been tabulated by Brown (92) and electron ranges by Berger and Seltzer (93).

The average ionization energy may be, very crudely, approximated by :-

$$(I/Z) = 11 \text{ eV} \qquad (2.1.3)$$

Fig.2.1 I/Z vs Z

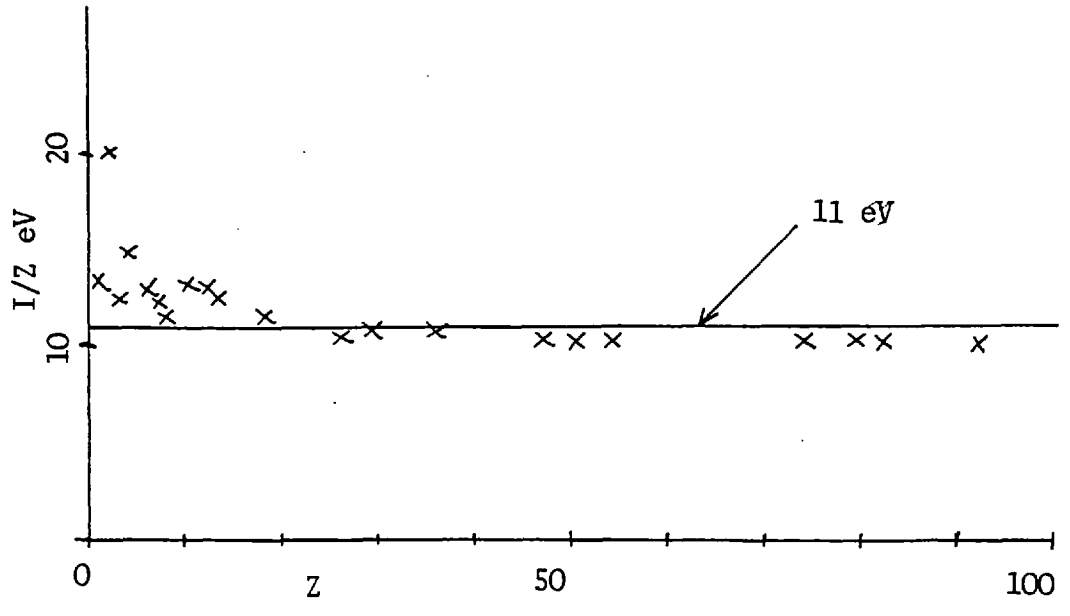

There are several inaccuracies / omissions in the theory which gives equation (2.1.2)

(1) The shell correction: This reduces the stopping power if the electrons energy is less than some of the ionization potentials of the atom.

(2) Straggling: Energy loss is not a determined function of ρs, there is some randomness.

(3) For electron energies of over 1 MeV Bremsstrahlung becomes an important loss machanism.

(4) The density effect: This is a reduction of the energy loss due to the polarisation of the medium. It is important for energies over 100 KeV.

(5) A correction to the continuous slowing down approximation which allows for the discrete nature of collisional energy loss (94).

Collisional Energy Loss in a Plasma

The collisional energy loss in a plasma has been given by Pines and Bohm (95). It is :-

$$\left(\frac{dE}{d(\rho s)}\right)_{class} \sim -\frac{1}{E} \ln \frac{E}{E_D} \qquad (2.1.4)$$

*

Where E_D, the Debye energy is $e^2/(4\pi\varepsilon_o\lambda_D)$.

This may be compared with the energy loss to collective oscillations of the plasma (an effect analogous to Cherenkov radiation) which is given by:-

$$\left(\frac{dE}{d(\rho s)}\right)_{coll} \sim -\frac{1}{E} \ln\left(1 + \frac{2E}{E_{th}}\right) \qquad (2.1.5)$$

Where $E_{th} = \frac{1}{2} m_e V_{th}^2$

The ratio of (2.1.5) to (2.1.4) gives :-

$$\frac{\left(\frac{dE}{d(\rho s)}\right)_{coll}}{\left(\frac{dE}{d(\rho s)}\right)_{class}} = \frac{\ln\left(1 + \frac{E}{E_{th}}\right)}{\ln\left(\left(\frac{E}{E_D}\right)^2\right)} \qquad (2.1.6)$$

Energy Loss in a Partially Ionized Medium

The energy loss in a partially ionized medium is the sum of the energy losses to the bound and free electrons. This is given by:-

$$-\frac{dE}{dx} = \frac{n_i e^4}{4\pi \varepsilon_o^2 m_e v_e^2}\left((Z_{nuc}-Z_{ion})\ln(2m_e v_e^2/I) + Z_{ion}\left(\ln(\lambda_D/\lambda_{DeB}) + \tfrac{1}{2}\ln\left(1+\frac{2m_e v_e^2}{\frac{3}{2}kT_{th}}\right)\right)\right) \qquad (2.1.7)$$

2.2 Deflection of Suprathermal Electrons

Deflection in a solid

As a suprathermal electron passes through a solid it experiences many collisions most of which result in small deflections. Typically 10^5 collisions will occur in the course of slowing down. Several Multiple Scatter models have been developed to describe the combined effect of many collisions (96 ,97 , 98). A simple model which neglects the effect of single large angle collisions and energy loss is given by Jackson(99). For electrons which are not so energetic that their De Broglie wavelength is smaller than the atomic nucleus the multiple scatter distribution may be approximated by :-

$$P(\theta_T)\ \theta_T\ d\theta_T \sim\ \theta_T \exp(-\theta_T^2/2\ \langle\theta_T^2\rangle\ ) \qquad (2.2.1)$$

where :-

$$\langle\theta_T^2\rangle = \frac{2\pi\ Z_{nuc}(Z_{nuc}+1)\ e^4 n_i}{(4\pi\varepsilon_o)^2\ E^2}\ \ln\left(\frac{1.1\ r_F}{\lambda_{DeB}}\right)\ L \qquad (2.2.2)$$

The cut-off distance $1.1\ r_F$ is taken from Goldsmit and Saunderson (96). θ_T is the angle between the direction of motion of the particle before and after travelling a distance, L. If instead we want the probability distribution for the projection of θ_T onto a plane, θ_p, this is given by :-

$$P(\theta_p) \sim \exp(-\theta_p^2 / 2\langle\theta_p^2\rangle) \qquad (2.2.3)$$

$$\langle\theta_p^2\rangle = \tfrac{1}{2}\langle\theta_T^2\rangle \qquad (2.2.4)$$

Equations (2.2.1) to (2.2.4) are valid for small $\langle\theta_T^2\rangle$ and for θ up to a few times $\langle\theta_T^2\rangle^{\frac{1}{2}}$.

Deflection in a Plasma

The deflection of a suprathermal electron in a plasma is discussed by Spitzer (100). In this case the electron may be interacting with many other particles at a given time. Thus the collisions are not true binary collisions. However since the deflections are small the collisions may be treated as if they were binary encounters. (This is discussed at length by Shkarofsky et al (101)).

The multiple scatter distributions are given by (2.2.1) and (2.2.3) with

$$\theta_T^2 = \frac{2\pi Z_{ion}(Z_{ion}+1)e^2 n_i}{(4\pi\varepsilon_o)^2 E^2} \ln\left(\frac{b_{max}}{b_{min}}\right) L \qquad (2.2.5)$$

In equations (2.2.2) and (2.2.5) the $Z(Z+1)$ accounts for scattering ions / nuclei (Z^2) and electrons (Z) per ion / nucleus. b_{max} and b_{min} in (2.2.5) are given by :-

$$b_{max} = \lambda_D$$

$$b_{min} = \lambda_{DeB} \qquad \text{where } \lambda_{DeB} > \text{Landau parameter}$$

for suprathermal energies of interest.

Deflection in a Partially Ionized Medium

A simple model for the screening of the charge of the nucleus is as follows. Up to a radius R_{ion} the charge of the nucleus is screened by the bound electrons. From R_{ion} to λ_D the charge of the ion

is Debye shielded by the plasma electrons. Thus the potential due to the nucleus as a function of distance would be approximately as shown below.

Fig.2.2 Screened Potential of Nucleus

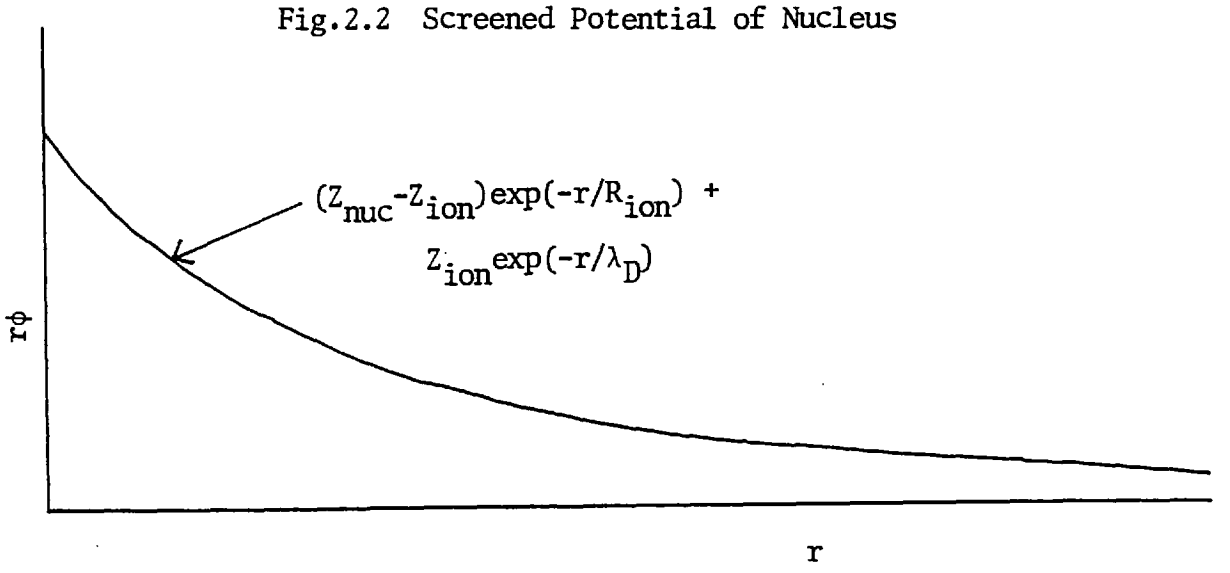

A crude approximation to the form factor is :

Fig.2.3 Approximate Form Factor

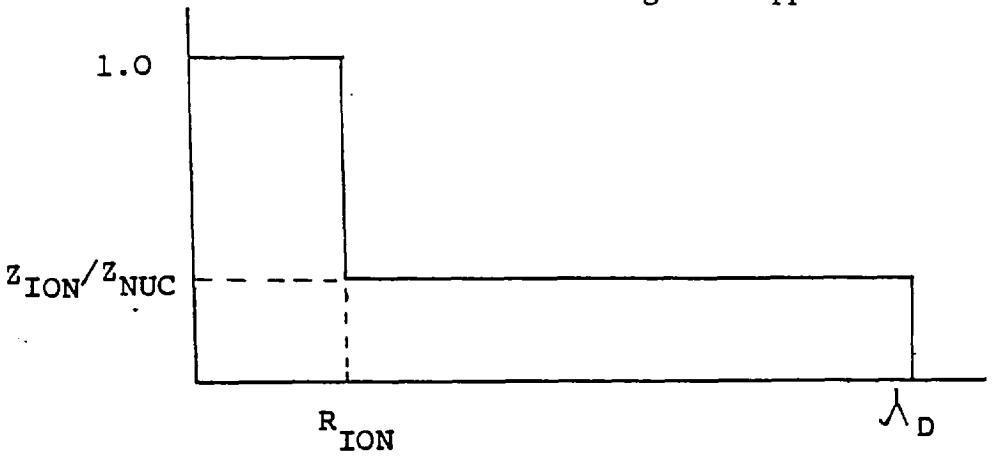

This suggests the following approach.Treat the collisions with impact parameter b in the range $b_{min}<b<R_{ion}$ as if the scattered electron "saw" the charge of the nucleus, and those with $R_{ion}<b<\lambda_D$ as if it "saw" the ionic charge. Such an approach gives:-

$$\langle\theta_T^2\rangle = \frac{\pi e^2 n_i L}{2 (4\pi\epsilon_o)^2 E^2} \left(Z_{nuc} (Z_{nuc} + 1) \ln\left(\frac{R_{ion}}{\lambda_{DeB}}\right) + Z_{ion}^2 \ln\left(\frac{\lambda_D}{R_{ion}}\right)\right)$$

(2.2.6)

This has the correct limits of (2.2.2) and (2.2.5) as $Z_{ion} \longrightarrow 0$ and $Z_{ion} \longrightarrow Z_{nuc}$.

2.3 Spencer's Range Calculations

Lewis (102) derived an equation for electron penetration in an infinite homogeneous medium which can, in the steady state, be written as follows:-

$$\cos\theta \frac{\partial I}{\partial z} = \int d\Omega' \sigma(r,\Theta) N \left\{ I(r,\theta',z) - I(r,\theta,z) \right\} + (2\pi)^{-1} \delta(z)\delta(r-r_0)\delta(\cos\theta - 1) \qquad (2.3.1)$$

Here I is the electron flux, N the density of atoms, $\sigma(r,\theta)$ is the collision cross section and z the distance from the source. r is the residual range of the electrons and θ is the angle the electron's velocity vector makes with the z-axis, and Θ the scattering angle. The source is at $z = 0$ with $\theta = 0$ and with residual range r_0. The use of the continuous slowing down approximation allows the energy loss, or alternatively the change in residual range, to be reexpressed. In this case the change of I due to energy loss, $\left(\frac{\partial I}{\partial s}\right)_{CSD}$ (where s is the path length) is :-

$$\frac{\partial}{\partial s} I(r) = \frac{\partial I}{\partial r} \frac{dr}{ds} = \frac{\partial I}{\partial r} (-1) \qquad (2.3.2)$$

Using $t = (r/r_0)$, $x = (z/r_0)$, $s(t,\theta) = r_0 N\sigma(r,\theta)$ and $I(r,\theta,z)\, dr = I(t,\theta,x)\, dt$ Spencer (103) derived :-

$$-\frac{\partial I}{\partial t} + \cos\theta \frac{\partial I}{\partial x} = \int d\Omega' \; S(t,\Theta)(I(t,\theta',x) - I(t,\theta,x)) +$$

$$+ (2\pi)^{-1} \delta(x)\delta(t-1)\delta(\cos\theta - 1) \qquad (2.3.3)$$

$-1 \leq x \leq +1 \qquad 0 \leq t \leq 1$

This was solved (103) by first expanding R and S in spherical harmonics and substituting into equation (2.2.3). Spatial moments of the resulting set of coupled partial differential equations are then taken. This yields a set of ordinary differential equations which may be solved.

Results of Spencer's calculations have been compared with experiments, see for example Zerby and Keller (104), and found to be in good agreement.

2.4 Monte Carlo Calculations

An excellent account of the application of Monte Carlo methods (methods involving random sampling) to the problem of charged particle transport has been given by Berger (105). The purpose of this section is to introduce the methods used in Monte Carlo electron transport. Emphasis will be given to the approach used in chapters 4 and 6 of this thesis.

Detailed Case Histories

It would be possible to describe the trajectory of an electron in a solid by the quantities $(E_0,\Omega_0,r_0;\ E_1,\Omega_1,r_1;\ \ldots)$ where E_n,Ω_n,r_n are the energy, direction and position after the n^{th} binary collision. Such trajectories could be generated by random sampling. However, because of the very large number of collisions made by an electron in the course of slowing down, this approach is very expensive.

Condensed Case Histories

In this approach the detailed description of the particle's trajectory is abandoned. The trajectory is split up into a number of steps, each of which contains many collisions. It may be described by:-

$$\begin{array}{cccc} 0 & S_1 & S_2 & \ldots. S_n \\ E_0 & E_1 & E_2 & \ldots. E_n \\ \Omega_0 & \Omega_1 & \Omega_2 & \ldots. \Omega_n \\ r_0 & r_1 & r_2 & \ldots. r_n \end{array}$$

where S is the distance travelled by the electrons and E_n,Ω_n,r_n the energy, direction and position after a distance S_n has been travelled. The relation between E_n and E_{n+1} and between Ω_n and Ω_{n+1} are

determined by the appropriate multiple scattering theories.

There are two competing factors influencing the choice of the distance between artificial scattering events ($S_{n+1} - S_n$). In order to minimise the length of the calculation the minimum number of steps must be used. On the other hand the accuracy of the models for energy loss and deflection will be better for small path lengths. This is due to the following:-

(1) Although the correlation between deflection and energy loss is not accounted for in a single step it will be, to some extent, over many steps.

(2) Some multiple scatter theories assume zero energy loss. The energy loss will be smaller if smaller steps are used.

(3) In a multi-material target more of the steps will lie wholly within a single material. Errors associated with boundaries will be reduced.

Choice of Pathlength

The choice of logarithmic spacing, ie choosing the pathlength so that the energy is reduced by a constant factor, k , is popular because the magnitude of the width of the multiple scattering distribution will not change in the course of the calculation. If this is required ΔS ($= S_{n+1} - S_n$) is prescribed by :-

$$1 - \frac{1}{E_n} \int_{S_n}^{S_{n+1}} \frac{dE}{ds}\, ds = k \qquad (2.4.1)$$

or aprroximately (if $\frac{1}{E}\frac{dE}{ds}\Delta S$ is small)

$$1 - \frac{1}{E_n}\frac{dE}{dS}_n \Delta S = k \qquad (2.4.2)$$

If material interfaces need careful treatment the pathlength may be reduced when the trajectory comes near a boundary.

Energy Loss

The simplest treatment of energy loss is to use the continuous slowing down (C.S.D) approximation. This gives :-

$$\Delta E = \int_{S_n}^{S_{n+1}} \frac{dE}{ds}\, ds \qquad (2.4.3)$$

where $\frac{1}{\rho}\frac{dE}{ds}$ is the stopping power of the material.

In fact the energy loss by the electrons will not be determined completely by the pathlength but will be distributed about the value given by (2.4.3). This is due to the random nature of the collisions. An expression for the distribution of energy losses, for small $\Delta E/E$, has been given by Landau (106), for the case where the energy loss is due to ionization, and by Blunck and Westphal (107) for the case when Bremsstrahlung must also be included.

Angular Deflection

Kinematic Relations

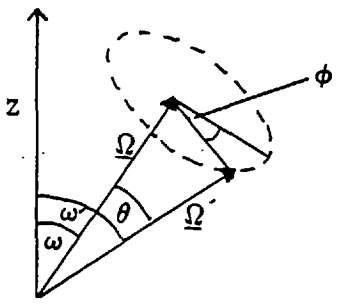

Fig.2.4

The effect of scattering from the pre-collision direction Ω to the post-collision direction Ω' may be described by two angles. θ; the angle between Ω and Ω' and ϕ; the angle $\Omega' - \Omega$ makes with the $\Omega \wedge (\Omega \wedge z)$ direction. The new polar angle ω' is given by:-

$$\omega' = \arccos(\cos\omega\cos\theta + \cos\phi\sin\omega\sin\theta) \qquad (2.4.4)$$

An alternative description valid for small deflections (small rotations approximately commute) is to consider the deflection $(\Omega \rightarrow \Omega')$ to be due to succesive rotations about the $z \wedge \Omega$ and $\Omega \wedge (\Omega \wedge z)$ axes.

Fig.2.5

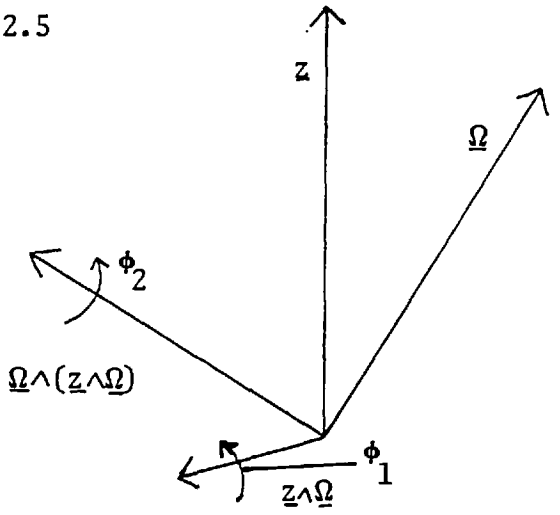

After the rotation, ϕ_1, about the $z \wedge \Omega$ axis the new value of θ, θ' is given by:-

$$\theta' = \theta + \phi_1 \qquad (2.4.5)$$

After the rotation, ϕ_2, about $\Omega \wedge (z \wedge \Omega)$ the new value of θ, θ'', is given by :-

$$\theta'' = \arccos(\cos\phi_2\cos\theta') = \arccos(\cos\phi_2\cos(\theta + \phi_1)) \qquad (2.4.6)$$

Equations (2.4.5) and (2.4.6) are less time consuming to evaluate than equation (2.4.4) and for this reason were used in the programme described in chapter 4.

Choice of Scattering Angles

The angles (ϕ_1,ϕ_2) or (θ,ϕ) are picked at random from an appropriate distribution of scattered angles, such as those described in section 2.2. If equation (2.4.6) is used both angles must be small (less than 10^{o} say).

2.5 Multi Group Diffusion

Although the Diffusion, or P_1, approximation is one of a set of approximations, the P_N set, it will be treated separately because of its comparative simplicity and its wide application to electron transport in Laser fusion target studies.

In the P_1 approximation the expansion of the angular dependence of the distribution, f, in Legendre polynomials is truncated after the first two terms. Thus, in 1-D, the angular dependence will be approximated by:-

$$f(x,v,t) \simeq A(x,v,t) + \mu B(x,v,t) \qquad (2.5.1)$$

The coefficients, A and B, are related to the zeroth and first moments of f by :-

$$N(x,v,t) = 2\pi \int_{-1}^{+1} (A + \mu B)\, v\, d\mu = 4\pi A \qquad (2.5.2a)$$

and

$$\Phi(x,v,t) = 2\pi \int_{-1}^{+1} (A + \mu B)\, \mu v\, d\mu = \frac{4\pi}{3} vB \qquad (2.5.2b)$$

Thus:-

$$f \simeq \frac{1}{4\pi} N + \frac{3}{4\pi v} \Phi \mu \qquad (2.5.3)$$

The transport equation for suprathermal electrons scattering and thermalising on a background thermal plasma with a Fokker Plank collision term has been given by Delettrez and Goldman (108). The form of the transport equation in various 1-D geometries is given in Appendix 3. For 1-D slab it is :-

$$\frac{\partial f}{\partial t} + v\,\mu\frac{\partial f}{\partial x} + a\left(\mu\frac{\partial f}{\partial v} + \frac{1}{v}(1-\mu^2)\frac{\partial f}{\partial \mu}\right) =$$

$$\frac{\Gamma}{2}(n_e + Z^2 n_i)\frac{\ln\Lambda_{sth}}{v^3}\frac{\partial}{\partial \mu}\left((1-\mu^2)\frac{\partial f}{\partial \mu}\right) + \frac{\Gamma n_e}{v^2}\frac{\partial}{\partial v}(\ln\Lambda_{sth}\, f)$$

in a stationary fluid (no PdV term) (2.5.4)

Two equations for the two unknowns A and B (alternatively N and Φ) are obtained by taking the first two moments of (2.5.4) with f given by (2.5.3). These give :-

$$\frac{\partial n}{\partial t} + \frac{\partial}{\partial x}\Phi - \frac{e}{m_e v^2}\frac{\partial}{\partial v}(E.J) - \frac{K_B}{v^2}\frac{\partial}{\partial v}(v^2 n) -$$

$$- \frac{K_f}{v^2}\frac{\partial}{\partial v}(n\ln\Lambda_{sth}) = \frac{\partial n}{\partial t})_{source} \qquad (2.5.5)$$

and

$$\frac{1}{v}\frac{\partial J}{\partial t} + \frac{v}{3}\frac{\partial n}{\partial x} - \frac{e}{3m_e}\frac{1}{v^2}\frac{\partial}{\partial v}(Env^2) - \frac{K_D}{v^2}\frac{\partial}{\partial v}(v^2\frac{J}{v}) -$$

$$- \frac{K_F}{v^2}\frac{\partial}{\partial v}(\ln\Lambda_{sth}\frac{J}{v}) + \frac{2K_d}{v^3}\ln\Lambda_{sth}\frac{J}{v} = \frac{\partial J}{\partial t})_{source} \qquad (2.5.6)$$

Where only μ is integrated over

The truncation of the infinite hierarchy of moment equations at (2.5.6), it does not involve the stress tensor, is due to the truncation of the Legendre polynomial expansion of the distribution function (2.5.4).

The approximation (2.5.4) is valid if the distribution function is nearly isotropic. This will be the case if $\lambda_{\pi/2}$ is less than the

scale length for the suprathermal density.

The numerical solution of equations (2.5.5) and (2.5.6) would present very great difficulties. Before considering what further simplifications can be made it is useful to discuss the numerical approach to the solution of the diffusion equations which is most convenient.

Numerical Solution of Simple Multi Group Diffusion Equations

Consider the equations:-

$$\frac{\partial n}{\partial t} + \frac{\partial \Phi}{\partial x} - \frac{\partial(\alpha n)}{\partial v} = \frac{\partial n}{\partial t})_s \qquad (2.5.7)$$

$$\Phi = -K(v,x)\nabla n \qquad (2.5.8)$$

where $\frac{\partial(\alpha n)}{\partial v}$ is a slowing down term. If the number (flux) of electrons in the speed range v_g to v_{g+1} is denoted n_g (Φ_g), and one sided differencing is used for the slowing down term, the difference equations are :-

$$\frac{\partial n_g}{\partial t} + \frac{\partial}{\partial x}(-K\frac{\partial n_g}{\partial x}) - \alpha_g n_g + \alpha_{g+1} n_{g+1} = \frac{\partial n_g}{\partial t})_s \qquad (2.5.9)$$

Equation (2.5.9) may be solved for one group at a time, starting with the highest speed group. The equation for a group is of the form :-

$$\frac{\partial n_g}{\partial t} + \frac{\partial}{\partial x}(-K\frac{\partial n_g}{\partial x}) - \alpha_g n_g = \text{source} \qquad (2.5.10)$$

where the source now includes the effect of downscatter from the immediately higher velocity group. Implicit differencing of equation (2.5.10), using the usual conservative 3 point differencing of the diffusion term, gives a stable and positive (for positive sources and initial conditions) algorithm.

Thus the solution of equations (2.5.10) involves solving one tridiagonal system of equations for each group. This may be accomplished very efficiently. Since the coefficients K and α, do not depend on n_g the equation is linear and no iteration is required. If a flux limit (section 3.6) is used K depends on n_g and this is no longer the case. *

Approach to the Solution of the Multi Group Diffusion Equations

The simplicity and efficiency of the scheme described above is very attractive. A common approach to the problems involved in solving equations (2.5.5) and (2.5.6) is to make approximations which allow this method of solution to be used. If this is to be done, the coupling between the groups and spatial zones must be as illustrated below:-

Fig.2.6 Coupling in a Simple Diffusion Model

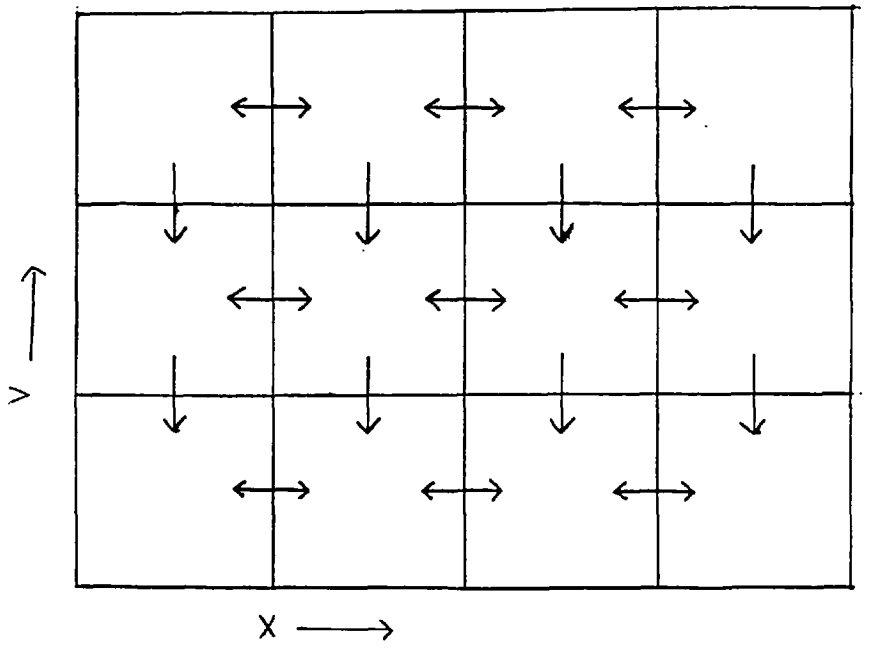

Such coupling clearly does not allow $\underline{J}.\underline{E}$ heating of the suprathermals or the treatment of a term with mixed derivatives.

The approach to the solution of the Multi Speed Group equations adopted by three authors (108, 109, 110) is described in section 3.4.

The inclusion of large energy transfer collisions in a Multi Group code is discussed by Greenspan and Shvarts (111).

2.6 The P_N Method

The P_N method has been described by Richtmyer and Morton (112) and Case and Zweifel (113). It was much used in early work on neutron transport but has largely been superceded by the S_N method (except for the P_1 (diffusion) method).

Description of the Method

The angular dependence of the distribution function may be expressed exactly, in one spatial dimension, as:-

$$f(x,\mu,t) = \sum_{l=0}^{\infty} (2l+1)^{\frac{1}{2}} \psi_l(x,t) P_l(\mu) \qquad (2.6.1)$$

where P_N are Legendre polynomials.

In the P_N method this exact description is replaced by the approximation:-

$$f(x,\mu,t) \simeq \sum_{l=0}^{N} (2l+1)^{\frac{1}{2}} \psi_l(x,t) P_l(\mu) \qquad (2.6.2)$$

N equations for the evolution of the coefficients, $\psi_l(x,t)$, are then required. This is achieved in the following manner. The scattering kernel is expanded in Legendre polynomials so that the transport equation is of the form :-

$$\frac{1}{v}\frac{\partial}{\partial t}\sum_{l=0}^{N}(2l+1)^{\frac{1}{2}}\psi_l(x,t)P_l(\mu) + \mu\frac{\partial}{\partial x}\sum_{l=0}^{N}(2l+1)^{\frac{1}{2}}\psi_l(x,t)P_l(\mu) =$$

$$= -\sigma\sum_{l=0}^{N}(2l+1)^{\frac{1}{2}}\psi_l(x,t)P_l(\mu) +$$

$$+ 2\pi\int_{-1}^{+1} d\mu' \left[\sum_{l=0}^{\infty}\sum_{m=-l}^{+l} K_l Y_{l,m}(\mu) Y_{l,m}(\mu')\right]\sum_{l=0}^{N}(2l+1)^{\frac{1}{2}}\psi_l(x,t)P_l(\mu)$$

$$\sum_{l=0}^{N}(2l+1)^{\frac{1}{2}}\psi_l(x,t)P_l(\mu') \qquad (2.6.3)$$

The term in the square brackets is an approximation to the scattering kernel. The Y_{lm} are associated Legendre polynomials . Multiplication of equation (2.6.3) by $P_k(\mu)$, k=0, ...L., and integration over solid angle , $2\pi\int_{-1}^{+1} d\mu$ gives N+1 coupled differential equations for the N+1 unknowns in equation (2.6.2).These may be solved to give the time evolution of $f(x,\mu,t)$. This method has been used by Kershaw (114) and Yabe et al (115) in suprathermal transport studies but without including E field effects.

2.7 The S_N Method

The S_N ,or discrete ordinate, method is the most widely used method in numerical neutron transport simulation. It was developed at Los Alamos by Carlson and co-workers (116). It has recently been applied to electron transport in a solid (117).

Description of the Method

Consider the 1-D transport equation :-

$$\frac{1}{v}\frac{\partial}{\partial t}I(v,\mu,t) + \mu\frac{\partial}{\partial z}I(v,\mu,t) = -\sigma_{UG}I(v,\mu,t) + \int\sigma_{IG}(\mu-\mu')(I(v,\mu,t)-I(v,\mu',t))d\mu' \qquad (2.7.1)$$

Here σ_{UG} and σ_{IG} are the out of group and in group cross sections respectively. I is the flux and $\mu = \cos\theta = \hat{z}.\hat{v}$.

In the discrete S_N approximation the μ dependence of the flux is approximated by :-

$$I(v,\mu) = \sum_{i=1}^{N} I(v,\mu_i)w_i\,\delta(\mu-\mu_i) \qquad (2.7.2)$$

where the w_i are the weights.

Substitution in equation (2.7.1) gives N equations of the form:-

$$\frac{1}{v}\frac{\partial}{\partial t}I(x,v,\mu_i,t) + \mu_i\frac{\partial}{\partial x}I(x,v,\mu_i,t) + \sum_j K_{IG}(w_jI(x,v,\mu_j,t) - K_{IG}I(x,v,\mu_j,t) - K_{UG}I(x,v,\mu_i,t) = \frac{\partial}{\partial t}I(x,v,\mu_i,t)_s \qquad (2.7.3)$$

where the subscripts IG and UG again refer to in and out of group scattering. (isotropic scattering has been assumed)

There is no unique procedure for determining the level weights, w_i, and level cosines, μ_i. However in order that the quadrature formulae give results analogous to analytic integration the following relations are usually satisfied.

$$\frac{1}{2}\int_{-1}^{+1} 1 \, d\mu = 1 \quad \text{(normalisation)} \qquad 1 = \sum_i w_i \tag{2.7.4a}$$

$$\frac{1}{2}\int_{-1}^{+1} \mu \, d\mu = 0 \qquad 0 = \sum_i \mu_i w_i \tag{2.7.4b}$$

$$\frac{1}{2}\int_{-1}^{+1} \mu^2 d\mu = \frac{1}{3} \qquad \frac{1}{3} = \sum_i \mu_i^2 w_i \tag{2.7.4c}$$

An example is the S_2 set

$$w_1 = w_2 = 0.5 \tag{2.7.5a}$$

$$\mu_1 = -\mu_2 = 3^{-\frac{1}{2}} \tag{2.7.5b}$$

In a geometry other than Cartesian the fluxes in different directions will be coupled by streaming as well as by collisions. This is referred to as angular redistribution.

An alternative approach, described by Case and Zweifel (118), is to split the interval $-1 \leq \mu \leq +1$ into N parts given by $\mu_{i-1} \leq \mu \leq \mu_i$. $I(x,v,\mu,t)$ is approximated by the linear interpolation formula :-

$$I(x,v,\mu,t) = \frac{1}{\mu_i - \mu_{i-1}} \left((\mu - \mu_{i-1}) \, I(x,v,\mu_{i-1},t) + (\mu_i - \mu) \, I(x,v,\mu_i,t) \right) \tag{2.7.6}$$

Integration of the transport equation over each interval gives N equations for the N+1 unknowns ($I(x,v,\mu_i,t)$: i=1,...N). A further equation, usually the transport equation for μ_0, is needed. In this case quadrature is achieved with the trapezoidal rule. Provided μ_i equals zero is not used there are N boundary conditions.

Comparatively little work has been done with S_N methods in charged particle transport. Antal and Lee (119) have used S_N methods in α-particle slowing down problems. Recently (117) electron penetration has been treated using the S_N method. Electron transport simulation is made more difficult than neutron transport simulation because of the very anisotropic scattering cross sections. To the knowledge of the author the effect of deflection due to steady state E fields has not been included in any S_N model.

CHAPTER 3

Introduction

In this chapter the models used to describe suprathermal electron transport in laser irradiated targets are reviewed. This includes both the numerical models used in target simulation codes and simpler models which are used to explain coronal phenomena. A minor extension, by the author, of some work by Shkarofsky is presented as section 3.8.

3.1 The Suprathermal Approximation

The problems associated with calculating the evolution of an arbitrary electron distribution are formidable. Two familiar simplifications are a thermal plasma; where by truncation of the moment expansion of the distribution function, fluid equations and appropriate transport coefficients may be used to advance the system in time, and a plasma in which electron-electron collisions are ignored; a Lorentz gas.

The nature of the "suprathermal approximation" is as follows. The electrons are divided into two classes, the bulk of the electrons which can be described by the equations for a thermal plasma and a small number of suprathermal electrons which, because of their large kinetic energy, will not thermalise on the time or length scales relevant to the thermal plasma. These electrons are assumed not to interact with each other but only with the thermal electrons and ions. Thus the inequality $n_{sth} \ll n_{th}$ must hold. The suprathermal electron will lose energy to the thermal plasma and, eventually, thermalise.

In this approximation the electrons are either part of a thermal class, which has energy and density sources and sinks from and to the suprathermals, or a suprathermal class for which the collision term is linear. In the absence of E and B field effects the suprathermals are described by linear equations. This represents a great simplification of the more general problem of non- thermal electron transport.

The most sweeping approximation involves ignoring the density and current associated with the suprathermal electrons, and any E or B field effects on them, and retaining only the energy deposition into the thermal plasma.

3.2 Core and Corona

The idealised state of affairs described in the previous section will not apply everywhere in the target. In the corona the suprathermal density may be comparable to or exceed the density of thermal electrons. Collisions with the thermal particles can become relatively unimportant and the E field can dominate the motion of the suprathermal electrons.

These differences will clearly have a great influence on the way in which suprathermal transport in the corona and in the higher density core are treated.

The approximations that are commonly used are :-

In the Core

1 $n_{sth} \ll n_{th}$

2 $\lambda_{\pi/2} \ll L$ (Diffusive)

3 $\underline{E}$ and $\underline{B}$ fields can be ignored

In the Corona

4 $\lambda_E \gg$ Length of corona

5 $\lambda_{\pi/2} \gg$ Length of corona

6 Collisionless

7 suprathermal electron transit time $\ll$ characteristic time for hydrodynamic motion

8 $L \gg \lambda_D (T_{sth})$

In the core the electron density of the $\gtrsim$ solid density material will greatly exceed the suprathermal density, which will be comparable to or less than critical density. Ionization of the target will soon give $n_{th} \gg n_{sth}$. Thus in the core condition (1) will hold in all cases of interest.

A suprathermal electron will have $\lambda_E > L$. In a high Z plasma $\lambda_E / \lambda_{\pi/2} = Z$ so condition (2) may hold. If it does a great simplification

results since the diffusion approximation is valid.

Next consider condition (3). To see if E fields are negligible we use simple Ohm's Laws for the thermals and suprathermal suprathermals.

consider a pair of equations:-

$$J_{sth} = (\nabla P_{sth}/(-en_{sth}) + E\ )\ \sigma_{th}\ \frac{n_{sth}}{n_i}\left(\frac{T_{sth}}{T_{th}}\right)^{3/2}$$

$$J_{th} = E\ \sigma\ \frac{n_{th}}{n_i}$$

If $J_{sth} + J_{th} = 0$ then:-

$$E = -\frac{\nabla P_{sth}}{(-en_{sth})}\left(\frac{1}{1 + \dfrac{n_{th}T_{th}^{3/2}}{n_{sth}T_{sth}^{3/2}}}\right)$$

and

$$J_{sth} = \frac{\nabla P_{sth}}{-en_{sth}}\ \sigma\frac{n_{st}}{n_i}\left(\frac{T_{sth}}{T_{th}}\right)^{3/2}\left(1 - \frac{1}{1 + \dfrac{n_{th}T_{th}^{3/2}}{n_{sth}T_{sth}^{3/2}}}\right) \qquad (3.2.1)$$

If $(n_{th}T_{th}^{3/2})\ /\ (n_{sth}T_{sth}^{3/2}) \gg 1$ then (3.2.1) becomes approximately :-

$$J_{sth} = \frac{\nabla P_{sth}}{-e}\ \frac{\sigma}{n_i}\left(\frac{T_{sth}}{T_{th}}\right)^{3/2}$$

In which case the effect of the E field is negligible.

A criterion for ignoring the effect of magnetic fields on the suprathermal transport is that :-

$$\left(\frac{\lambda_{\pi/2}}{r_{eL}}\right)_{sth} \ll 1 \qquad (3.2.2)$$

The inclusion of the B field greatly complicates the calculation of quasineutral E field effects. The condition $J = 0$ is replaced by the condition $\nabla \cdot J = 0$ for $B \neq 0$.

If (1), (2) and (3) all hold then the simulation of suprathermal transport is comparatively easy.

The quantity of matter in the corona is usually "small" so the energy loss by the suprathermal electrons in crossing the corona once will be small. Thus for electrons which pass through both the core and the corona the collisional energy loss in the core will vastly exceed that in the corona. Condition (4) will generally hold in the corona. The modelling of collisional energy loss is greatly complicated if $n_{sth} \sim n_{th}$ since suprathermal-suprathermal collisions will be important.

Momentum transfer due to collisions may be important in a high Z corona. In a low Z corona condition (5) will hold.

The assumption that the suprathermal electrons are collisionless in the corona, condition (6), is sometimes used. It is more restrictive than conditions (4) and (5) which require collisions to be a "small" term.

Since $v_{sth} \gg v_{is}$ the changes caused by hydrodynamic motion in the course of a suprathermal electron transit time will be small. Condition (7) allows the time dependence of the state of the corona to be included perturbatively.

Finally condition (8) allows quasineutrality to be used. It is not always valid.

3.3 Fluid Models for Suprathermal Electrons

A fluid model for the suprathermal electrons is a crude approximation. Since suprathermal-suprathermal collisions are unimportant compared to suprathermal-thermal collisions, the suprathermals will not become Maxwellian. Moreover even if the suprathermals are created with a Maxwellian distribution they will not stay that way. Collisions do not form a basis for truncating the moment expansion of the distribution function. The disparity between the timescales for the suprathermal electron and hydrodynamic motion may be used to justify truncating the moment expansion. Although there is no physical basis for it it is often found convenient to assign a temperature to the suprathermals.

Basis for Truncation of the Moment Expansion

It is instructive to consider the one dimensional Vlasov-Poisson system:-

$$\frac{\partial f}{\partial t} + v \frac{\partial f}{\partial x} + a \frac{\partial f}{\partial v} = 0 \qquad (3.3.1)$$

$$a = \frac{e}{m_e} \frac{\partial \phi(x,t)}{\partial x}$$

$$\frac{\partial^2 \phi}{\partial x^2} = \varepsilon_o \rho$$

Following Bernstein et al (120) introduce the energy, $\frac{1}{2} m v_e^2 - e\phi$ as an independent coordinate. Equation (3.3.1) becomes

$$\frac{\partial f}{\partial t} - e \frac{\partial \phi}{\partial t} \frac{\partial f}{\partial \varepsilon} + v \frac{\partial f}{\partial x} = 0 \qquad (3.3.2)$$

If there is no time dependence ($\frac{\partial}{\partial t} = 0$) the solution to (3.3.2) is $f = f(\varepsilon)$.

We may write:-

$$f = f_+(\varepsilon) + f_-(\varepsilon)$$

Where the subscript denotes the direction of motion.

The electron distribution may be divided into two parts. One with energy less than ε_{crit} which is trapped and the other with energy greater than this which is not trapped by the electrostatic potential.

Fig.3.1

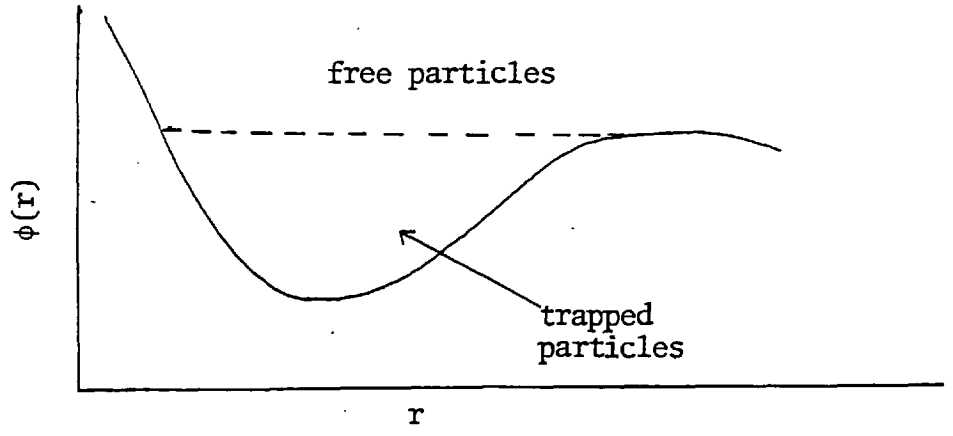

If the electrons are trapped in a time independent potential then $f_+ = f_-$ and all odd moments of the distribution function will be zero. Valeo and Bernstein (75) expand the distribution function

$$f = f_0 + \lambda f_1 + \lambda^2 f_2 + \ldots.$$

where λ is a formal expansion parameter of order τ_{sth}/τ_{hydro}. $v\frac{\partial}{\partial x}$ is zeroth order in λ, $\frac{\partial}{\partial t}$ and $\frac{e}{m}\frac{\partial \phi}{\partial t}\frac{\partial}{\partial \varepsilon}$ are first order in λ.

Thus to zeroth order :-

$$v \frac{\partial}{\partial x} f_0 = 0 \tag{3.3.3}$$

and to first order :-

$$\frac{\partial f_0}{\partial t} + \frac{e}{m} \frac{\partial \phi}{\partial t} \frac{\partial f_0}{\partial \varepsilon} + v \frac{\partial f_1}{\partial x} = 0 \tag{3.3.4}$$

From (3.3.3) $f_0 = f_0(\varepsilon;t)$. (3.3.4) then gives, when integrated round a closed orbit with ε and t held constant,:-

$$\frac{\partial f_0}{\partial t} \oint \frac{dx}{v} + \frac{\partial f_0}{\partial \varepsilon} \oint \frac{dx}{v} \frac{e}{m} \frac{\partial \phi}{\partial t} = 0 \tag{3.3.5}$$

since f_1 must be single valued.

It can be shown by substitution that a function $f_0(J)$, $J = \oint v\, dx$ is a solution to (3.3.5). Using this (3.3.4) may be integrated to give :-

$$f_1 = \frac{\partial f_0}{\partial J} \left[\left(\oint \frac{dx}{v} \right) \int dx\, v - \left(\int \frac{dx}{v} \right) \oint dx\, v \right] \tag{3.3.6}$$

Using $$\frac{dJ}{dv} = \frac{\partial J}{\partial \varepsilon} \frac{\partial \varepsilon}{\partial v} + \frac{\partial J}{\partial x} \frac{\partial x}{\partial v} + \frac{\partial J}{\partial t} \frac{\partial t}{\partial v} =$$

$$= mv \frac{\partial J}{\partial \varepsilon}$$

they derived first order (in λ) expressions for the moments of the distribution functions.

$$u = \int dJ \left(\frac{\partial J}{\partial \varepsilon}\right)^{-1} (f_+ - f_-)$$

$$q = -3nTu + \int dv\ v^3 f_1$$

Where $nT \simeq m \int dv\ v^2 f_o$

Thus both u and q are first order quantities. They use calculations with an assumed potential to justify

$$q = \beta p u \tag{3.3.7}$$

β of order unity.

(3.3.7) truncates the moment expansion. The fluid equations are closed by :-

$$\frac{\partial p}{\partial t} + \frac{\partial}{\partial x}(q + 3pu) - 2e \frac{\partial \phi}{\partial x} nu = 0$$

$$q = \beta p u \tag{3.3.8}$$

They use :-

$$\frac{\partial}{\partial t} n + \frac{\partial}{\partial x} nu = 0 \tag{3.3.9}$$

$$-en \frac{\partial \phi}{\partial x} - \frac{\partial p}{\partial x} = 0 \tag{3.3.10}$$

Equation (3.3.10) is valid if $v_{sth} \gg u_{sth}$, the full momentum equation being :-

$$\frac{\partial}{\partial t} nu + u \frac{\partial}{\partial x} nu = -en \frac{\partial \phi}{\partial x} - \frac{\partial p}{\partial x}$$

In the limit of E field effects being unimportant this becomes :-

$$\frac{\partial}{\partial t} nu + u \frac{\partial}{\partial x} nu + \frac{\partial p}{\partial x} = 0$$

which describes streaming particles.

Any model based on equations (3.3.8), (3.3.9) and (3.3.10) must be tested to see if the results it gives are consistent with $v_{sth} \gg u_{sth}$.

If the suprathermal electrons were truly collisionless then any electron streaming into the high density core would pass through it, reflect at the other side and stream back. This would be consistent with no zero order current. A more realistic situation is illustrated below.

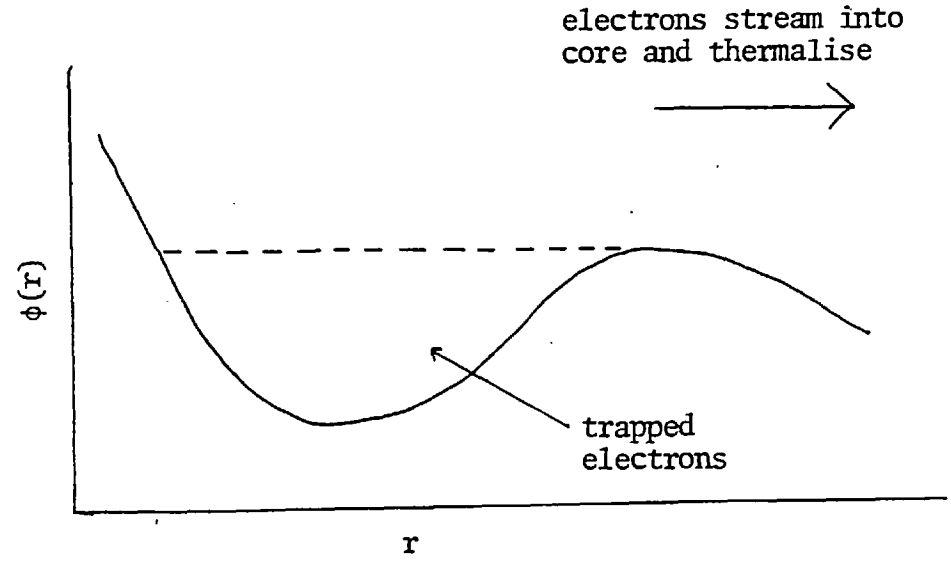

Fig.3.2

An assumption which has been used is that the suprathermals are in equilibrium with the E field and have a Maxwellian distribution. The equations governing the suprathermal electrons are then :-

$$n_{sth} = n_{sth_o} e^{-e\phi/kT_{sth}} \qquad (3.3.11)$$

$$T_{sth} = \text{constant}$$

n_{sth_o} is the suprathermal density when $\phi = 0$. (3.3.11) can be simply derived from :-

$$v\frac{\partial f}{\partial E_T} = 0 \qquad f = f(E_T) \qquad (3.3.12)$$

and

$$f_{(\phi=0)} = e^{-\frac{1}{2}mv^2/kT} \qquad (3.3.13)$$

The effect of the neglect of the small terms due to the time dependence of ϕ in deriving (3.3.11) in self-similar expansion models has been considered by Mora and Pellet (121).

Mason (54) has used a model in which both thermals and suprathermals are described by collision dominated fluid equations in an investigation of B field production by suprathermals.

3.4 Multi Group Models

In this section the implementation of multi group models (section 2.5) in laser target simulation codes is illustrated by three examples. These are due to Delettrez and Goldman (108), Zimmerman (110) and Kershaw (109,122). The first was used in the University of Rochester 1-D code "LILAC" and the other two in the Livermore 2-D code "LASNEX".

Implementation in LILAC

The suprathermal electrons are treated by a three component model. Those for which a diffusive model is valid ($\lambda_{\pi/2} < L$) are treated by multi group diffusion. Those for which such a model is not valid are treated by the forward- reverse model (123). Deflection is ignored for these electrons, the coupling between the two groups is introduced by the angular redistribution (cf S_N) and the boundary conditions.

The multi (velocity) group diffusion equations (section 2.5) are used with the underlined terms omitted:-

$$\frac{\partial n}{\partial t} + \frac{\partial}{\partial \underline{r}} \cdot \underline{J} - \frac{e}{m_e v^2} \frac{\partial}{\partial v} (\underline{E} . \underline{J}) - \frac{K_B}{v^2} \frac{\partial}{\partial v} (v^2 n) - \frac{K_f}{v^2} \frac{\partial}{\partial v} (n \ln \Lambda_{sth}) = \left(\frac{\partial n}{\partial t}\right)_s \qquad (3.4.1)$$

$$\frac{1}{v} \frac{\partial \underline{J}}{\partial t} + \frac{v}{3} \frac{\partial n}{\partial \underline{r}} - \frac{e}{3 m_e v^2} \frac{1}{\partial v} (\underline{E} n v^2) - \frac{K_B}{v^2} \frac{\partial}{\partial v} \left(v^2 \frac{\underline{J}}{v}\right) - \frac{K_f}{v^2} \frac{\partial}{\partial v} \left(\ln \Lambda_{sth} \frac{\underline{J}}{v}\right) + 2 \frac{K_d}{v^3} \ln \Lambda_{sth} \frac{\underline{J}}{v} = \left(\frac{\partial \underline{J}}{\partial t}\right)_s \qquad (3.4.2)$$

These approximations reduce equations (3.4.1).and (3.4.2) to a simple Fickian diffusion term. In equation (3.4.1) the ohmic heating ($\underline{E}.\underline{J}$) term is only allowed to demote the suprathermals to the thermals. It cannot premote thermals to suprathermals.

The model for the streaming suprathermals assumes two semi-isotropic distributions .

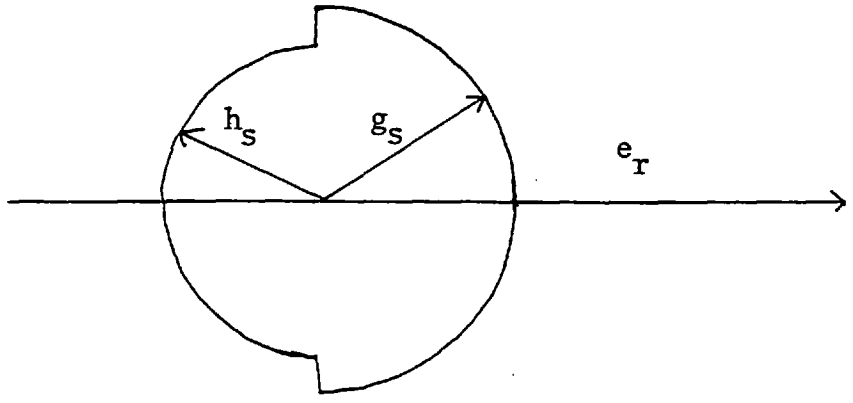

Fig.3.3 Forward-Reverse Model

The particle currents are simply given by $-v_{sth}h_{sth}/2$ and $+v_{sth}g_{sth}/2$. The zeroth order moment gives:-

$$\frac{\partial h_{sth}}{\partial t} - \frac{\partial}{\partial \underline{r}} \cdot J_h - \frac{e}{2mv^2}\frac{\partial}{\partial v}(vE.J_h) - \frac{K_B}{v^2}\frac{\partial}{\partial v}(h_{sth}v^2) -$$

$$- \frac{K_f}{v^2}\frac{\partial}{\partial v}(h_{sth} \ln \Lambda_{sth}) = \frac{\partial h_{sth}}{\partial t})_s \qquad (3.4.3)$$

where $\underline{J}_h = -v_{sth}h_s/2$, and a similar equation for g_{sth}.
The source / sink terms $\frac{\partial h_{sth}}{\partial t})_s$, $\frac{\partial g_{sth}}{\partial t})_s$ include the angular redistribution terms. All outgoing electrons are specularly reflected

at the boundary of the last cell. The E field is calculated using Gauss' equation. The effect of P dV cooling on the suprathermal electrons has now been included (124).

Lasnex Implementation (1)

The multi velocity group implementation described in (110) uses the "Ohm's Law":-

$$\Phi = - \alpha_j (n_j eE + \nabla P_j) \qquad (3.4.4)$$

where $P = \int (n_g v^2 \frac{1}{3}) 4\pi v^2 \, dv$ and α_j the flux limited group diffusion coefficient.

The E field is determined from $\Sigma \text{ flux}_j = 0$

$$\text{ie} \quad E = - \frac{\Sigma \alpha_j \nabla P_j}{e \Sigma \alpha_j n_j} \qquad (3.4.5)$$

The zeroth moment eqations are :-

$$\frac{\partial n_g}{\partial t} + \nabla . \Phi - \frac{4 e^2}{(4\pi\varepsilon_o)^2 m_e} n_e \ln\Lambda_{sth} \frac{n_g}{v} = \frac{\partial n_g}{\partial t})_s \qquad (3.4.6)$$

The J.E term is omitted.

Lasnex Implementation (2)

The implementation of a more refined model, in one spatial dimension, has recently been described by Kershaw (122). It uses a model first used in relativistic electron beam-target interaction studies (109).

The multi total energy group equations, using a relativistic collision term (125), are :-

$$\underbrace{\frac{\partial n_g}{\partial t} + \frac{\partial}{\partial x}.(v_f n_g)}_{1} = \underbrace{-\frac{\partial}{\partial \underline{r}}.\Phi + \frac{2}{m_e}\frac{\partial}{\partial E_T}\left(\frac{C_e \ln\Lambda}{u} n_g\right)}_{2} +$$

$$\underbrace{+\left(\frac{\partial n_g}{\partial t}\right)_{Brem} + \left(\frac{\nabla.v_f}{3}\right)\frac{\partial}{\partial E_T}(pun_g)}_{3} \underbrace{- e\frac{\partial\Phi}{\partial t}\frac{\partial n_g}{\partial E_T}}_{4} = \left(\frac{\partial n_g}{\partial t}\right)_s \qquad (3.4.7)$$

$\underline{V}_f$ = fluid velocity

$C_k = 2\pi m_k Z_k^2 r_o^2 (m_e c^2)^2$ k denotes species (e=electrons)

p = momentum u = velocity

and

$$-\frac{2(m\gamma)^2}{p^3}\ \Sigma C_k \ln\Lambda_k \quad \Phi = \frac{p^3}{3}\frac{\partial}{\partial \underline{r}}\left(\frac{n_a}{pm\gamma}\right) \qquad (3.4.8)$$

(C_k, $\ln \Lambda_k$ refer to the different ion species)

The groups of terms in (3.4.7) labeled (1) -(4) are treated in the following fashion:-

(1) This term is $\frac{1}{V}\frac{D}{Dt}(Vn_g)$.

V = specific volume.

It is treated by the Lagrangian hydrodynamics.

(2) These terms are treated by implicit three point differencing with the friction term acting as a sink to the lower groups and a source from the higher groups; ie the standard multi group treatment.

(3) These terms are regarded as "small". They are treated implicitly but split off from the main calculation. If the operator equation for the main calculation is (I + A) and for the total calculation including the small terms is (I + A + B). This approximation is equivalent to (I + A + B) $\simeq$ (I + A) (I + B).

(4) The $\frac{\partial \phi}{\partial t}\frac{\partial n_g}{\partial E_T}$ term can be written $\frac{\partial}{\partial E_T}\left[\left(\frac{\partial \phi}{\partial t}\right)n_g\right]$

Its treatment is illustrated below:-

Fig.3.4 Bin-Bin Mapping

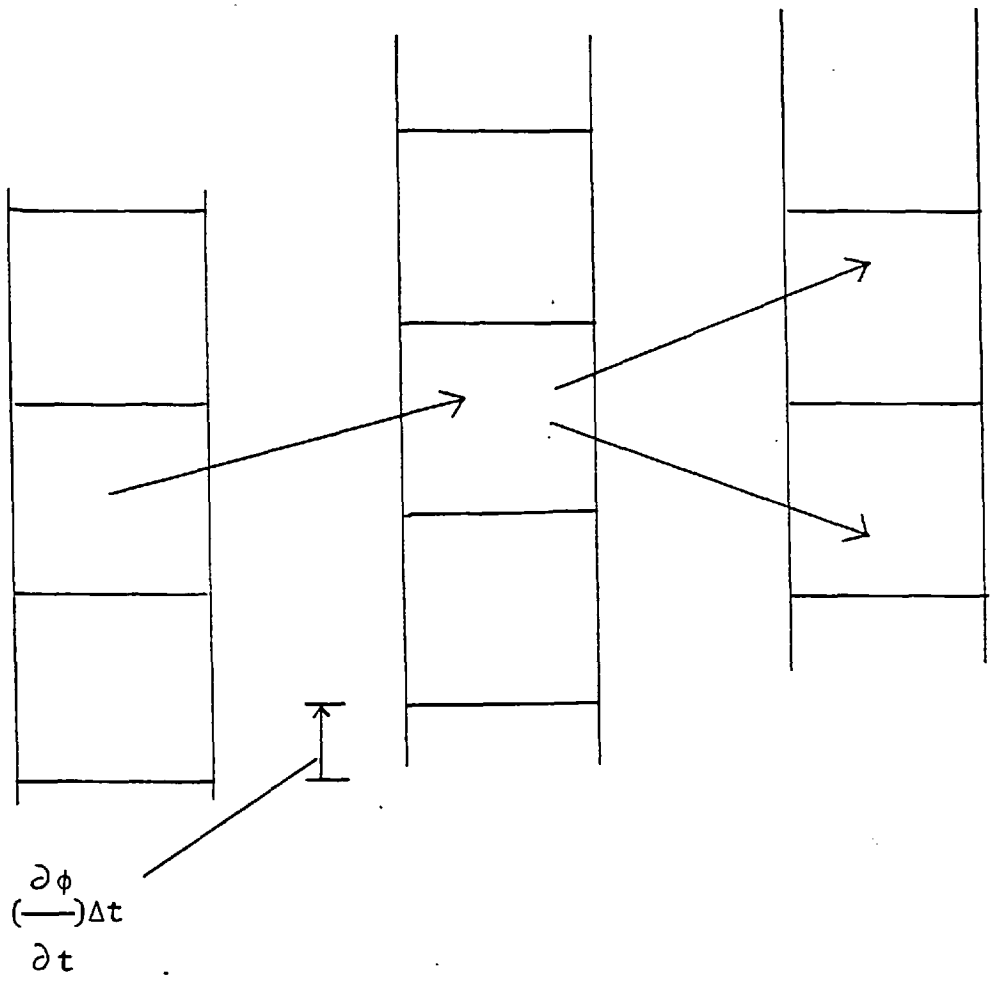

There are energy conservation problems associated with the mappings.

J and E Calculation

The current is calculated from :-

$$\frac{\partial \rho}{\partial t} + \frac{\partial}{\partial \underline{r}} \cdot J = 0 \qquad (3.4.9)$$

The thermal electron motion is treated implicitly (120).

The E field is found iteratively using:-

$$E_i^{n+1} = E_i^n - \alpha J_i^n / \left(\frac{\partial J}{\partial E}\right)_i^n \qquad (3.4.10)$$

$$\text{where} \quad \left(\frac{\partial J}{\partial E}\right)_i^n = \frac{J_i^n - J_i^{n-1}}{E_i^n - E_i^{n-1}}$$

where the superscript denotes the number of iterations.
At the end of each step the thermal density is given by:-

$$n_{th} = Zn_i - \Sigma n_{sth} \qquad (3.4.11)$$

Multi group codes have also been described by Shvartz and Jablon (127), Shvartz et al (81), Yabe et al (128) and Evans (129).

3.5 Monte Carlo Models

A Monte Carlo suprathermal electron transport model has been used in conjunction with the KMSF 1-D Lagrangian code "TRHYD" (130) and has recently been used to model experiments (131). The condition $J_{total} = 0$ and the Ohm's law for the thermals are used to calculate the E field. The simulation particles are reflected at the outer boundary of the last cell. The pressure due to the suprathermal electrons is calculated in each cell and this is used in the hydrodynamic calculation and the calculation of P dV energy loss.

A Monte Carlo model for suprathermal transport has been used by Mason(132,133) in work on the effect of suprathermal transport on the thermal transport. In this work ion motion is suppressed and the E field is calculated using a dilated plasma period technique. This will be further discussed in chapter 6.

3.6 The Flux Limit

A diffusive model will give a flux :-

$$\Phi_{diff} = -\frac{v}{3}\frac{1}{\lambda_{\pi/2}}\nabla n \qquad (3.6.1)$$

If $\lambda_{\pi/2}$ exceeds the scale length for the suprathermal density then Φ_{diff} may exceed Φ_{fs} where :-

$$|\Phi_{fs}| = vn \qquad (3.6.2)$$

Φ_{fs} is clearly the greatest flux that can be carried by particles with velocity v and density n. It is necessary to limit the flux given by (3.6.1) to some value, such as Φ_{fs}, when the diffusion approximation is invalid. There are several possible limits.

(1) A unidirectional beam of particles. This has a flux Φ_{fs} (by the definition of Φ_{fs}) .

(2) In diffusion theory the angular dependence is approximated by:-

$$F(v, \mu) = A(v) + \mu B(v) \qquad (3.6.3)$$

If $F(v, \mu) \geq 0$ for all v, μ is imposed then the maximum flux corresponds to $B = \pm A$. In this case :-

$$n = 2\pi\int_{-1}^{+1} A \, d\mu$$

$$\Phi = 2\pi\int_{-1}^{+1} Av\mu^2 \, d\mu = \frac{1}{3} nv = \frac{1}{3}\Phi_{fs}$$

(3) The flux out of a region in which the flux is isotropic

$$n = 2\pi\int_{-1}^{+1} A \, d\mu$$

$$\Phi = 2\pi\int_0^1 A\,\mu\,d\mu = \frac{1}{4}nv = \frac{1}{4}\Phi_{fs}$$

The limit $|\Phi| \leq \Phi_{lim}$ may be included in a diffusion model, $\Phi = -D\nabla n$, by modifying the diffusion coefficient, D. One choice is:-

$$\frac{1}{D^*} = \frac{1}{D} + \frac{|\nabla n|}{\Phi_{lim}} \qquad (3.6.4)$$

or

$$\frac{1}{D^*} = \frac{\Phi_{lim} + D\,\nabla n}{\Phi_{lim}}$$

In the limit $D|\nabla n| \ll \Phi_{lim}$

$$\frac{1}{D^*} \simeq \frac{1}{D} \qquad (3.6.5)$$

and in the limit $D|\nabla n| \gg \Phi_{lim}$

$$\frac{1}{D^*} \simeq \frac{\nabla n}{\Phi_{lim}} \qquad (3.6.6)$$

and $$D^*\nabla n = \Phi_{lim}\frac{\nabla n}{|\nabla n|} \qquad (3.6.7)$$

(3.6.5) and (3.6.6) are the desired limits of the modified diffusion coefficient.

Equation (3.6.7) gives a flux which is in the direction of the density gradient. For free streaming particles it is the initial motion of the particles and not the density gradient which "drives" the flux. An example in which the flux is not parallel to the density gradient is shown below.

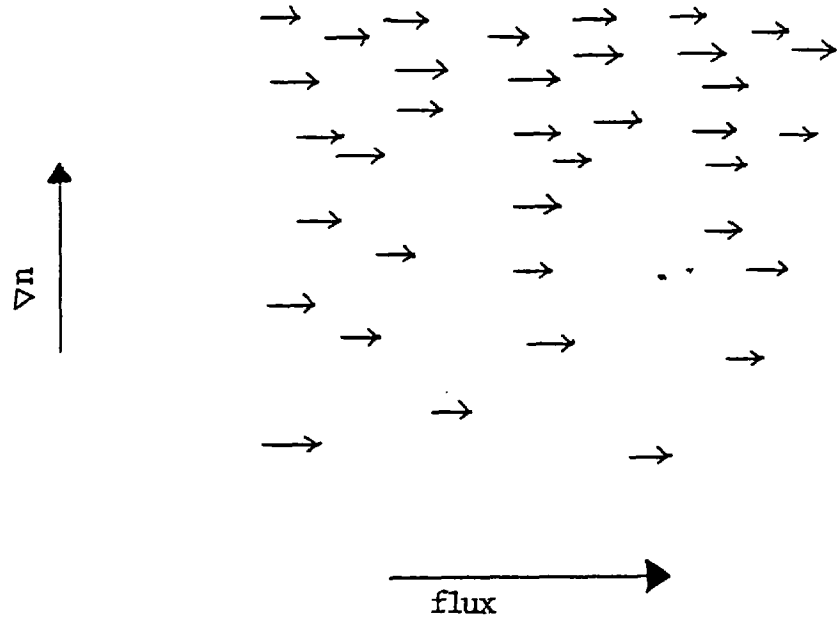

Fig.3.5 A Flux Which is not in the-∇n Direction

Corman et al (134) describe several approaches to flux limiting. They give a method, due to D.Post and J.Wilson, of including limits (1) or (3), described earlier in this section, where appropriate, viz:-

$$\Phi_{lim} = nv(1 + 3\exp(-\frac{\lambda}{2}\frac{1}{n}\left|\frac{\partial n}{\partial x}\right|))^{-1}$$

The flux limit used in chapter 5 is limit(2). This is the limit which is "in the spirit of" the diffusion approximation.

Kershaw (114) has compared higher order P_n methods with flux limited diffusion (P_1).

> He found $n > 10$ was needed for P_n to give better results than flux limited P_1.

3.7 Analytic Work

Two analytic models for suprathermal transport are described in this section. Albritton et al(135) considered the transport of large mean-free-path electrons and Shkarofsky (136) describes a Lorentz gas model.

Large Mean-Free-Path Transport

Figure 3.6 shows, schematically, the trajectory of a suprathermal electron in the corona of a spherical microballoon.

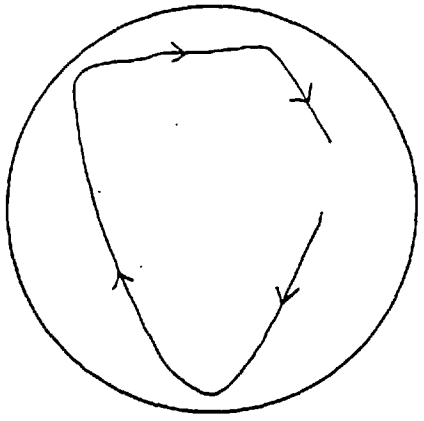

Fig.3.6 Trajectory of Electron in the Corona

Clearly the inward radial flux due to such orbiting electrons will be much less than the naive flux limiting value $v(\frac{1}{2}m_e v^2)$. Indeed the flux may be outward, due to ion expansion. The motion of the electron is dominated by the E fields in the corona. The effective potential the electron experiences, for motion in the radial direction, is illustrated

below:-

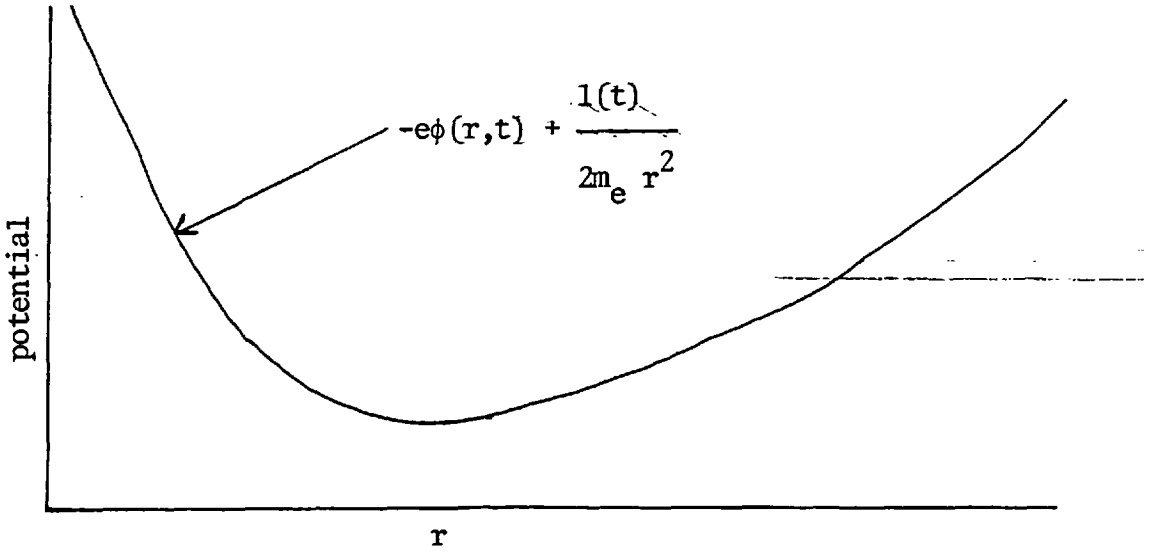

Fig.3.7 Effective Potential of Orbiting Electron

l is the angular momentum of the electron.

This potential has the same effect as the purely electrostatic potential well considered by Valeo and Bernstein (75) and discussed in section 3.3. The flux, with no collisions and no time dependence of ϕ , will be, for appropriate boundary conditions, zero. Albritton et al use the assumption of an infinite potential jump at some "sheath" which is moving slowly, compared with the suprathermal electrons, and assuming $\lambda_{\pi/2} \gg$ Radius of the Microballoon everywhere. They calculate the first order "bounce average" diffusion coefficients in impact parameter. The flux calculated scales as :-

$$q \sim (\tfrac{1}{2}m_e v^2)v \frac{R}{\lambda_E}$$

Double Maxwellian Heat Conduction

Shkarofsky (136) used a model in which the zero order electron distribution function was taken to be the superposition of two Maxwellians

$$f_o = \left(\frac{m}{2\pi}\right)^{2/3} \frac{n_{th}}{T_{th}^{3/2}} \exp(-mv^2/2T_{th}) + \frac{n_{sth}}{T_{sth}^{3/2}} \exp(-mv^2/2T_{sth}) \qquad (3.7.1)$$

The distribution function is expanded to first order and the first term of the spherical harmonic expansion is used. Thus:-

$$f \simeq f_o + \underline{f}_1 \frac{\underline{v}}{\underline{v}} \qquad (3.7.2)$$

It is assumed that the effect of laser energy deposition and energy transport maintain a stationary n_{th} , T_{th} , n_{sth} and T_{sth} profile. Using the Lorentz gas approximation the equation for $\underline{f}_1$ is :-

$$\underline{f}_1 = -\frac{1}{\nu_c}\left[v \nabla f + e/m(\partial f_o/\partial v)\, \underline{E}\right] \qquad (3.7.3)$$

This may be used to calculate the current ,

$$\underline{J} = -\frac{4}{3}\pi\, e \int_o^\infty \underline{f}_1 v^3\, dv \qquad (3.7.4)$$

and the energy flux,

$$\underline{q} = \frac{2}{3}\pi \int_o^\infty \underline{f}_1 v^5\, dv \qquad (3.7.5)$$

The factors of 1/3 in equation (3.7.4) and (3.7.5) are due to the integration over angle. Using equation (3.7.1) for f_o in equation (3.7.3) to obtain an expression for $\underline{f}_1$ Shkarofsky finds the energy flux, for $J = 0$ to be :-

$$q = -\frac{32}{m^2}\frac{1}{n_+ Y}\left(\frac{1}{n_{th}T_{th}^{3/2} + n_{sth}T_{sth}^{3/2}}\right) \cdot$$

$$2n_{sth}T_{th}^{5/2}\,T_{sth}^{3/2}\,(T_{th}-T_{sth})\nabla n_{th} + 2n_{th}T_{th}^{3/2}\,T_{sth}^{5/2}\,(T_{th}-T_{sth})\nabla n_{sth} +$$

$$+ n_{th}T_{th}^{3/2}(n_{th}T_{th}^{5/2} + n_{sth}T_{sth}^{3/2}(7T_{th}-5T_{sth}))\nabla T_{th} +$$

$$+ n_{sth}T_{sth}^{3/2}\,(2n_{sth}T_{sth}^{5/2} + n_{th}T_{th}(7T_{sth}-5T_{th}))\nabla T_{sth} \qquad (3.7.6)$$

*

The condition for the reversal of the sign of the ∇T_{th} heat flux can be seen from this.

The Lorentz gas approximation is also used to investigate the heat flow, when both thermal and suprathermal electrons are magnetised, and the generation of B fields.

* Where Y is given on page 75.

3.8 An Extension of Shkarofsky's Work

Shkarofsky used the collision frequency:-

$$\nu_1 = n_+ Y/v^3 \qquad (3.8.1)$$

where $Y = 4\pi(Z_{ion} e^2/4\pi\varepsilon_o m)^2 \ln\Lambda$

The applicability of this term to both thermal and suprathermal electron transport in a high Z corona is dubious for two reasons. Firstly since $\ln\Lambda_{th}$ may be small taking $\ln\Lambda_{th} = \ln\Lambda_{sth} = \ln\Lambda$ will not be accurate. Secondly the plasma may not be fully ionized. In this case, as has been seen in section 2.2, the suprathermal electrons will "see" a larger effective Z^2 and the use of Z^2_{ion} in equation (3.8.1) will lead to inaccuracies.

Since the Lorentz approximation is being used we may write:-

$$f \simeq f_{o_{th}} + \underline{f}_{1_{th}} \cdot \frac{\underline{v}}{|\underline{v}|} + f_{o_{sth}} + \underline{f}_{1_{sth}} \cdot \frac{\underline{v}}{|\underline{v}|} \qquad (3.8.2)$$

and the equations for $f_{1_{th}}$ and $f_{1_{sth}}$ are:-

$$\nu_{th}\, \underline{f}_{1_{th}} = -\left[v \nabla f_{o_{th}} - \frac{e}{m}(\partial f_{o_{th}}/\partial v)\, \underline{E}\right] \qquad (3.8.3a)$$

and

$$\nu_{sth}\, \underline{f}_{1_{sth}} = -\left[v \nabla f_{o_{sth}} - \frac{e}{m}(\partial f_{o_{sth}}/\partial v)\, \underline{E}\right] \qquad (3.8.3b)$$

where

$$f_{o_{th}} = n_{th}\left(\frac{m}{2\pi\, T_{th}}\right)^{3/2} \exp(-mv^2/2T_{th}) \qquad (3.8.4a)$$

$$f_{o_{sth}} = n_{sth}\left(\frac{m}{2\pi\, T_{sth}}\right)^{3/2} \exp(-mv^2/2T_{sth}) \qquad (3.8.4b)$$

The drift velocities of both zero order distribution functions are zero. If this were not so electron-ion collisions would act on f_o.

$$\nu_{th} = n_+ Y_{th}/v^3 \quad , \quad Y_{th} = 4\pi\,(Z_{ion}e^2/4\pi\varepsilon_o)^2 \ln\Lambda_{th} \qquad (3.8.5a)$$

$$\nu_{sth} = n_+ Y_{sth}/v^3 \quad , \quad Y_{sth} = 4\pi\,(Z_{eff}e^2/4\pi\,\varepsilon_o)^2 \ln\Lambda_{sth} \qquad (3.8.5b)$$

The expressions for the electron current and the electron energy flux are then given by :-

$$\underline{J} = \frac{e}{n_+ Y_{th}}\left[\frac{1}{3}\nabla(n_{th}\langle v^5\rangle_{th}) + \frac{Y_{th}}{Y_{sth}}\frac{1}{3}\nabla(n_{sth}\langle v^5\rangle_{sth}) + \right.$$

$$\left. + \frac{2e}{m}\cdot\left\{n_{th}\langle v^3\rangle_{th} + n_{sth}\langle v^3\rangle_{sth}\right\}\underline{E}\right] \qquad (3.8.6)$$

and

$$\underline{q} = \frac{m}{3n_+ Y_{th}}\left(-\tfrac{1}{2}\left[\nabla(n_{th}\langle v^7\rangle_{th}) - \frac{Y_{th}}{Y_{sth}}\nabla(n_{sth}\langle v^7\rangle_{sth})\right] - \right.$$

$$\left. - \left(\frac{4e}{m}\right)(n_{th}\langle v^5\rangle_{th} + n_{sth}\langle v^5\rangle_{sth})\,\underline{E}\right) \qquad (3.8.7)$$

where $$\langle v^k\rangle_{sth/th} = \frac{4\pi}{n_{sth/th}}\int_o^\infty v^{k+2} f_{o_{sth/th}}\, dv \qquad (3.8.8)$$

using $$\int_o^\infty x^{2n+1} e^{-px^2}\, dx = \frac{n!}{2p^{n+1}} \qquad (p>0)$$

we can write:-

$$\langle v^k \rangle_{sth/th} = \frac{2}{(\pi)^{\frac{1}{2}}} \left(\frac{2}{m}\right)^{k/2} T^{k/2}\left(\tfrac{1}{2}k+\tfrac{1}{2}\right) \qquad (3.8.9)$$

for odd k.

Using equation (3.8.6) to eliminate the E field from equation (3.8.7) and putting the total current equal to zero the expression for q becomes:-

$$q = -\frac{32}{m^2}\frac{1}{n_+ Y_{th}}\left(\frac{1}{n_{th}T_{th}^{3/2} + (Y_{th}/Y_{sth})n_{sth}T_{sth}^{3/2}}\right) \cdot$$

$$\Big\{2n_{sth}(Y_{th}/Y_{sth})T_{th}^{5/2}\,T_{sth}^{3/2}\,(T_{th}-T_{sth})\nabla n_{th} + 2n_{th}(Y_{th}/Y_{sth})T_{th}^{3/2}\,T_{sth}^{5/2} \cdot$$

$$(T_{sth}-T_{th})\nabla n_{sth} +$$

$$n_{th}T_{th}^{3/2}(2n_{th}T_{th}^{5/2} + n_{sth}(Y_{th}/Y_{sth})T_{sth}^{3/2}(7T_{th}-5T_{sth}))\nabla T_{th} +$$

$$+ n_{sth}T_{sth}^{3/2}(2n_{sth}(Y_{th}/Y_{sth})^2 T_{sth}^{5/2} + n_{th}(Y_{th}/Y_{sth})T_{th}^{3/2}(7T_{sth}-5T_{th}))\nabla T_{sth}\Big\}$$

(3.8.10)

If $Y_{sth} = Y_{th} = Y$ this reduces to equation (3.7.6) with $J = 0$.

The condition for reversal of the flux due to T_{th} becomes:-

$$n_{sth}(5T_{sth}-7T_{th})T_{sth}^{3/2}(Y_{th}/Y_{sth}) > 2n_{th}T_{th}^{5/2} \qquad (3.8.11)$$

Since $Y_{th}/Y_{sth} < 1$ this will be harder to satisfy than the condition by Shkarofsky where Y_{th}/Y_{sth} in equation (3.8.11) is replaced by unity.

CHAPTER 4

Introduction

In this chapter we briefly describe an experiment by Hares, Kilkenny, Key and Lunney (67) which investigated suprathermal electron preheat in layered targets. The effect of the E field which drives the thermal return current is crudely estimated and a design for a target which will increase this effect is given. A numerical model is developed to give a more quantitative description of resistive E field effects. Its application to the analysis of the experiments in (67) and to the design of, and analysis of, experiments with resistive targets (137) is described. Finally the importance of resistive targets to I.C.F. target design is discussed.

4.1 The experiment of Hares et al

K_α radiation

The primary diagnostic used on this experiment was a measurment of the K_α X-radiation from fluorescent elements (fluors) within the target. This diagnostic has been discussed by Choi(138) and references therein.

There are two relevant causes of K shell ionisation, firstly the absorption of photons with energy greater than the K shell ionisation energy. Such ionisation is most efficient for energies close to the ionisation energy. Secondly there is ionisation by collisions with suprathermal electrons with energies greater than the K shell ionisation energy. Typically 1% of the energy deposited by suprathermal electrons will go into K shell ionisation.

As the target is ionised the ionisation potentials of the

remaining bound electrons are changed. Thus the "positions" of the characteristic X-radiation lines will be shifted. This will result in K_α radiation not being detected as such and a saturation of the observed yield.

The experiment of Hares et al (67) was the first from which, by suitable choice of fluors, the problems of radiation pumping and saturation were eliminated.

The experiment

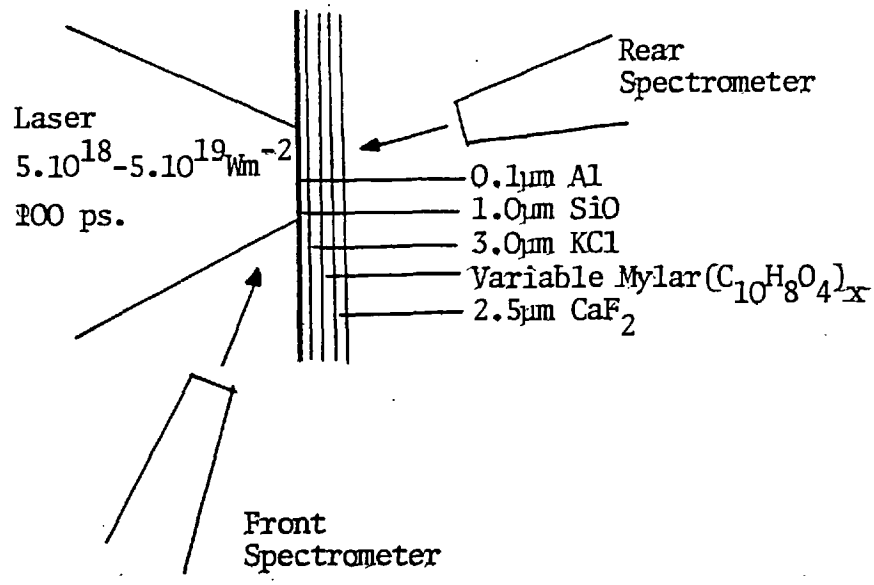

Fig.4.1 Layout of Experiment

In an experiment conducted at the Rutherford Labaratory Central Laser Facility layered targets, as shown in Fig 4.1, were irradiated with 1.06μm laser light. A thermal plasma is formed which is isolated from the front fluor by the Aluminium and Silicon layers. Suprathermal electrons created by the laser-plasma interaction preheat

the target. Some of the energy which is deposited in the fluor layers will give rise to K_α radiation which is detected by the spectrometers. For fixed power and focusing conditions, and hence fixed intensity, a series of experiments were conducted using targets with different Mylar thicknesses.

The idealisation involved in the analysis of the experiment, described by Hares (139), is illustrated by fig 4.2.

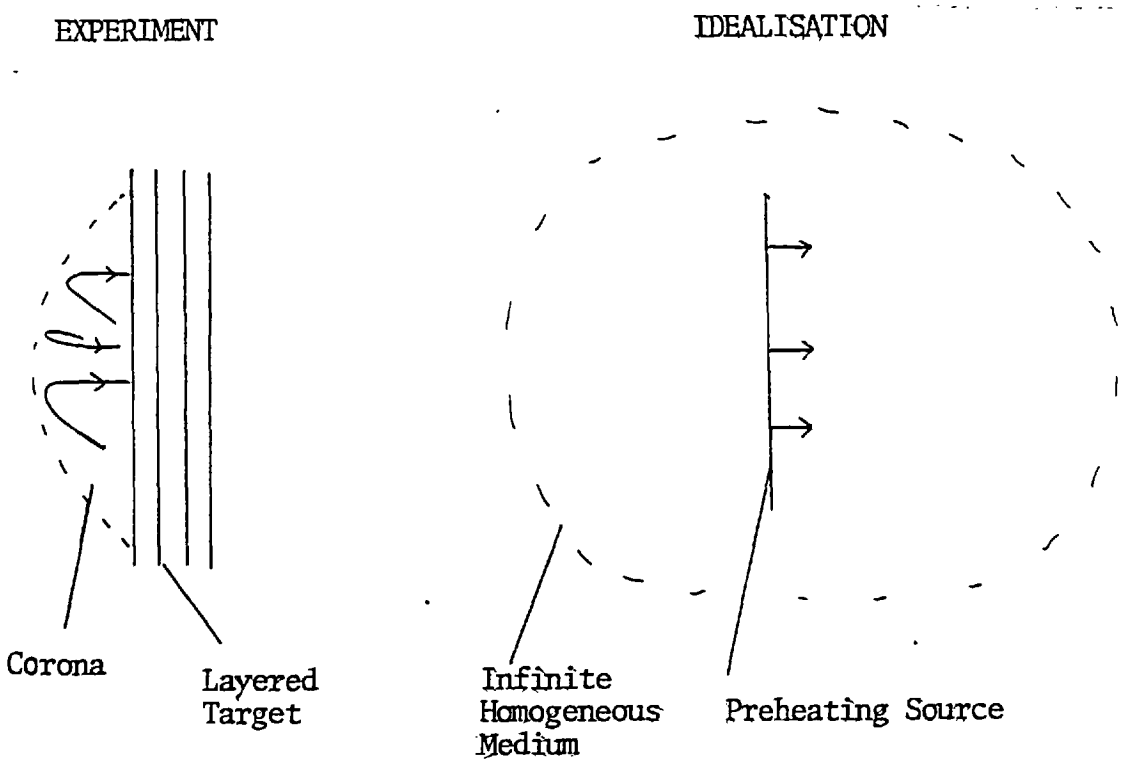

Fig.4.2 Idealisation of the Experiment

In the analysis the following assumptions were used:-

(1) Spencer's results for electron energy deposition in a solid (see also section 2.3)

(2) The result from (140) of the fraction of deposited energy going into K shell ionization .

(3) An assumed form of the preheating source :-

$$f_{preheating}(E) = N\, E^{n+\frac{1}{2}} \exp(-E / T_{sth}) \qquad (4.1.1)$$

By fitting the K_α yields of the front and rear fluors with that predicted by the above, a preheating distribution of the form :-

$$f_{preheating}(E) = N\, E^{3/2} \exp(-E / T_{sth}) \qquad (4.1.2)$$

was inferred. Experiments using different intensities of laser irradiation and the assumption that the form of the preheating distribution remained the same were used to determine the variation of the suprathermal "temperature" with intensity.

This experiment gave the following results:

(1) The form of the preheating distribution.

(2) The scaling of T_{sth} with intensity.

(3) The scaling of the fraction of incident energy causing target preheat.

It was the first experiment to give direct measurment of suprathermal electron preheat. This experiment is described more fully in (139, 141, 67).

4.2 The role of resistivity

If the suprathermal electrons carry a current J_{sth} then, in a one dimensional experiment, a thermal return current $J_{th} = -J_{sth}$ must flow. If the thermal plasma has a resistivity η_{th} there must be a E field $J_{th} \cdot \eta_{th}$. A crude estimate of the effect of the E field on the suprathermal transport may be found as follows. Let the canonical values of the suprathermal range, suprathermal current density and the resistivity of the thermal plasma be R_c, J_{sth_c} and η_c . Then a potential $-R_c J_{sth_c} \eta_c$ is established if the suprathermal transport is unaffected by the E field. The energy lost by an electron in crossing this potential is $e R_c J_{sth_c} \eta_c$. Typical current carrying electrons have an energy $f k T_{sth}$, where f is a constant of order one, the value of which depends on the form of the suprathermal electron distribution function. It is inconsistant to assume that E fields do not affect the suprathermal transport if:-

$$\frac{e R_c J_{sth_c} \eta_c}{k} \gtrsim T_{sth} \qquad (4.2.1)$$

When the condition in equation (4.2.1) pertains linear transport analysis, as described in the previous section, is no longer valid.

The range of the electrons may be rewritten as r_c / ρ where r_c is the stopping power and ρ the density of the target. Using this equation (4.2.1) becomes:-

$$\frac{e r_c J_{sth_c} \eta_c(\rho)}{k \rho} \gtrsim T_{sth} \qquad (4.2.2)$$

Note that the canonical resistivity is a function of the density.

Ignoring this for the moment it can be seen that E field effects may be increased by reducing the density of the target.

In (141) scaling of T_{sth} and the fraction of incident energy going into suprathermal electron preheat are given. This may be used to find out how E field effects will scale with intensity. Experimentally (in the range 5-50 10^{18} W m^{-2})

$$T_{sth} = (T_{sth})_o \left(\frac{I}{I_o}\right)^{\frac{1}{2}}$$

Power into preheat $\sim I$

The energy flux into the target $\sim (\frac{1}{2} m_e v_e^2).n_e v_e \sim T_{sth}\, J_{sth}$. Thus:-

$$J_{sth} = (J_{sth})_o \cdot \left(\frac{I}{I_o}\right)^{\frac{1}{2}}$$

The range $\sim T_{sth}^2$ so $r = r_o \left(\frac{I}{I_o}\right)$

The energy deposition per unit mass is independent of intensity so the resistivity will be independent of intensity. Thus:-

$$\left(\frac{r\, J\, n}{T_{sth}}\right) = \left(\frac{I}{I_o}\right) \left(\frac{r_o\, J_o\, n_o}{T_{sth_o}}\right) \qquad (4.2.3)$$

The effect of resistivity will be more important for higher intensity illumination.

The preceding discussion only deliniates a range of parameters for which it is invalid to ignore the effect of the resistive E field. In the next section a numerical model which was developed to study the E field effects on the suprathermal transport is described.

4.3 Details of a numerical model

The simulation model uses the following assumptions:-

(1) That one dimensional slab geometry is appropriate.

(2) That the target is in local thermodynamic equilibrium (L.T.E.)

(3) Spitzer resistivity is used for the thermal electrons.

(4) Thermal transport, radiation transport and hydrodynamic motion are all ignored.

(5) The density of suprathermal electrons is much less than that of thermal electrons.

(6) The timescale for change of the state of the target is much greater than the suprathermal electron "lifetime".

Each of these will be discussed in turn.

Assumption (1)

If we first ignore the effects of E and B fields a necessary condition for ignoring two dimensional effects is that the laser spot size is much greater than the range of the suprathermal electrons. A rough estimate of the effect of finite spot size may be found by using single group diffusion theory. The single group diffusion equation is:-

$$\frac{\partial N_g}{\partial t} + \nabla \cdot \Phi_g + \frac{N_g}{\tau_E} = \frac{\partial N_g}{\partial t})_s \qquad (4.3.1)$$

where $\tau_E = \lambda_E / v_g$

$$\Phi_g = -\frac{v_g}{3} \lambda_{\pi/2} \nabla N_g \qquad (4.3.2)$$

Thus in the steady state ($\frac{\partial}{\partial t} = 0$) the single group equation is, from (4.3.1) and (4.3.2) :-

$$\nabla^2 N_g - \left(\frac{3}{\lambda_E \lambda_{\pi/2}}\right) N_g = \text{source} \qquad (4.3.3)$$

To estimate the spreading effect due to finite source size equation (4.3.3) has been solved in an infinite medium for a disk source. The flux across any plane can then be calculated from equation (4.3.2).

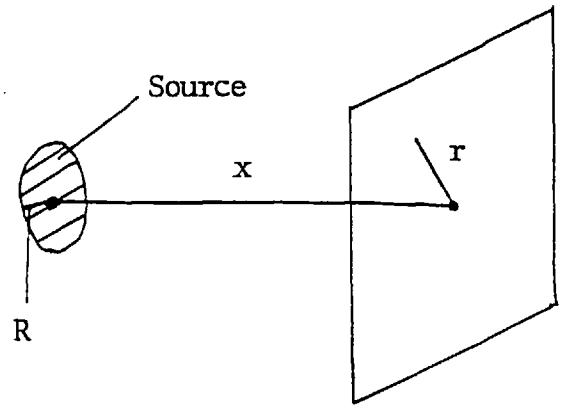

Fig.4.3 Geometry for One Group Diffusion Model

The Green's function for the one group diffusion operator, the solution of:-

$$\left(\nabla^2 - \frac{3}{\lambda_E \lambda_{\pi/2}}\right) G(\underline{r}, \underline{r}') = \delta(\underline{r} - \underline{r}')$$

is:-

$$\frac{1}{4\pi\, r-r'} \exp\left(- \underline{r}-\underline{r}' \left(\frac{3}{\lambda_E \lambda_{\pi/2}}\right)^{\frac{1}{2}}\right) \qquad (4.3.4)$$

where $G(\underline{r}, \underline{r}') \to 0$ as $|\underline{r} - \underline{r}'| \to \infty$ has been used.

Using (4.3.4) the value of N_g can be found at any point in space by integrating over the source. The flux may also be calculated. This has been accomplished by numerically integrating over the source. Fig. 4.4 gives typical results.

These results may be used to justify a one dimensional simulation.

$x/R = 0.5$ $\qquad$ $x/R = 0.5$

$R(3/\lambda_E\lambda_{\pi/2})^{\frac{1}{2}} = 2$ $\qquad$ $R(3/\lambda_E\lambda_{\pi/2})^{\frac{1}{2}} = 10$

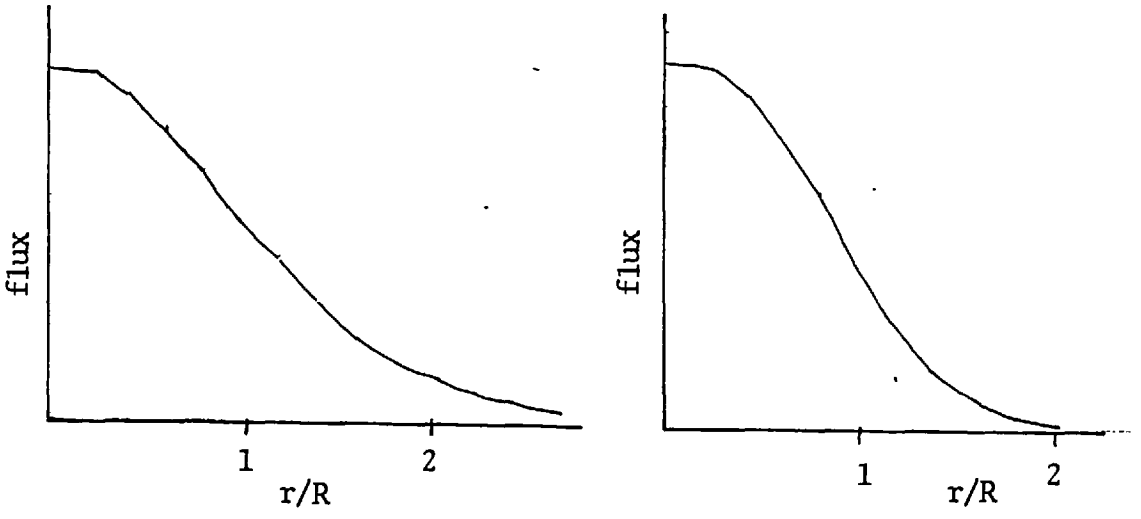

Fig.4.4 Flux from a Disc Source

Now consider the effect of E and B fields. If B = 0 then quasineutrality dictates $\underline{J}_{total} = 0$. A departure from $\underline{J}_{total} = 0$ is possible if the B field can diffuse into the target. The equations governing this are:-

$$\underline{J}_{sth} + \underline{J}_{th} = (\nabla \wedge \underline{B}) / \mu_o$$

$$\underline{E} = \eta \underline{J}_{th} \qquad (4.3.5)$$

$$\frac{\partial \underline{B}}{\partial t} = -\nabla \wedge \underline{E}$$

If the assumption that $\underline{J}_{sth}$ is irrotational is made then, from (4.3.5), :-

$$\frac{\partial \underline{B}}{\partial t} = -\nabla^2 \frac{\eta}{\mu_o} \underline{B} \qquad (4.3.6)$$

using $\nabla.\underline{B} = 0$

Equation (4.3.6) can be used to estimate the depth into the target to which the magnetic field diffuses, L_c , by using:-

$$\frac{1}{\tau_c} = \frac{1}{L_c^2} . \frac{\eta_c}{\mu_o} \qquad (4.3.7)$$

τ_c, the characteristic time, will be the length of the laser pulse. If L_c is much less than the range of the suprathermal electrons then ignoring the $\underline{B}$ field effects will be justified.

The value of L_c for the experiments described in (67) was typically 5 microns.

Assumption (2)

The criteria for the validity of L.T.E. are given by Griem (142). For a uniform (in space and time) optically thin plasma this is :-

$$n_e > 7.4\ 10^{24} (\langle z \rangle + 1)^7 \left(\frac{kT}{\langle z \rangle^2 E_H}\right)^2 \qquad (4.3.8)$$

The condition for the spatial scale length is :-

$$d\rangle \frac{7\ 10^{24}}{A^{1/4}} \left(\frac{kT}{E_H}\right)^{\langle z\rangle} \exp\left(\frac{\langle z\rangle^2 E_H}{2\ kT}\right) \qquad (4.3.9)$$

and for the characteristic time:-

$$\tau\rangle \frac{1.15\ 10^{13}(\langle z\rangle+1)^3 n^{\langle z\rangle+1}}{n_e(n^{\langle z\rangle}+n^{\langle z\rangle+1})} \frac{kT}{\langle z\rangle^2 E_H} \exp\left(\frac{\langle z\rangle^2 E_H}{kT}\right) \qquad (4.3.10)$$

Because of the Z dependence of (4.3.8) this inequality will not be satisfied by cool high Z plasmas. However the L.T.E. equation of state may be used if the plasma is optically thick to its own thermal radiation.

Assumption (3)

Only in the two extreme cases, fully ionized and very slightly ionized, are there adequate theories for the resistivity of an ionized gas. The latter case is of no interest here as the resistivity is much greater than that calculated using the assumption that electron-neutral collisions dominate. The Spitzer theory (58, 143) is applicable to a fully ionized gas with ionic charge Z. It gives :-

$$\eta = \frac{10^{-4}\ Z\ \ln\Lambda\ \gamma}{T^{3/2}} \qquad (T \text{ in eV}) \qquad (4.3.11)$$

where $\Lambda = b_{max}/b_{min}$

b_{max}, the maximum impact parameter, is usually taken to be the Debye length, λ_D. However if there are very few particles in a Debye sphere, as there will be if λ_D becomes comparable to the inter ionic distance, this will need modifications. (Clearly if there are $\lesssim Z$ electrons in the Debye sphere λ_D cannot be used as the distance over which the ion ionic charge is screened.) b_{min} is the larger of the classical distance

of closest approach and the DeBroglie wavelength of a thermal electron. The coefficient γ can be evaluated numerically (143). It is 1 if $Z \gg 1$.

The Spitzer formula should give an accurate value for the resistivity in a plasma which is fully ionized, non-degenerate, has $\ln \Lambda \gg 1$ and is not turbulent.

We wish to apply the Spitzer formula to cases where the above conditions do not all hold. It is important to know whether the errors introduced by this will be large.

Ignoring degeneracy will introduce serious errors if the thermal energy of the plasma is comparable to or less than the Fermi energy, ie if :-

$$kT \lesssim \frac{h^2}{2\,m_e} (3\,\pi^2 n_e)^{2/3}$$

Fig.4.5 Fermi-Dirac Distribution for Two Temperatures

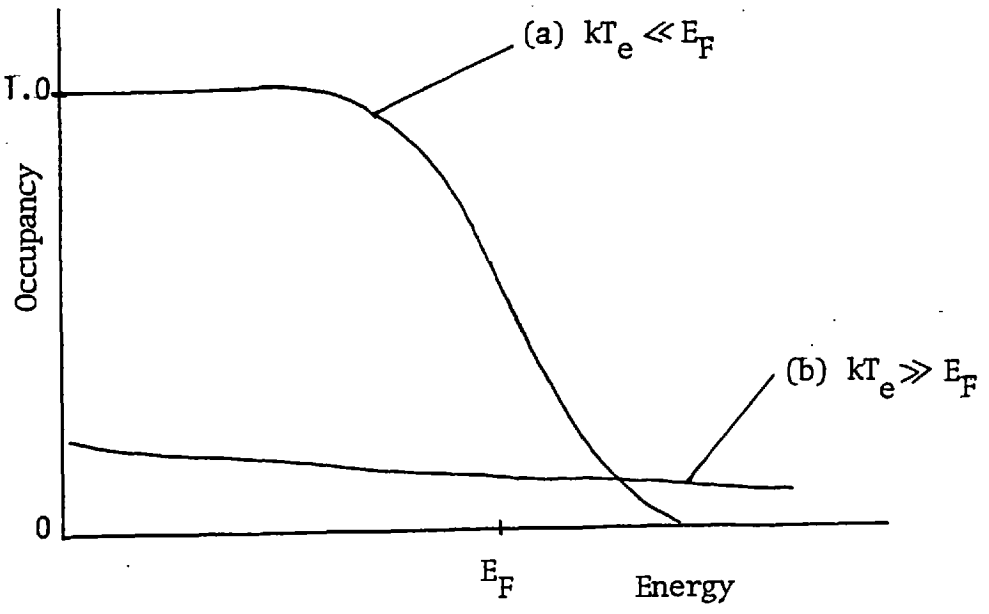

Clearly in case (b) the effect of the Pauli exclusion principle in "disallowing" some collisions is negligible. If E_F and kT_E are comparable use of the Spitzer formula overestimates the resistivity. For $kT_E \gg E_F$ the average occupancy of states with energy below kT_E will be of order $(E_F/kT_E)^3$ · $(E_F/kT_E)^3$ is typically 10^{-3}.

The target material will not be fully ionized. In the partially ionized "gas" there will be ions in more than one charge state present. An approximate treatment of this is as follows. A simple, mean free path (mfp) , theory gives the conductivity of a plasma as:-

$$\frac{e^2 n_e}{m_e \tau}$$

where $\tau = \lambda_{\pi/2} / v_{th}$ is the collision time, and $\lambda_{\pi/2} \sim (Z^2 n_Z)^{-1}$.

Thus the collision times for collisions with each ionization state $\tau_Z \sim (Z^2 n_Z)^{-1}$.

$$\frac{1}{\tau_{total}} = \sum \frac{1}{\tau_Z} \sim \sum Z^2 n_Z = n_i \bar{Z}^2$$

also $n_e = n_i \bar{Z}$.

$n_e / \tau_{total} \sim \bar{Z}/\bar{Z}^2$

This leads us to the conclusion that Z in equation (4.3.11) should be replaced by $\bar{Z}^2/\bar{Z}$ (which is $\geq Z$). If the material is multiply ionized and in L.T.E. $\bar{Z}^2/\bar{Z} \simeq \bar{Z}$ (this approximation was checked using a full L.T.E. code supplied by R.W.Lee). Two further effects are relevant. The Spitzer theory only deals with elastic scattering. In a partially ionized gas inelastic collisions will also occur. Also the nuclear charge is screened out over a distance $a_o/Z^{1/3}$ (144) (a_o is the Bohr radius). If this is comparable to the minimum impact parameter the plasma electrons will "see" some of the nuclear charge. Both these

effects will increase the resistivity from the Spitzer value.

A condition for the validity of the classical transport coefficients is that $\ln\Lambda$ is large (cf 1). If this is not the case then the effect of single large angle scatters due to collisions with impact parameters $\lesssim b_{min}$ and the effect of the interaction of an electron with plasma oscillations in its wake (95) may be as important as the cumulative effect of small angle deflections. The Spitzer theory is only valid to order $1 / \ln\Lambda$.

Assumption (4)

The burn depth of the thermal plasma is $\sim 0.1\,\mu$m. This will have little effect on the suprathermal transport since it will only affect the state of a target for a small part of the suprathermal electron's range.

To consider the effect of thermal transport and hydrodynamic motion in the preheated target we consider the following canonical values:-

Atomic Number	12
Charge State	5
Temperature	100 eV
Scale Length	20 μm
Density of Ions	10^{28} m^{-3}

Then the thermal diffusion time is 10^{-8} secs and the sound transit time is $3\cdot10^{-10}$ secs compared to a pulse length of $9\cdot10^{-11}$ secs. From this it is clear that thermal transport can be ignored and plausible that hydrodynamic motion may be ignored.

Radiation from the thermal plasma will have a negligible preheating effect because of its short range (for the targets illustrated in fig.4.1) . Although hard x-rays will be able to preheat the target, their preheating effect will be small; only a small fraction of the

suprathermal electron energy loss goes into hard x-rays. Thus radiation transport may be ignored.

Assumption (5)

If the thermal electron density is much greater than the suprathermal density then the model described in section 2.1 is applicable. Typical electron densities in solids are 10^{28} m^{-3} - $5 \cdot 10^{29}$ m^{-3}. A typical suprathermal density would be of the order of or less than 10^{26} m^{-3} (10% of critical density for 1 μm radiation). $n_{sth} \ll n_{th}$ in all cases of interest.

Assumption (6)

Since the time dependence of the problem is treated by performing a series of time independent transport calculations we require that the source and the scattering properties and resistivity of the target do not change greatly during the time it takes a suprathermal electron to thermalise. The timestep which is used must satisfy the inequality :-

(lifetime of suprathermal electron) $\leq$ (timestep) $\leq$ (timescale for change of target / source properties)

Calculation of the Suprathermal Transport

The sequence of calculations used to simulate the effect of suprathermal transport are summarised below:-

Fig.4.6

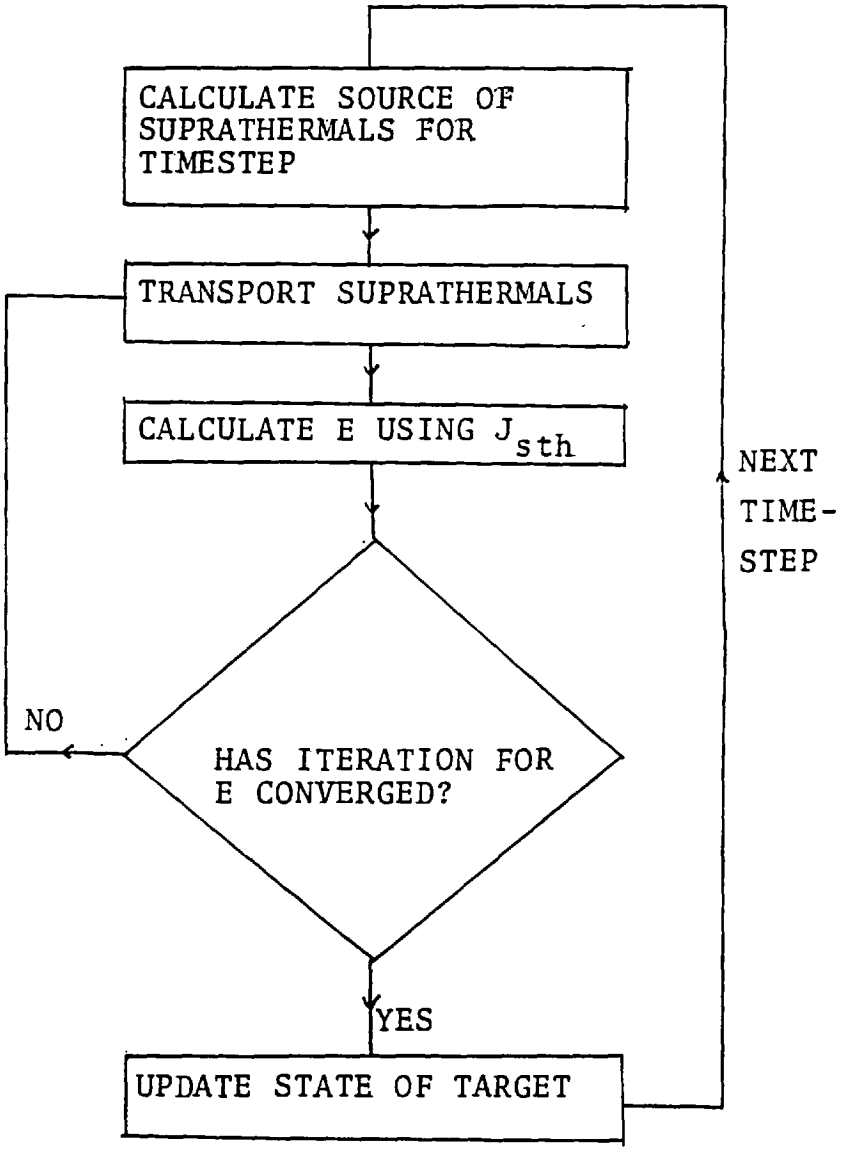

The stages shown above will now be described.

Source of Suprathermals

Weights

A source distribution of the form (4.1.2) is represented by a number of Monte Carlo particles. These particles are weighted to represent a large number of real electrons. If the source is given by $f(E)$ electrons $s^{-1}m^{-2}$ incident on the target, then for an energy range $E_a - E_b$ the weights of the particles in that range should satisfy :-

$$\sum_{\substack{\text{particles} \\ \text{in range} \\ E_a - E_b}} w_i = \int_{E_a}^{E_b} f(E)\, dE$$

The choice which has been used is to split the energy range $(1KeV - 6kT_{sth})$ up into many small intervals. One simulation particle is used to represent the source in each interval and its weight is given by:-

$$W = f(E_{mid})\,(E_{max} - E_{min})$$

where E_{mid} is the middle of the energy range. Energy WE_{mid} and charge $-eW$ are associated with each particle. The rate of energy deposition of a simulation particle is given by :-

$$\Delta E_{\text{simulation particle}} = W^{\bullet}\, \Delta E_{\text{electron}}$$

The current due to a simulation particle is $-eW$ between the points where the particle is created and where it thermalises.

The initial direction of the simulation particles may be specified.

The Monte Carlo Electron Transport

Monte Carlo electron transport has been discussed previously (section 3.4). A very simple model is used here. The continuous energy loss approximation and a Gaussian multiple scatter distribution are employed to simulate the effects of collisions; condensed case histories are used. The effect of the E field is included by following the Monte Carlo particles along parabolic trajectories between scattering "events", and changing the particles' energy accordingly. The formulae used for the energy loss due to collisions and the width of the Gaussian multiple scatter distribution are equations (2.1.6) and (2.2.6) respectively. The method for calculating the change in the polar angle due to collisions is given by equations (2.4.5) and (2.4.6). Particle histories are terminated when their energy becomes comparable to the ionization potential , or Debye energy, of the target material. All the remaining energy is then deposited.

The E field acting on the particle is taken to be the field at the centre of the cell containing the particle. The energy lost is deposited in the cell containing the particle or, if the particle crosses the cell boundary, half is deposited in each cell.

As described above the particles are weighted so as to represent the source function of suprathermal particles. Normally 400 - 1000 simulation particles are used.

At the two boundaries of the simulation reflection or free flow conditions could be applied. In all work described in this chapter free flow conditions were used at both boundaries.

The inclusion of E field effects complicates the treatment of the collisional energy loss and deflection. Because the E field changes the electrons' kinetic energy it is no longer possible to choose path lengths to give preselected energies after each step with a continuous slowing down (C.S.D.) approximation. Since a high order evaluation of the

C.S.D. energy loss $\int (dE/ds) ds$ would be expensive, and also no longer as accurate, because the E field will also affect the energy, a simple first order expression for the collisional energy loss was used:-

$$E_{C.S.D.} = \left(\frac{dE}{ds}\right)_{E=E_I} \Delta s$$

where E_I is the kinetic energy at the start of a step and Δs the path length. Δs must be chosen so that :-

$$\left(\frac{dE}{ds} \Delta s\right) / E$$

is small. The conventional approach to the treatment of scattering [105] is to store the multiple scatter distribution functions for a number of preselected energies. Since, as was mentioned above, the energies after each step can no longer be selected and also because the state of the target, and hence its scattering properties, are a function of time, such an approach is not practicable. Such problems do not occur if a Gaussian multiple scatter distribution is used, as in this case, but would greatly complicate the implementation of a more sophisticated model.

Deflection and energy loss due to collisions and the E field are treated independently. This is justified since the scale length for deflection due to the E field will always be far greater than the Debye length.

The Choice of "Random" Quantities

When random numbers were needed these were "picked" by using the C.D.C. pseudo random number tables "RANF". During an iteration for the E field the random numbers used for a given case history at each iteration started at the same place in the RANF tables by using

the "RANSET" routine. This simplifies consideration of the iteration for the E field. The noise due to the small number of particles used may be estimated by comparing simulations with different sets of random numbers , see below:-

Fig.4.7 Effect of Noise on Energy Deposition

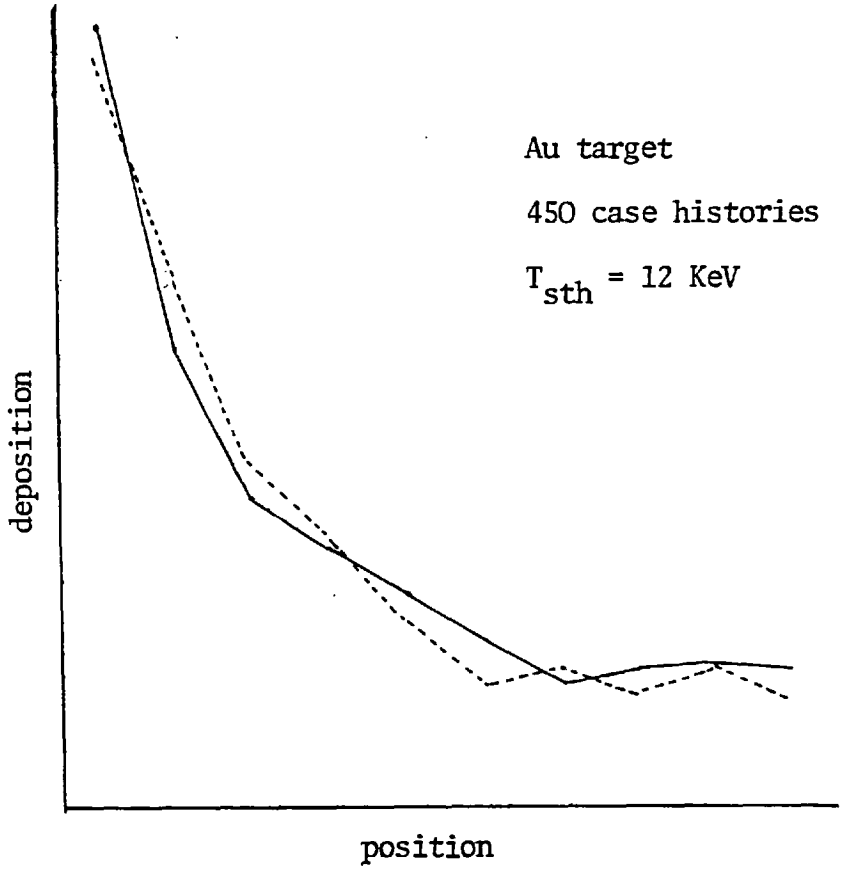

E Field Calculation

The E field is calculated by using:-

$$J_{total} = J_{sth} + J_{th} = J_{sth} + \eta^{-1}E = 0 \qquad (4.3.12)$$

J_{sth} is calculated by summing the contribution of all the Monte Carlo particles. This is a simple matter because the contribution of a particle is constant between the places where it is created and the case history is terminated and zero elsewhere. The E field needed to give $J_{th} = - J_{sth}$ is then calculated and used in the iterative scheme:-

$$E^{n+1} = (1-\alpha)E^{n} + \alpha(-J_{sth}/\eta) \qquad (4.3.13)$$

E is calculated at the cell centres and J is found by taking the average of the currents through the cell's boundaries. The convergence of the scheme is illustrated by plotting $J_{sth}(x)$ at each iteration.

Fig.4.8 Iteration For E Field

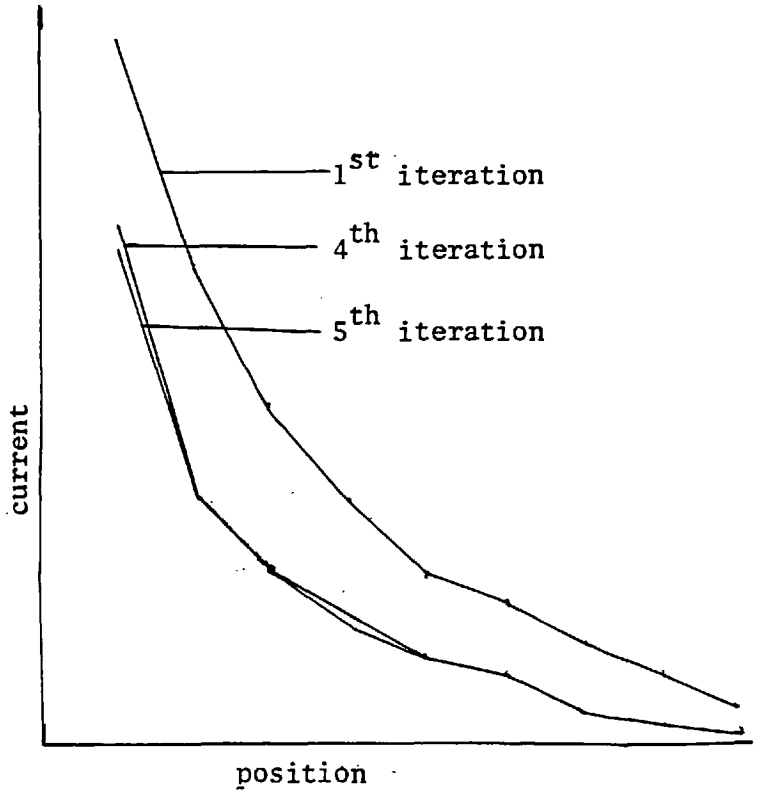

Updating the State of the Target

At the end of each time step the energy deposition in the target is incremented and the "state" of the target is calculated. The L.T.E. equation of state is used for the average ionization. This is described below. The resistivity is given by the "Spitzer formula", equation (4.3.11). The Debye energy of the free electrons and the average ionization energy of the bound electrons must be calculated. The latter is taken to be:-

$$I_{av} = 11\ (Z_{nuc} - Z_{ion})\ \left(\frac{Z_{nuc}}{Z_{nuc} - Z_{ion}}\right)^2 \text{ eV} \qquad (4.3.14)$$

where a Z^2 scaling of isoelectronic ions and the approximate formula (2.1.3) are assumed.

The Equation of State

From the specific energy deposition the state of ionization of the target material must be calculated. It is necessary to satisfy:-

$$E_{deposited} = 1.5\ n_i (1 + \bar{Z}) kT + E_{ionization} \qquad (4.3.15)$$

where $\bar{Z}$ is the average ionization state.

A subroutine FINDZ (supplied by R.W.Lee) was used to calculate the approximate L.T.E. average ionization state for a given temperature and the energy required to ionize the material to this state. This subroutine uses the approximate L.T.E. calculation described by Zel'dovich and Raiser (145) and ignores ionization potential depression. Equation (4.3.15) was satisfied by solving the equation:-

$$E_{deposited} - 1.5\ n_i (1 + \bar{Z})\ kT - E_{ionization} = f(T) = 0$$

by the iterative scheme :-

$$T^{n+1} = T^{n} - \frac{f'(T^{n})}{f(T^{n})} \quad ; \quad f'(T^{n}) = \frac{f(T^{n}) - f(T^{n-1})}{T^{n} - T^{n-1}} \qquad (4.3.16)$$

The first value of $f'(T)$ was found by calculating $f(T^{1})$ and $f(1.01T^{1})$.

The results given by the subroutine FINDZ have been compared with a full L.T.E. calculation which included a crude treatment of ionization potential depression. Results were found to be in good agreement for low Z materials. The full L.T.E caclulation could not be carried out for high Z (Z >20) materials.

The calculation of the state of the target was compared with the "SESAME" (146) equation of state tables. For gold they were found to be in good agreement for densities < 10% of solid density.

4.4 Application of the model to the design of and analysis of experiments

Two applications of the model will be described in this section: firstly analysis of the targets described in reference(67), and section 1 of this chapter; secondly the design of targets in which resistivity inhibits the flow of suprathermal electrons into the target and the analysis of experiments with such targets.

Analysis of ordinary targets

An initial test of the model was its application, with E field and ionization effects omitted, to the targets described in section 1. Using a source of the form given by equation (4.1.2), and varying T_{sth}, the ratio of the energy deposition in the front and rear fluor layers was used to determine T_{sth}. This was compared to the value of T_{sth} deduced from the analysis using Spencer's method (139) and was in good ($\pm$ 5 %) agreement. This should be the case since the targets contained only low / medium Z materials and the crude application of Spencer's theory with an average Z should be reasonabaly accurate.

The inclusion of ionization and E field effects with Spitzer resistivity showed a potential of a few hundred Volts across the target. This has a negligable effect on the transport of electrons with $T_{sth} \approx$ 14 KeV.

Resistive inhibition

As has been seen the effect of the E field in inhibiting suprathermal transport in solid density, low Z, targets is very small. How should a target be designed so as to increase the effect of the E field? Equation (4.2.2) shows that reducing the density of the target material will enhance the effect of the E field.

The resistivity, for a given specific energy deposition, is a function of density. If the L.T.E. equation of state is applicable in both cases then the average ionization state will be higher in the low density target. Fig 4.[9] shows the resistivity plotted against specific energy deposition for solid and 1% solid density Gold and Carbon targets.

Fig.4.9 Resistivity vs Energy Deposition

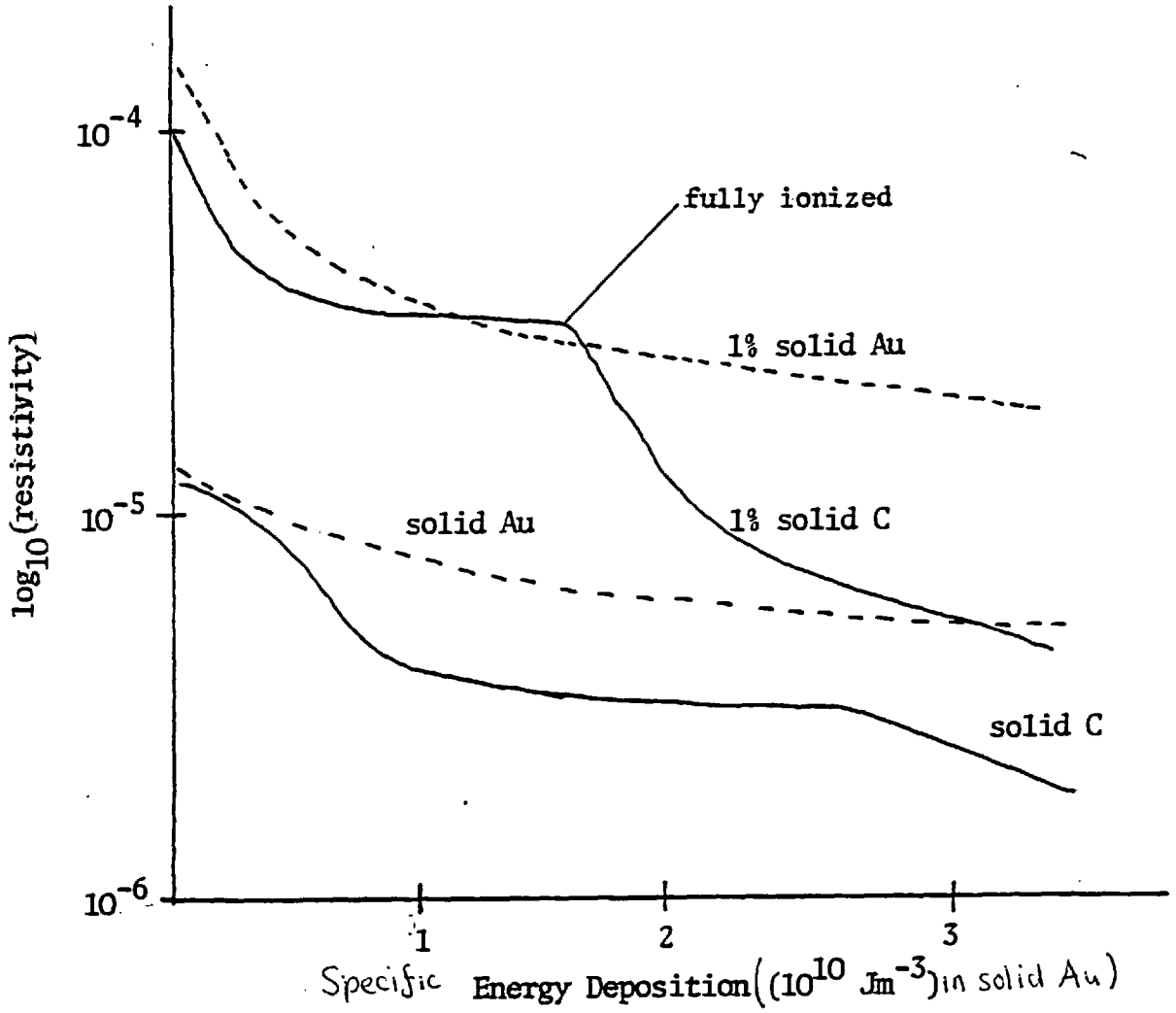

It can be seen that the resistivity decreases relatively slowly with increasing energy deposition, until the material becomes fully ionized. If the target becomes fully ionized the resistive effect will "burn out" due to the $T^{-3/2}$ dependence of the resistivity.

These considerations lead to the the idea of employing a low density high Z layer to increase the effect of the resistivity. Fig. 4. shows the energy deposition into a 0.5% solid density

Gold layer with and without E field effects after a 90ps. pulse of intensity 3. 10^{19} Wm^{-2} with 10% of the energy going into suprathermal electrons with T_{sth} = 14 KeV.

Fig.4.10 E Field Effects on Energy Deposition

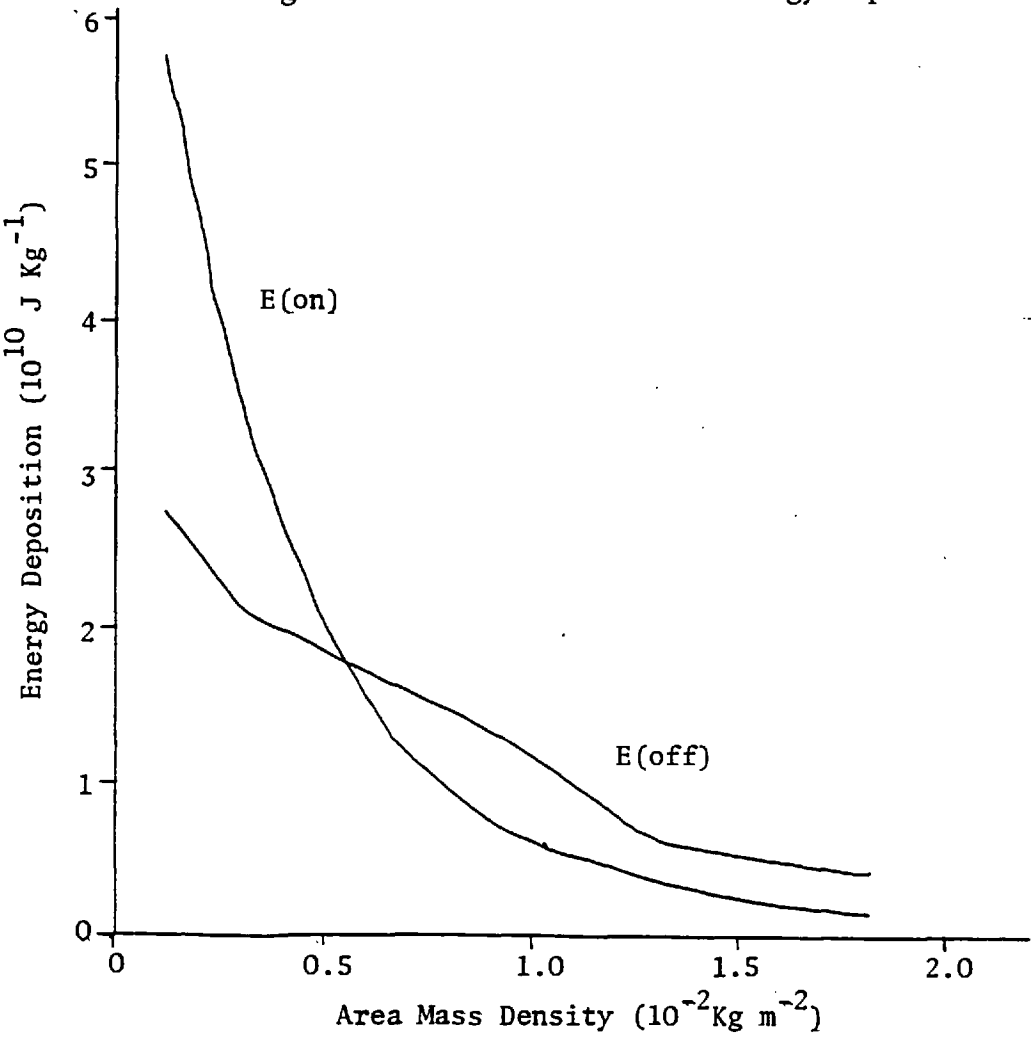

An experiment was conducted at the Rutherford Laboratory using the following target design.

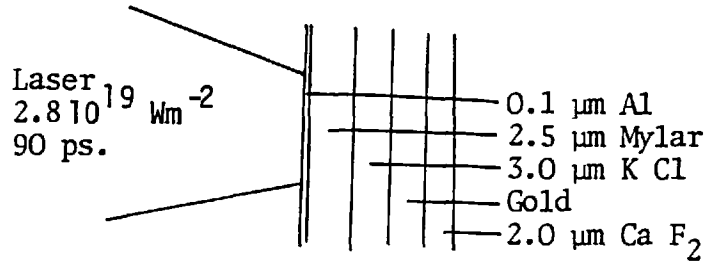

Fig.4.11 Target Construction

Pairs of targets with the same area mass density of Gold were used. In one the Gold was solid density and in the other it was approximately 1% of solid density. The K_α emission from the rear and front fluor layers was compared with the emission predicted by the simulation. (The simulation gives the energy loss by suprathermal electrons from which the K_α emission may be calculated). This shows that the reduction in energy deposition in the rear fluor layer is greater than can be explained by Spitzer resistivity. The simulations were repeated, using an arbitary multiple of Spitzer resistivity.* It was found that four times Spitzer resistivity brought the simulation results just inside the experimental error bars.

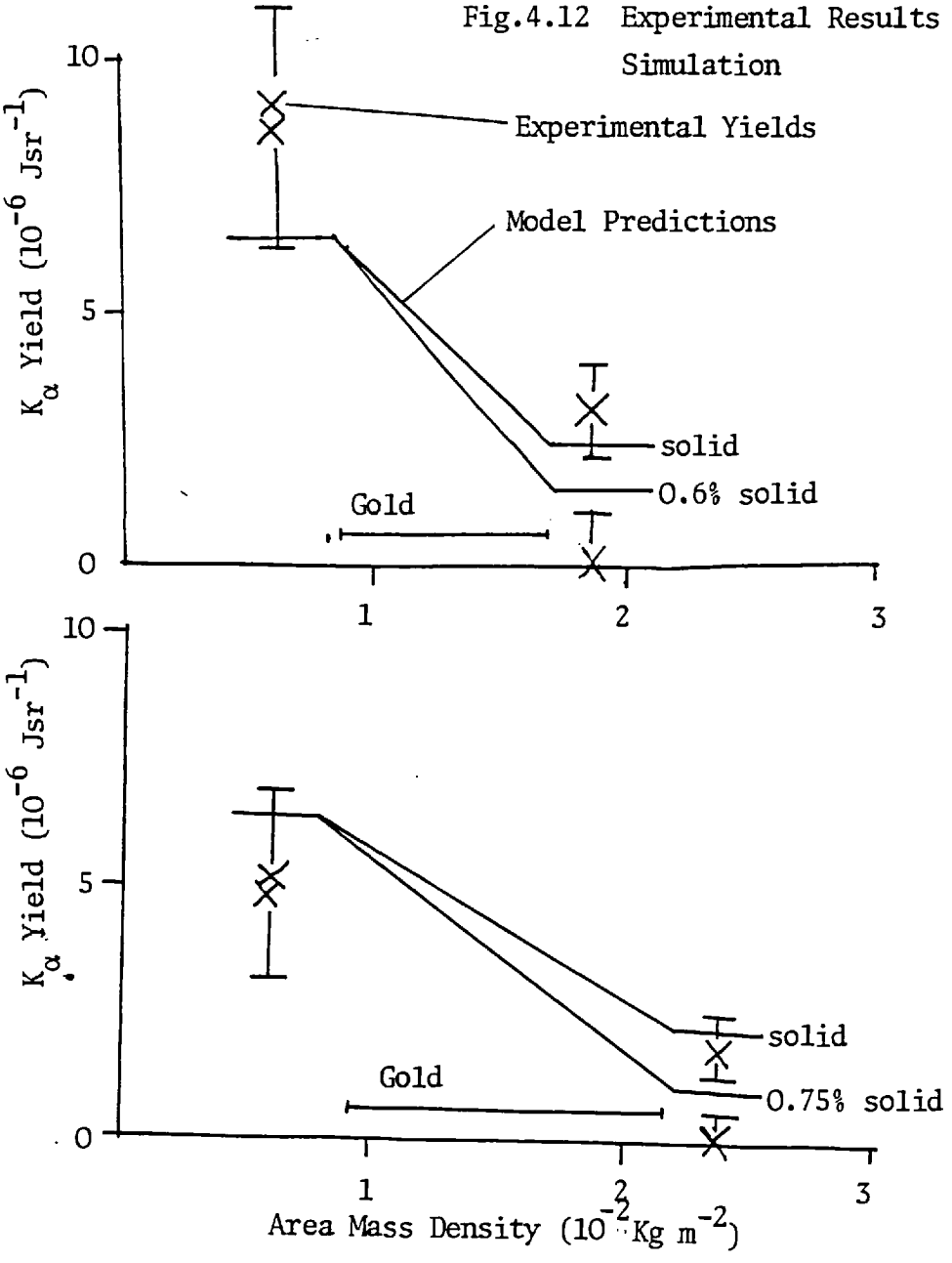

Fig.4.12 Experimental Results and Simulation

One deficiency of the target design used above is that the suprathermal current is considerably attenuated before it reaches the Gold layer. Experiments were conducted with targets in which no front fluor layer was used and in which the area mass density infront of the gold layer was minimised. (Some mass was needed for for structural and fabrication purposes.) These experiments confirmed the results described above.

4.5 Resistive Targets and Target Design

Can resistive inhibition be used in an I.C.F. target? To answer this question the possible ways of reducing suprathermal preheat must be considered.

Ablative Targets

The simplest way of stopping preheat is to use targets with a large area mass density between the surface and the fuel.(section 1.7). Since the acceptable level of preheat of the fuel is low ($\lesssim$1eV), electrons of several times T_{sth} must be stopped. This may result in a large and undesirable (section 1.2) increase in the mass of the target. At the energies of interest (10-100 KeV) the area mass density requirement is almost independent of Z; the effects of scattering and average ionization energy counterbalance each other.

In (147) the inclusion of a high Z layer is suggested.

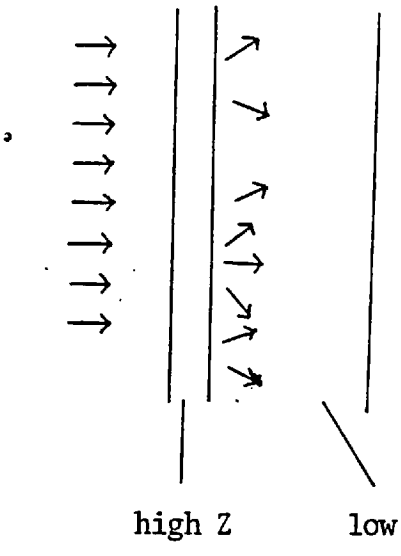

Fig.4.13

Although this layer is insufficiently thick to greatly reduce the energies of the suprathermal electrons it will make a beam of electrons incident on it more isotropic and hence reduce the quantity of low Z material needed to obtain a given reduction of the suprathermal energy flux.

Vacuum Insulation

Lee et al (148) have suggested using vauum gap insulation, see below.

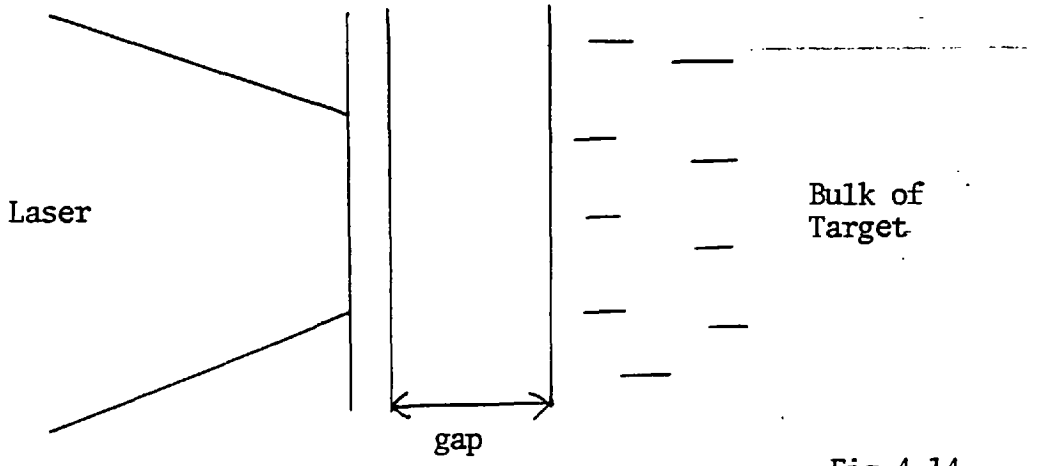

Fig.4.14

With a gap $\gg \lambda_D$(sth) the flux of suprathermal electrons into the bulk of the target will be small. However hydrodynamic motion of the laser heated layer will close up the gap and "short out" the insulation. If the size of the gap is dictated by the condition that it does not close during the laser pulse, it may be large. This would preclude the use of this method for long (> 5ns)pulses. Even for shorter pulses the mass of the outer layer, due to its larger area in spherical geometry, can become undesirably large. Additionally there are structural problems in producing such targets.

Seeded Targets

Tidman (149) suggested using "seeded targets", targets with small regions of high Z materials within them. The idea behind this is that the $\nabla n_e \wedge \nabla T_e$ generated B fields will impede the suprathermals.

Resistive Inhibition

As has been seen in section 4.2, resistive targets would be expected to perform better at higher laser intensities. Such targets require less area mass density than non resistive targets to prevent fuel preheat. (experiments suggest 1/3 as much.) Because the resistive layer is thicker, there will be a mass penalty in spherical geometry. This will not be as great as the penalty for vacuum gap insulation. The fabrication of low density gold coated microballoons presents no problems (150).

CHAPTER 5

Introduction

In this chapter we discuss the advantages of using total energy groups vis-a-vis speed or kinetic energy groups in a multi group diffusion model. A model which treats all the terms in the multi group equations implicitly is developed. The resulting set of linear equations are shown to give positive results for any choice of timestep. The application of a flux limiter is discussed. The numerical solution of the multi group equations using an ILUCG algorithm (Appendix 2) is then described and some results are given. Finally we compare our method of solution with that of Kershaw (109,122).

5.1 The Advantage of Total Energy Groups

In one spatial dimension or in the steady state the electric field;

$$\underline{E} = -\nabla\phi + \frac{\partial \underline{A}}{\partial t} = -\nabla\phi$$

($\underline{A} = \frac{\mu_o}{4\pi}\int \frac{\underline{J}}{r}\, d(\text{volume})$ in 1-D $\frac{\partial \rho}{\partial t} = 0 \rightarrow J = \text{constant} = 0$, since there is no current flowing into the target. Thus $\underline{A} = 0$).

The total energy of an electron;

$$E_T = \tfrac{1}{2} m_e v_e^2 - e\,\phi(x,t)$$

will change due to two causes, collisions and the time dependence of the electric potential. (In the absence of these mechanisms the Lagrangian has no explicit time dependence and E_T is a constant of the motion). If $\phi = \phi(x)$ then a suprathermal electron will only lose total energy but its kinetic energy may increase.

Fig.5.1 Total vs Kinetic Energy

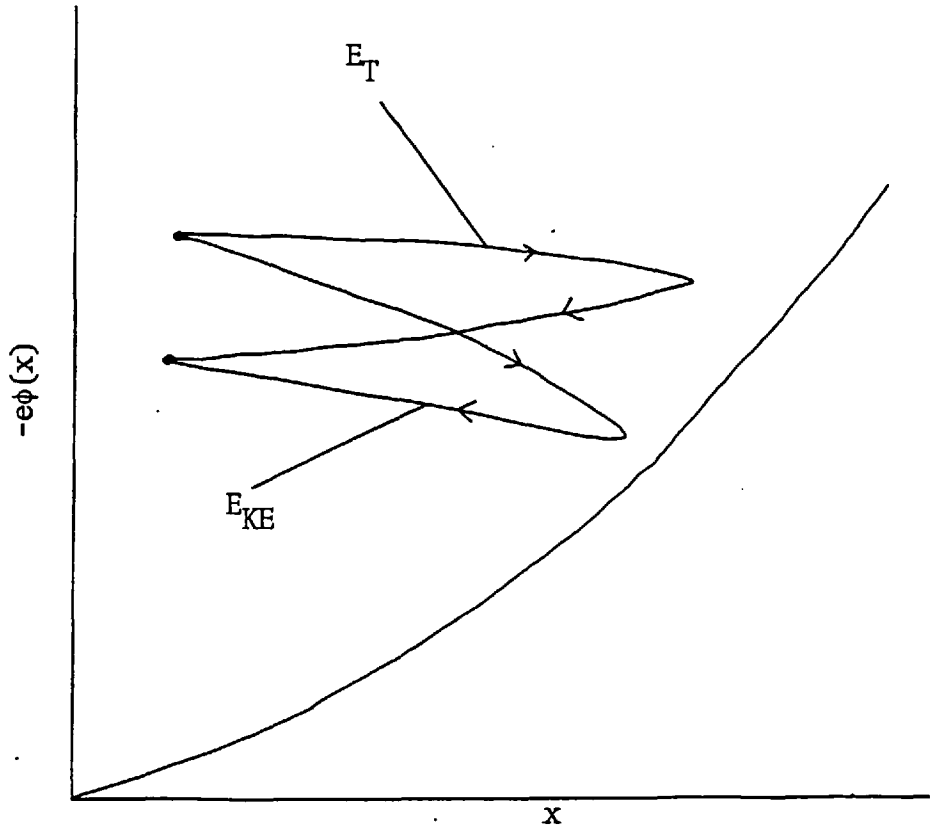

This suggests that, at least for time independent calculations, using total energy as a coordinate may be advantageous. In this case the fact that a suprathermal electron may only lose total energy allows us to solve the multi group equations one group at a time with a resulting great reduction in computational effort . In the time dependent case the use of total energy considerably simplifies the coupling between the groups and the spatial zones, and consequently simplifies the set of linear equations which must be solved.

5.2 The Fokker-Planck Equation Using E_T, x, t and μ as Independent Coordinates

From Appendix 3 the Fokker-Planck equation in an Eulerian frame may be written as :-

$$\frac{\partial f}{\partial t} + v\mu\frac{\partial f}{\partial x} + a\left(\mu\frac{\partial f}{\partial v} + \frac{1}{v}(1-\mu^2)\frac{\partial f}{\partial \mu}\right) = \left(\frac{\partial f}{\partial t}\right)_{coll} \qquad (5.2.1)$$

where x, t, μ and v are independent coordinates.

To transform this equation so that x', t', μ' and E_T are independent coordinates the following may be used:-

$$\frac{\partial}{\partial x} = \frac{\partial}{\partial x'}\frac{\partial x'}{\partial x} + \frac{\partial}{\partial \mu'}\frac{\partial \mu'}{\partial x} + \frac{\partial}{\partial t'}\frac{\partial t'}{\partial x} + \frac{\partial}{\partial E_T'}\frac{\partial E_T}{\partial x}$$

and similar transformation for the other variables. This gives the transformation (dropping primes) :-

$$\frac{\partial}{\partial x} \longrightarrow \frac{\partial}{\partial x} - e\frac{\partial \phi}{\partial x}\frac{\partial}{\partial E_T}$$

$$\frac{\partial}{\partial \mu} \longrightarrow \frac{\partial}{\partial \mu}$$

$$\frac{\partial}{\partial v} \longrightarrow mv\frac{\partial}{\partial E_T}$$

$$\frac{\partial}{\partial t} \longrightarrow \frac{\partial}{\partial t} - e\frac{\partial \phi}{\partial t}\frac{\partial}{\partial E_T}$$

where $v = (2/m)^{\frac{1}{2}}(E_T + e\phi)^{\frac{1}{2}}$

(5.2.1) now becomes :-

$$\frac{\partial f}{\partial t} - e\frac{\partial \phi}{\partial t}\frac{\partial f}{\partial E_T} + a\,\mu mv\frac{\partial f}{\partial E_T} + v\,\mu\frac{\partial f}{\partial x} - v\,\mu e\frac{\partial \phi}{\partial x}\frac{\partial f}{\partial E_T} + \frac{a}{v}(1-\mu^2)\frac{\partial f}{\partial \mu} =$$

$$= \text{collision term}$$

using $a = -(e/m)(-\frac{\partial \phi}{\partial x})$ this simplifies to :-

$$\frac{\partial f}{\partial t} - e\frac{\partial \phi}{\partial t}\frac{\partial f}{\partial E_T} + v\,\mu\frac{\partial f}{\partial x} + (e/m)\frac{\partial \phi}{\partial x}\frac{(1-\mu^2)}{v}\frac{\partial f}{\partial \mu} = \text{collision term} \qquad (5.2.2)$$

One may recast (5.2.2) into a more convenient form by substituting $F = fv$. This yields :-

$$\frac{1}{v}\left(\frac{\partial F}{\partial t} - e\frac{\partial \phi}{\partial t}\frac{\partial F}{\partial E_T} + v\,\mu\frac{\partial F}{\partial x} + (e/m)\frac{\partial \phi}{\partial x}\frac{(1-\mu^2)}{v}\frac{\partial F}{\partial \mu} - (e/m)\frac{F}{v}\,\mu\frac{\partial \phi}{\partial x}\right) =$$

$$= \text{collision term} \qquad (5.2.3)$$

We must now transform the collision term. Using a non-relativistic Fokker-Planck equation (Appendix 3) :-

$$\frac{\Gamma}{2}(n_e + Z^2 n_i)\frac{\ln\Lambda_{sth}}{v^3}\frac{\partial}{\partial \mu}\left((1-\mu^2)\frac{\partial f}{\partial \mu}\right) + \frac{\Gamma\, n_e}{v^2}\frac{\partial}{\partial v}(\ln\Lambda_{sth}\, f)$$

which transforms to :-

$$\frac{\Gamma}{2}(n_e + Z^2 n_i)\frac{\ln\Lambda_{sth}}{v^3}\frac{\partial}{\partial \mu}\left((1-\mu^2)\frac{\partial f}{\partial \mu}\right) + \frac{\Gamma\, n_e m}{v}\frac{\partial}{\partial E_T}(\ln\Lambda_{sth}\, f)$$

and on substituting $f = F/v$ this becomes:-

$$\text{(Diffusion term)} \quad \frac{\Gamma}{2}(n_e + Z^2 n_i)\frac{\ln\Lambda_{sth}}{v^3}\frac{\partial}{\partial\mu}\left((1-\mu^2)\frac{\partial}{\partial\mu}\frac{F}{v}\right)$$

$$\text{(Friction term)} \quad + \frac{\Gamma n_e}{v} m \frac{\partial}{\partial E_T}\left(\ln\Lambda_{sth}\frac{F}{v}\right) \qquad (5.2.4)$$

(5.2.3) and (5.2.4) combine to give :-

$$\frac{\partial F}{\partial t} - e\frac{\partial\phi}{\partial t}\frac{\partial F}{\partial E_T} + v\mu\frac{\partial F}{\partial x} + (e/m)\frac{(1-\mu^2)}{v}\frac{\partial F}{\partial\mu}\frac{\partial\phi}{\partial x} - \frac{F}{v}(e/m)\mu\frac{\partial\phi}{\partial x} =$$

$$= \frac{\Gamma}{2}(n_e + Z^2 n_i)\frac{\ln\Lambda_{sth}}{v^3}\frac{\partial}{\partial\mu}\left((1-\mu^2)\frac{\partial F}{\partial\mu}\right) + \Gamma n_e m\frac{\partial}{\partial E_T}\left(\ln\Lambda_{sth}\frac{F}{v}\right) \qquad (5.2.5)$$

Equation (5.2.5) will be used to derive the multi energy group equations in the next section.

5.3 Derivation of the Multi Total Energy Group Equations

Making the standard diffusion approximation we use :-

$$F = F_o + \mu F_1 \tag{5.3.1}$$

where F_o and F_1 are not functions of μ. By definition :-

$$N = \int_{-1}^{+1} d\mu F_o \quad , \quad \Phi = \int_{-1}^{+1} d\mu \, \mu v \, \mu F_1$$

The zeroth moment of equation (5.2.5) gives :-

$$\frac{\partial N}{\partial t} - e \frac{\partial \phi}{\partial t} \frac{\partial N}{\partial E_T} + \frac{\partial}{\partial x} \Phi = \Gamma n_e m \frac{\partial}{\partial E_T} \left(\frac{\ln \Lambda_{sth} N}{v} \right) + \text{source} \tag{5.3.2}$$

The first moment (multiplying by μv and integrating over μ) gives:-

$$\frac{v^3}{3} \frac{\partial}{\partial x} \left(\frac{N}{v} \right) = - \frac{\Gamma}{2} (n_e + Z^2 n_i) \frac{\ln \Lambda_{sth}}{v^3} 2 \Phi \tag{5.3.3}$$

where terms of order $1/Z^2$, the first moment of the source term, and the $\partial \Phi / \partial t$ term have been ignored. These approximations have been discussed previously (section 2.4) . Equations (5.3.2) and (5.3.3) constitute a closed set of equations. Closure was achieved by the truncation of the moment expansion of F in Hermite polynomials used in equation (5.3.1), it does not depend on the approximations used to get equation (5.3.3). These approximations do, however, simplify the solution of the multi group equations.

Equations (5.3.2) and (5.3.3) must now be recast into multi group equations. The number of electrons in a cell in the speed range

v_g to v_{g+1} is:-

$$N_g = \int_{cell} dx \int_{-1}^{+1} d\mu \int_{v_g}^{v_{g+1}} 2\pi v^2 dv\, f$$

If v_g, v_{g+1} correspond to total energies E_g, E_{g+1} then this may be reexpressed as :-

$$N_g = \int_{cell} dx \int_{-1}^{+1} d\mu \int_{E_g}^{E_{g+1}} \frac{2\pi}{m} F\, dE_T$$

Using $dv = \frac{dv}{dE_T} dE_T = dE_T/mv$ and $F = fv$.

Similarly:-

$$\Phi_g = \int_{cell} dx \int_{-1}^{+1} d\mu \int_{E_g}^{E_{g+1}} \frac{2\pi}{m} F\mu\, dE_T$$

Thus:- $$N_g = \int_{cell} dx \frac{2\pi}{m} \int_{E_g}^{E_{g+1}} N dE_T$$

and:- $$\Phi_g = \int_{cell} dx \frac{2\pi}{m} \int_{E_g}^{E_{g+1}} \Phi dE_T$$

Using these, and approximating terms of the form $\int_{E_g}^{E_{g+1}} f(E_T)\, N\, dE_T$ by $N_g f(E_T)\, \Delta E_T$ where $E_T = \frac{1}{2}(E_g + E_{g+1})$ and $\Delta E = E_g - E_{g+1}$, the multi total energy group equations become :-

$$\frac{\partial N_g^*}{\partial t} - e\frac{\partial \phi}{\partial t}\frac{N_g^*}{E_T} + \frac{\partial}{\partial x}\phi_g^* = -\Gamma n_e m \frac{\partial}{\partial E_T}\left(\frac{\ln \Lambda_{sth}\, N_g}{\bar{v}}\right) + \text{source} \qquad (5.3.4)$$

$$\frac{\bar{v}^3}{3}\frac{\partial}{\partial x}\left(\frac{N_g^*}{\bar{v}}\right) = -\frac{\Gamma}{2}(n_e + Z^2 n_i)\frac{\ln \Lambda_{sth}}{\bar{v}^3}\, 2\, \phi_g^* \qquad (5.3.5)$$

where $N_g^* \Delta x\, \Delta E = N_g$, $\phi_g^* \Delta x\, \Delta E = \Phi_g$ and Δx is the volume of the cell and N_g and ϕ_g are the total density and flux in a cell between the energies E_g and E_{g+1}.

Equations (5.3.4) and (5.3.5) may be combined to give an equation of the form:-

$$\frac{\partial N}{\partial t} + \frac{\partial}{\partial E_T}(\beta N) + \frac{\partial}{\partial x}\alpha\frac{\partial}{\partial x}\left(\frac{N}{v}\right) = \text{source} \qquad (5.3.6)$$

where β can be of either sign.

This equation must be solved using fully implicit differencing. It is important that this differencing should ensure the physical inequality $N_g \geq 0$. It is instructive to consider two simplifications of equation (5.3.6)..Firstly:-

$$\frac{\partial N}{\partial t} + \frac{\partial}{\partial x}\alpha\frac{\partial}{\partial x}\left(\frac{N}{v}\right) = \text{source}$$

This is a parabolic equation. It can be differenced fully implicitly in such a way as to ensure positivity and satisfy conservation using centred differencing (ie the standard three point scheme). Secondly consider the equation :-

$$\frac{\partial N}{\partial t} + \frac{\partial}{\partial E_T}(\beta N) = 0$$

This is a hyperbolic equation and describes advection of N with "velocity" β. If such an equation is to be differenced implicitly, one sided differencing is required. The differencing should reflect the domain of dependence of the equation. Thus the way in which the equation is differenced will depend on the sign of β. With such a scheme the flux out of a region depends on the density in that region. This ensures that the density will stay positive. Our approach to the differencing of equation (5.3.6) is to treat the diffusion terms as one would treat a parabolic equation and the $(\partial/\partial E_T)$ term like a hyperbolic equation. Figure (5.2) illustrates the mesh which is used.

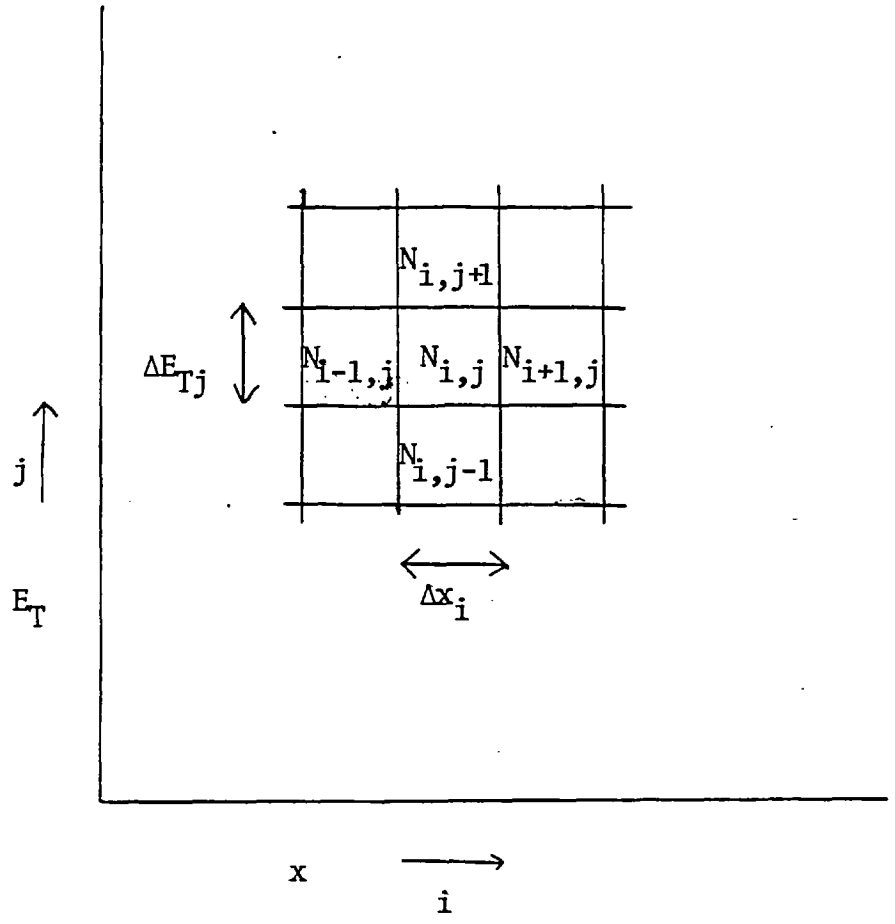

Fig.5.2 The Mesh

Two subscripts are used to label the number of electrons in a group and a spatial zone. (This notation is not reflected in our computer programme where single index arrays are used for efficiency). The electric potential, ϕ_i , is defined at the centre of each spatial zone. For some bins $-e\phi > E_T$. There can be no electrons in such a bin. The diffusion coefficient at the spatial boundary of these bins is set to zero. Physically this represents reflection by the E field. Electrons will not downscatter into these bins. They will enter the thermal population instead. The difference equations allow electrons which were, at one time level, in a bin for which $-e\phi > E_T$ at the next time level to "advect" to higher total energy. There is a large damping associated with the one sided differencing which is used. Such differencing, called Leleviers method in hydrodynamics (151) replaces

$$\frac{\partial f}{\partial x} \quad \text{by} \quad \frac{\partial f}{\partial x} \pm \frac{\Delta x}{2} \frac{\partial^2 f}{\partial x^2}$$

where the sign depends on the direction of the flow. Thus the advection equation is replaced by:-

$$\frac{\partial f}{\partial t} + v \frac{\partial f}{\partial x} = \frac{v \ \Delta x}{2} \frac{\partial^2 f}{\partial x^2}$$

Thus, even though the downscatter terms for these negative kinetic energy cells are zero, there will some density associated with them. This is set to zero and the density added to the thermal density.

The energy that is associated with the electrons in the j^{th} group is $\frac{1}{2}(E_j + E_{j+1})N_{g\ i,j}$. After each timestep the energy lost by the electrons in the bins is added to the thermal electrons' energy.

The details of the differencing scheme for (5.3.6) will now be given. Consider a cell in x, E_T space.

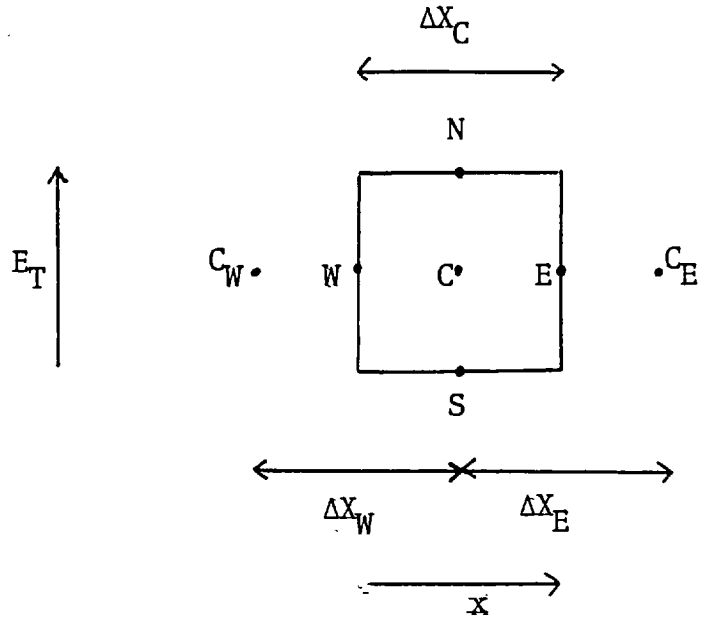

Fig.5.3

Since the potential is defined at the centre of the spatial zones the kinetic energy is defined at the points N, S and C . The coefficient , α , is calculated at the W and E points using spatial averaging of the coefficient between adjacent cells. If the kinetic energy at the S point of either cell is less than zero, no flux is allowed between the cells. The flux, Φ_W , at the W boundary of the ij^{th} cell is :-

$$\frac{\alpha^W_{ij}}{\Delta x^W_i}\left(\frac{N^*_{ij}}{v^c_{ij}} - \frac{N^*_{i-1,j}}{v^c_{i-1,j}}\right)$$

In Cartesian geometry the areas of the W and E faces are taken to be $1 \cdot \Delta E$ (the scale factors equal 1) and the diffusion term becomes :-

$$\frac{\Phi_E - \Phi_W}{\Delta x^c_i} = \frac{1}{\Delta x^c_i}\left(\frac{N^*_{i-1,j}}{v^c_{i-1,j}\,\Delta x^W_i} + \frac{N^*_{i+1,j}}{v_{i+1,j}\,\Delta x^E_i} - \frac{N^*_{ij}}{v^c_{ij}\,\Delta x^W_i} - \frac{N^*_{ij}}{v^c_{ij}\,\Delta x^E_i}\right) \qquad (5.3.7)$$

The coefficient, β , is calculated at the N and S points. The sign of β determines the direction of "flow" at each of these boundaries. The possible combinations of signs of β at N and S are illustrated below:

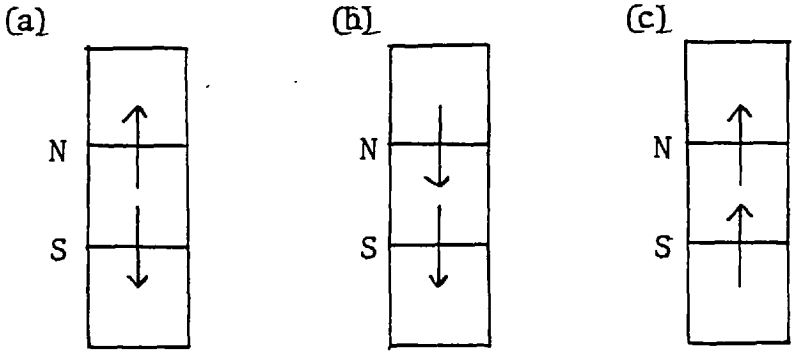

Fig.5.4

First consider case (a).

The $(\partial/\partial E_T)$ term is differenced as:-

$$\frac{1}{\Delta E_j}\left(\beta_N N^*_{gi,j+1} - \beta_S N^*_{gi,j}\right) \qquad (5.3.8a)$$

Consider the equivalent expression for the $j+1^{th}$ energy group. That is:-

$$\frac{1}{\Delta E_{j+1}}\left(\beta_{NN} N^*_{gi,j+2} - \beta_N N^*_{gi,j+1}\right)$$

The loss in $N_{gi,j+1}$ is thus :-

$$\left(\frac{\beta_N N^*_{gi,j+1}}{\Delta E_{j+1}}\right) \Delta E_{j+1}\, \Delta x_i$$

Which also equals the gain in N_{gij} from equation (5.3.8a). Thus the scheme conserves the number of electrons.

Case (b) is differenced as :-

$$\frac{1}{\Delta E_i}\left(\beta_S N^*_{gi-1,j} - \beta_N N^*_{gij}\right) \qquad (5.3.8b)$$

and case (c) as :-

$$\frac{1}{\Delta E_i}\left(-\beta_S N^*_{gij} - \beta_N N^*_{gij}\right) \qquad (5.3.8c)$$

(5.3.8a,b and c) provide a conservative differencing scheme for the $(\partial/\partial E_T)$ term. Equations (5.3.7) and (5.3.8) are differenced at the advanced time level, ie fully implicit differencing of these terms is used. $\frac{\partial N^*_g}{\partial t}$ is simply differenced as :-

$$\frac{N^{*n+1}_{gij} - N^{*n}_{gij}}{\Delta t} \qquad (5.3.9)$$

Boundary conditions must be specified :-

Fig.5.5 Boundaries of Simulation Region

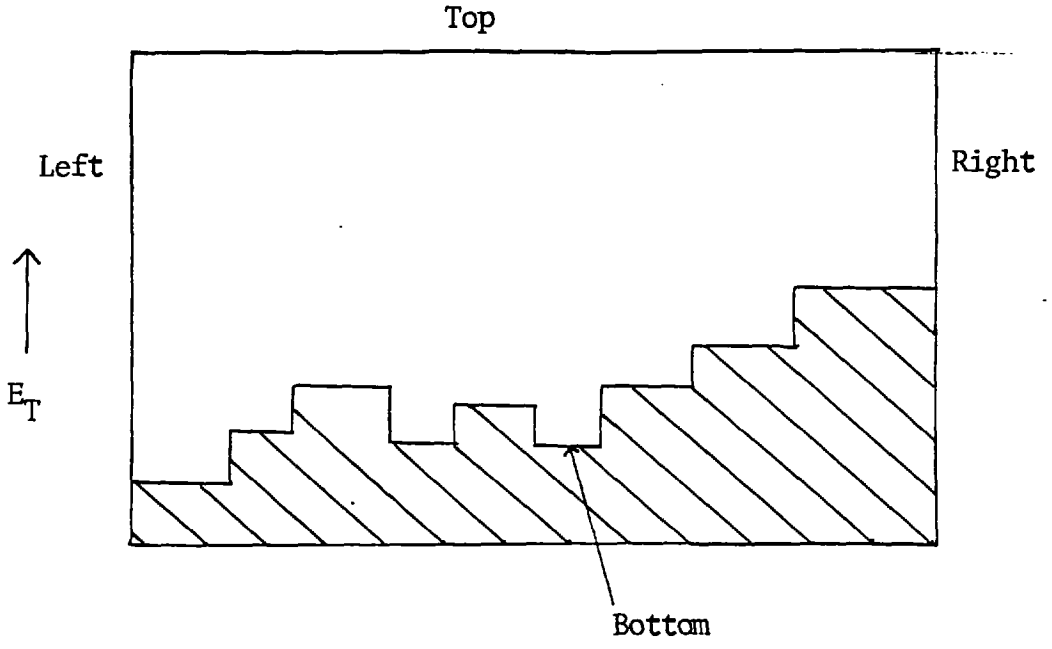

KE < 0 in shaded area.

No flux or free flow may be allowed at the left and right boundaries (no flow may be allowed into the region). No downward flux is allowed into the shaded region. No flux is allowed out at the top. To achieve this β is set to zero at the top boundary. To maintain energy conservation any energy lost because of this is dumped into the thermals. Electrons from the lowest bin with positive kinetic energy downscatter into the thermals.

These equations must be solved to update the suprathermal density. It is assumed at this stage that the potentials at the advanced time level are known. The equations may couple one cell in the x, E_T

plane to any of its four neighbours. One cannot solve the multi group equations in the standard way (section 2.5). Instead one must solve for all the groups at once. This is done by first scaling the equations, so the diagonal elements of the resultant set of linear equations are all one, and then solving the equations using a quindiagonal ILUCG algorithm (Appendix 2).

5.4 Calculation of $\underline{J}$ and Iteration for $\underline{J}_{total} = 0$

In the previous section a description of how the multi group equations are solved, with a given electric potential, was given. The E field and hence the potential are calculated by the condition that $J_{total} = 0$. The procedure used to calculate J_{total}, and to iteratively determine E, will now be described.

The total suprathermal current is calculated using the expressions for the suprathermal particle fluxes. These are calculated from the suprathermal densities and the potential at the advanced time. (Recall that the assumption that the flux relaxes to its new value in a time shorter than the time step has been made). These fluxes are calculated at the cell boundaries.

In the cases which are to be considered, suprathermal transport in a partially (or fully) ionized solid, the E field is resistive in character (section 3.2).

In this case we may use a scheme similar to that used in chapter 4. Using the simple thermal Ohm's law :-

$$J_{th} = \eta_{th} E \tag{5.4.1}$$

and

$$J_{th} = -J_{sth} \tag{5.4.2}$$

we can find the E field which would give $J_{total} = 0$ if the suprathermal current was unaffected by the E field. The iterative scheme:-

$$E^{n+1} = \alpha E^{n} + (1-\alpha)(E^{n+1})'$$

$$(E^{n+1})' = - J_{sth}\, \eta_{th} \tag{5.4.3}$$

is used to find the new E field. (Here n denotes the number of

iterations). E^o is taken as the value of E at the last time level. The choice of $\alpha = 0.5$ has been found to be satisfactory. When the potential developed across the target is small (cf kT_{sth}), $\alpha = 1.0$ gives more rapid convergence.

The initial choice :-

$$\alpha = MAX(0.5, \exp(e\,\Delta\Phi / kT_{sth}))$$

has been used , where $\Delta\Phi$ is the change in the potential across the target in the first iteration.

The E field is defined at the cell boundaries, where the current is defined. This is integrated to give the potential at the cell centres, which is where it is required for the transport calculation .

The sequence of calculations for one time step is :-

Fig.5.6

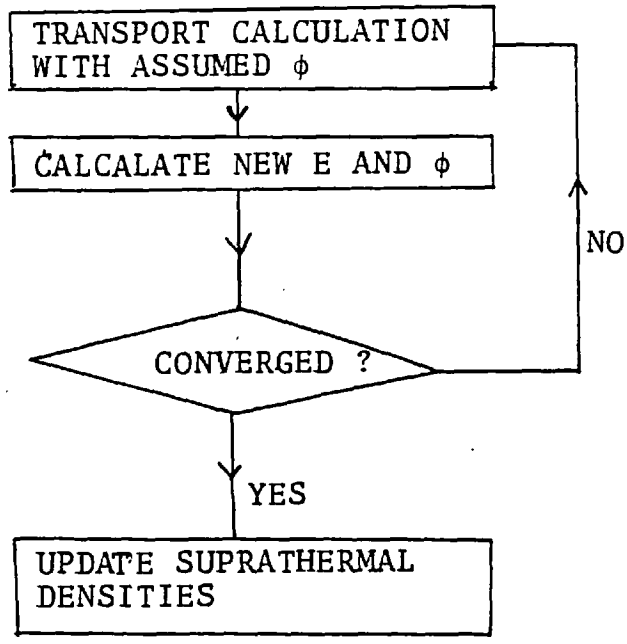

The convergence test requires $\Sigma |E^{n+1} - E^n| <$ some specified value.

5.5 Flux Limiter

The concept of flux limiting has been discussed previously (section 3.6). The expression for the flux (5.3.5) includes E field effects. A flux limiter is chosen so that the flux is limited to $\frac{1}{3}$ Nv where Nv is evaluated at the boundary between cells by interpolation. The unlimited flux :-

$$\alpha \frac{\partial}{\partial x}\left(\frac{N_g}{v}\right) \tag{5.5.1}$$

is modified to :-

$$\alpha^* \frac{\partial}{\partial x}\left(\frac{N_g}{v}\right) \tag{5.5.2}$$

$$\frac{1}{\alpha^*} = \left(\frac{1}{\alpha} + \frac{\left| \frac{\partial}{\partial x}\left(\frac{N_g}{v}\right) \right|}{\frac{1}{3} Nv} \right)$$

N and v are the values at the last iteration. If N is zero $\alpha = \alpha^*$ is used.

5.6 Results from the Model

Number of Groups

In Figure 5.7 the energy deposition profile in a Gold target is shown for multi group calculations using 5,10 and 15 groups. Equal group widths were used in all cases. This suggests that 10 group resolution is adequate.

Fig.5.7 Effect of Number of Groups

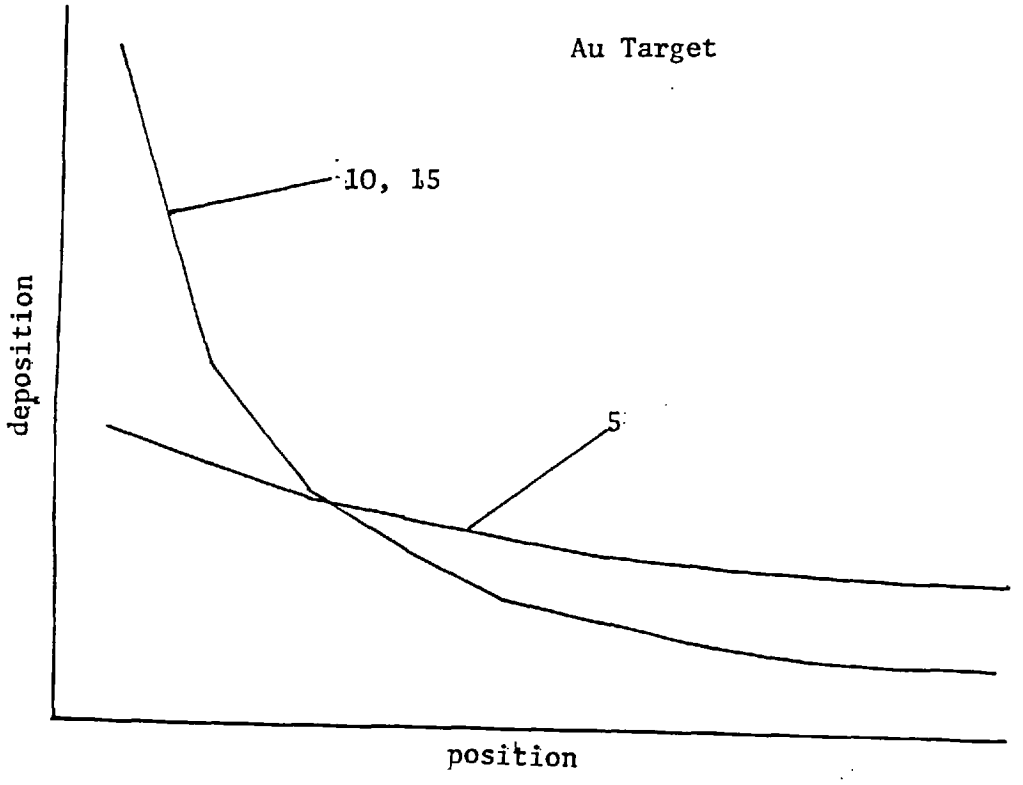

Comparison with Monte-Carlo Calculations

Figures 5.8 and 5.9 show a comparison of the steady state energy deposition in low Z (Hydrogen) and high Z (Gold) targets. The former was fully ionized (T_{th} = 100eV) and the latter unionized. The boundary conditions were that no flux was allowed through the boundaries of the simulation region. In the Monte-Carlo calculation

reflection boundary conditions were imposed. The source was of the form:-

$$f(E) = \exp(-E/kT_{sth}) \qquad (5.6.1)$$

$$T_{sth} = 12KeV$$

In the Monte-Carlo calculation the particles were initially moving in the +x direction. 10 groups equally spaced in the range 10-100 KeV were used in the Multi Group calculation.

The agreement between the two calculatios is better for the gold target; as would be expected.

When the Multi Group calculations were repeated without a flux limiter the calculation for the Gold target was only slightly altered but that for the Hydrogen target was greatly changed.

Fig.5.8 Energy Deposition in Hydrogen

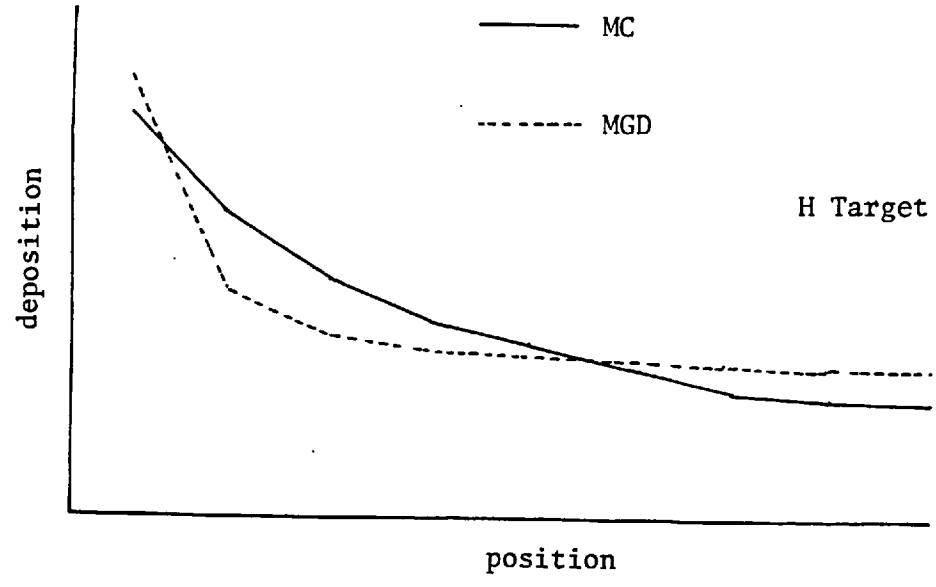

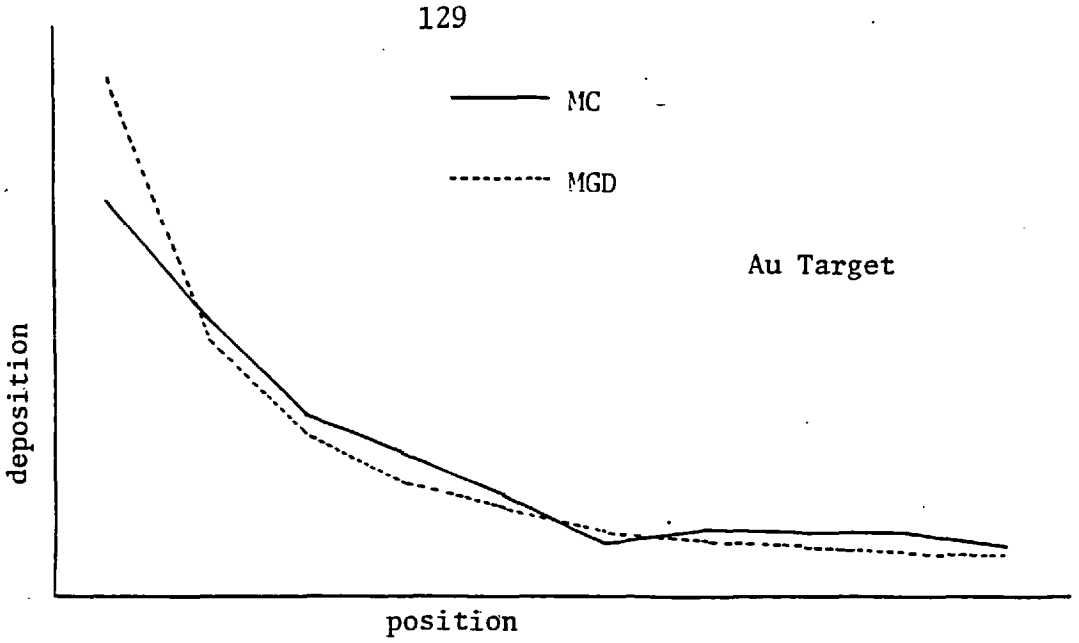

Fig.5.9 Energy Deposition in Gold

The potential calculated using the condition $J_{total} = 0$ is shown in Figure 5.10 . The target was solid Gold and the resistivity was chosen so that a potential of approximately $2kT_{sth}$ was developed across the target. The two calculations can be seen to be in reasonable agreement.

Fig.5.10 E Field Calculations

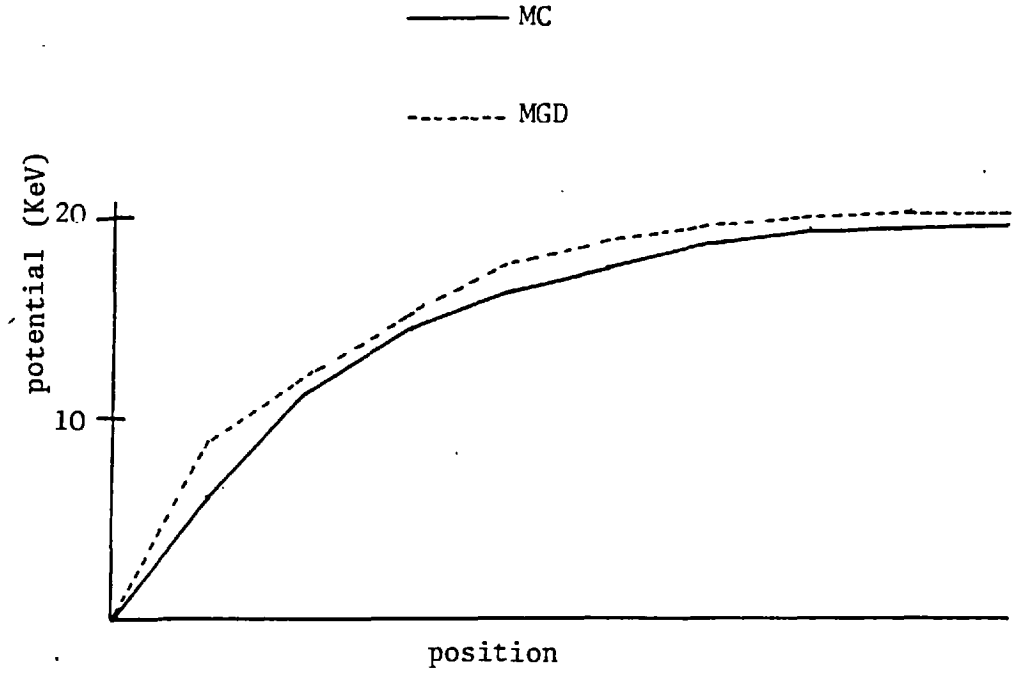

Time Dependent Calculations

The application of the model to time dependent calculations has been only briefly investigated. In Figure 5.12 the energy deposition profile after a 0.2 ps. burst of suprathermal electrons is shown. (The source and state of the Gold target were the same as in the steady state calculations described above). The ratio of this to the deposition calculated excluding the $\partial\phi/\partial t$ term is shown in Figure 5.11 . This shows that the $\partial\phi/\partial t$ term will increase the range of the suprathermals when $\partial\phi/\partial t$ is positive.

Fig.5.11 Energy Deposition in Gold

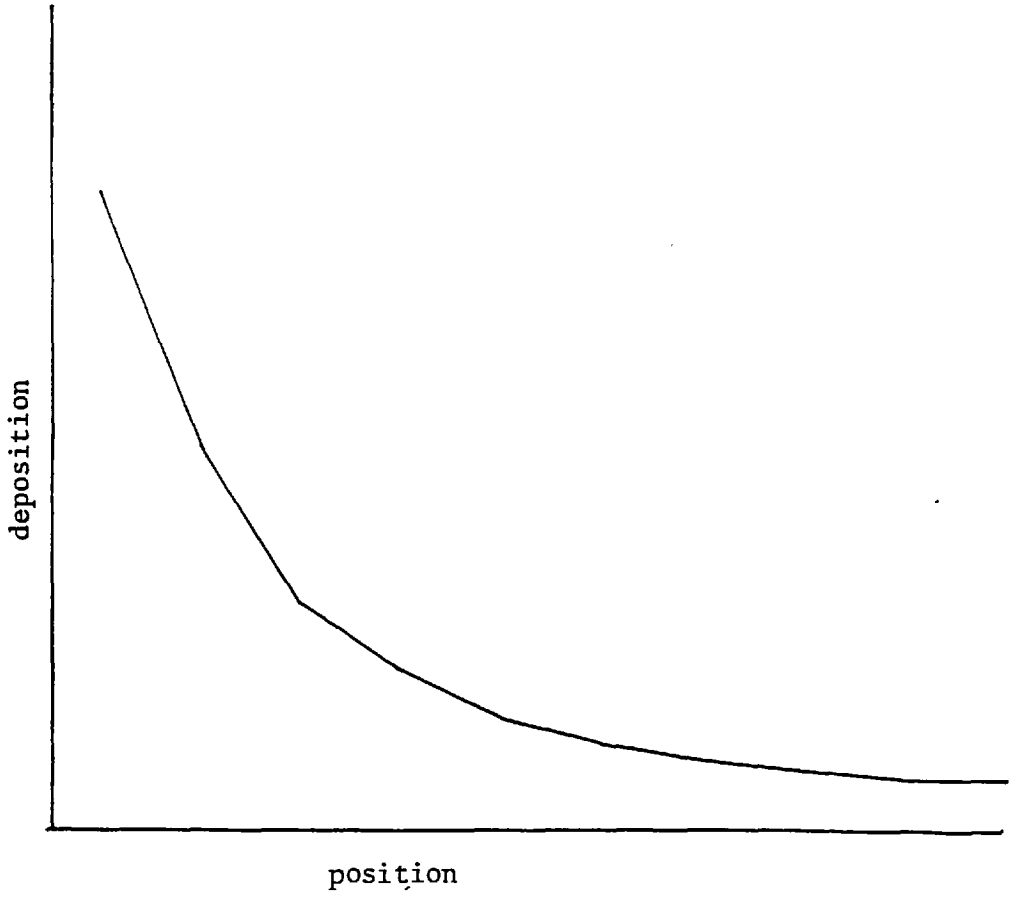

Fig.5.12 Ratio of Energy Depositions

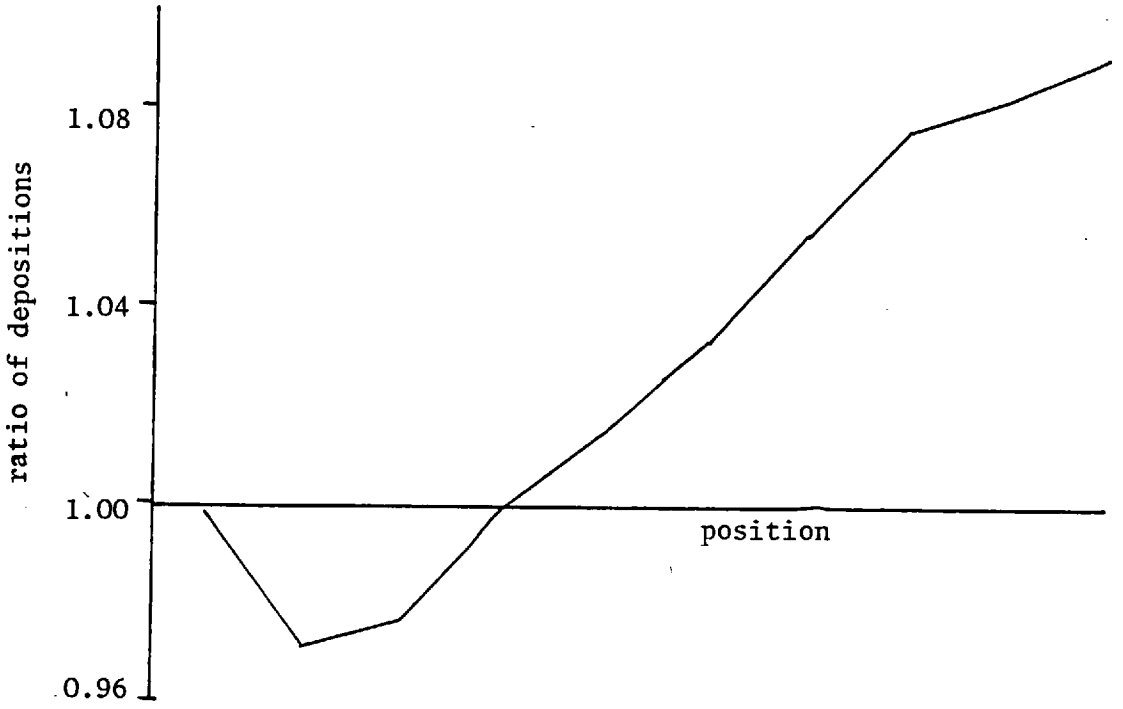

5.7 Discussion

A numerical model which solves the multi group diffusion equations, with E field effects included, in a way which is implicit, positive and conservative has been introduced. The penalty which has been paid for this is that the multi group equations cannot be solved group by group but must all be solved together.

Kershaw (122) recently reported the successful implimentation, in 1-D, of a new multi group diffusion model in the LASNEX laser fusion code. This has been briefly discussed in section 3.4.

The solution of a (number of groups, N_G) * (number of zones, Nz) quindiagonal system, which is done iteratively, is clearly far more time consuming than solving N_G tridiagonal systems of size N_Z. However it avoids the inaccuracies associated with the split of calculations which Kershaw uses. The use of fixed bins avoids the energy non conservation problems associated with the bin-bin mapping. The large computing time penalty would, however, probably preclude the use of such a scheme in a hydro-code. The efficiency of the scheme could however be improved by noting that some region in the x, E_T plane is not connected to higher values of E_T. This is illustrated below.

Fig.5.13

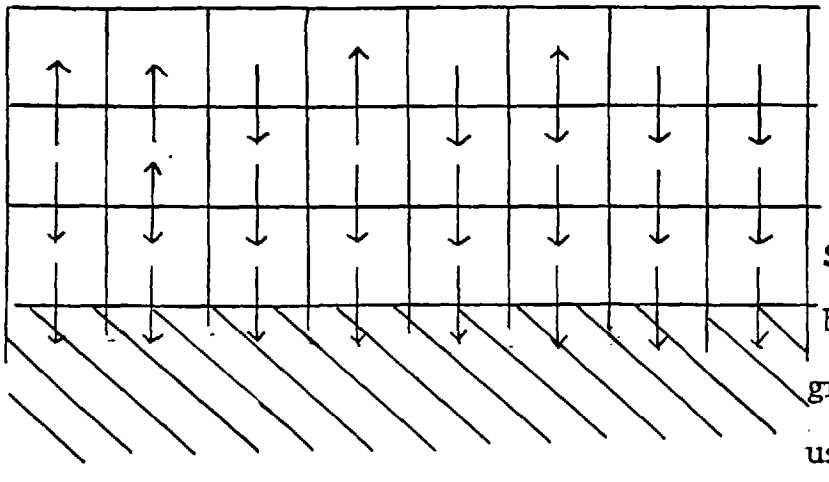

Another inefficiency in the method described in this chapter is that instead of excluding negative kinetic energy bins from the calculation the equation $1 \cdot N_G(\text{negative kinetic energy}) = 0$ is solved.

For problems where the time step is very large, such that the $(\partial\phi / \partial t)$ term never exceeds the collisional downscatter, the method is ideally suited and is clearly far superior to multi velocity group methods for this problem.

The application of a flux limit using multi total energy group methods is more straightforward than for multi speed groups. For the former it is simple to flux limit the total suprathermal flux. In the flux limited regime the E field and ∇n terms may be of comparable sizes in the flux calculated using speed groups: limiting only the ∇n term is clearly wrong.

The difference between the fully implicit calculation described in this chapter and time split calculations can be illustrated by analogy with approximate matrix factorisation.

The method used in this chapter may be represented by :-

Fig.5.14

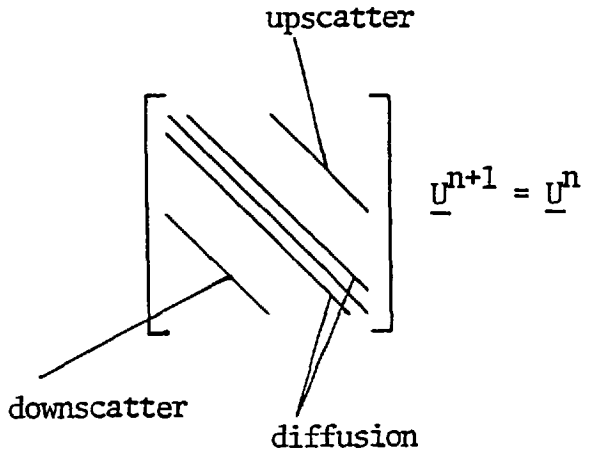

The time splitting approach described by Kershaw (122) and reviewed in section 3.4 is equivalent to an approximate factorisation of M of the form:-

Fig.5.15

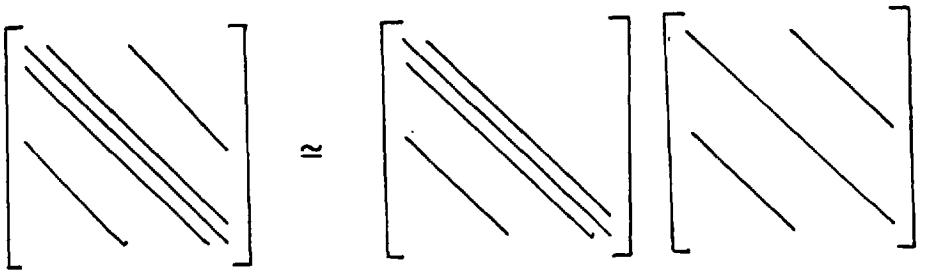

(It should be noted that (a) time splitting for the P dV term is unavoidable, unless the hydrodynamics is iterated about, and (b) the $(\partial \phi / \partial t)$ term is accounted for separately).

An approach used in multi velocity group models (152) is to neglect the E field driving term and to deal with $\underline{J} \cdot \underline{E}$ downbinning and upbinning in two sweeps through the groups: top to bottom and then bottom to top. This may be represented by the following:-

Fig.5.16

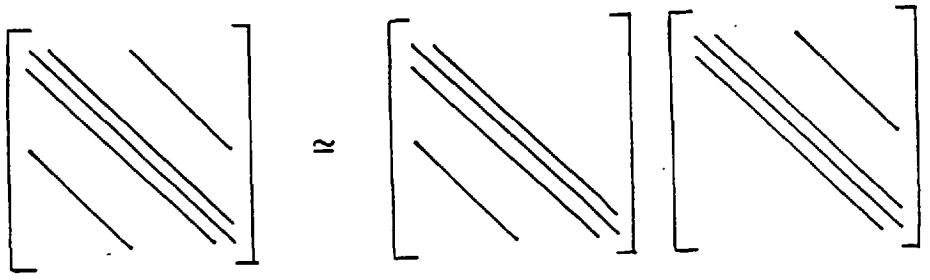

It is clear that such approximate factorisation introduces errors. If the second approximate factorisation is considered the sparsity pattern of the product of the matrices is given, schematically, by:-

Fig.5.17

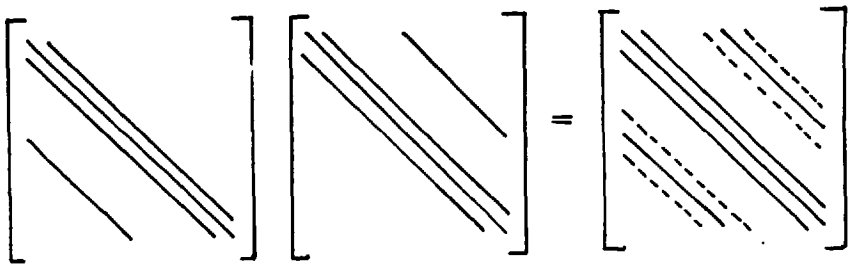

From this it can be seen that exact decomposition corresponds to an overspecified problem. In a 2-D hydrodynamic simulation Beam and Warming (153) have used a decomposition which is accurate to second order in Δt. However due to the large time steps which must be used in suprathermal transport such an approach does not seem applicable.

CHAPTER 6

Introduction

In this chapter a one (spatial) dimensional electron transport model, which includes electron-ion collisions by using the Monte Carlo method, is described. Various methods for calculating the quasi neutral E field are discussed and their implimentation in the computer model are described. We describe first a variant of a model due to Mason (133) which uses "plasma period dilation", the problems associated with it and an approach to mitigating these problems. Secondly an iterative approach is described. This uses a Newton-Raphson method to get $J_{total}(E) = 0$. Careful consideration of the effects of P.I.C. weighting and interpolation of the E field lead to an efficient scheme.

6.1 Monte Carlo Transport Model

In this section we will describe all aspects of the model except the calculation of the E field. This will be discussed in sections 6.2, 6.3 and 6.4.

The Mesh

The mesh is 1-D Cartesian with constant cell size Δx. It is possible to use a non-uniform cell size but in this case interpolation for the density is no longer equivalent to P.I.C. weighting.

P.I.C. Weighting

The particle in cell (P.I.C.) method is used to calculate the contribution of each simulation particle to the densities in each cell. The P.I.C. weighting is equivalent to having a particle, the size of which equals the mesh spacing, Δx, and the density of which is uniformly distributed throughout this region.

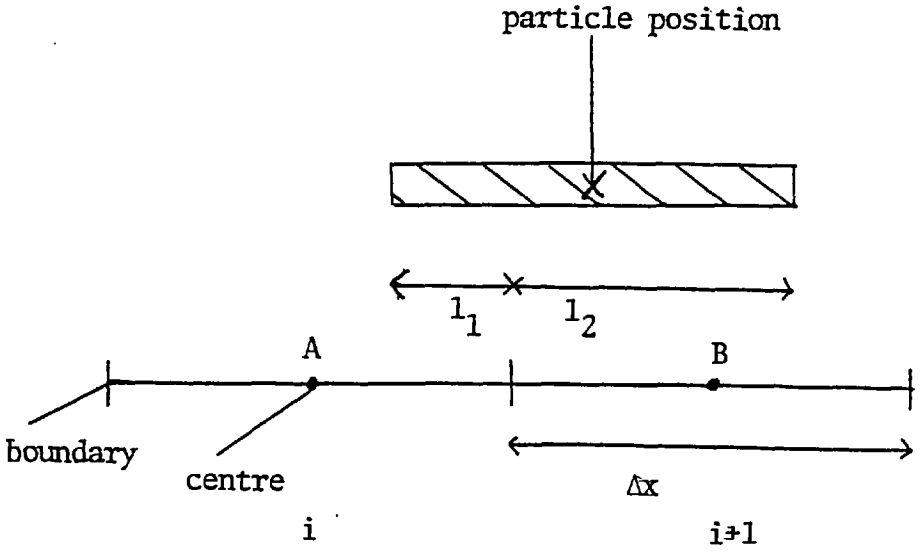

Fig.6.1 P.I.C. Weighting Scheme

The density associated with cell i is (weight of particle)$\cdot \frac{I_1}{\Delta x}$ and with cell i+1 is (weight of particle)$\cdot \frac{I_2}{\Delta x}$. This is equivalent to linearly interpolating the density between A and B . Linear interpolation is more readily extended to the case of a non-uniform mesh. The P.I.C. method has the advantage, in common with all methods which use finite size particles, of reducing noise compared to that of a point particle simulation. It has been found (154) to be preferable to Nearest Grid Point weighting for energy conservation in Vlasov plasma simulations. The wider application of P.I.C. methods is described by Morse(155).

Particle Moving

A Leap-frog scheme is used to move the particles. It is :-

$$\left.\begin{aligned} x^{n+1} &= x^n + v_x \Delta t \\ \underline{v}^{n+3/2} &= \underline{v}^{n+1/2} - (e/m)E^{n+1/2}\,\underline{i}\,\Delta t \end{aligned}\right\} (6.1.1)$$

$$\left.\begin{aligned} \underline{v}^{n+3/2'} &= \underline{v}^{n+3/2} + \text{effect of scattering} \\ \omega^{n+3/2'} &= \omega^{n+3/2} + \text{effect of scattering} \end{aligned}\right\} (6.1.2)$$

This scheme is second order accurate and, in the absence of scattering, is reversible. Reversibility is important since non-reversible schemes may create entropy numerically. The model for deflection is superior to that used in chapter 4 and its implimentation will be described in more detail. Particles are not allowed to leave the simulation region. When a particle reaches a boundary it is specularly reflected.

Calculation of Change in Polar Angle due to Scattering.

The kinematics of scattering have been discussed in section 2.4. To get the new polar angle, ω', we use equation (2.2.6) to give a probability distribution for the deflection, θ. Due to the simple, Gaussian, form of the chosen multiple scatter distribution the probability distribution can be written as :-

$$P(\theta) = KP_o(\theta)$$

where $P_o(\theta)$ is independent of the state of the scattering material and the speed of the scattered particle.

$P(\phi)$ is uniform in the range $0 \leq \phi \leq 2\pi$.

θ and ϕ are chosen using random numbers. These random numbers are used to refer to one element of an array, the elements of which have been chosen to reflect a given probability distribution function. These arrays are generated in a preparatory programme as follows. To generate an array whose elements are in the range $x_1 < x < x_2$ with a probability distribution $P(x)$, the following procedure is carried out:-

Fig.6.2

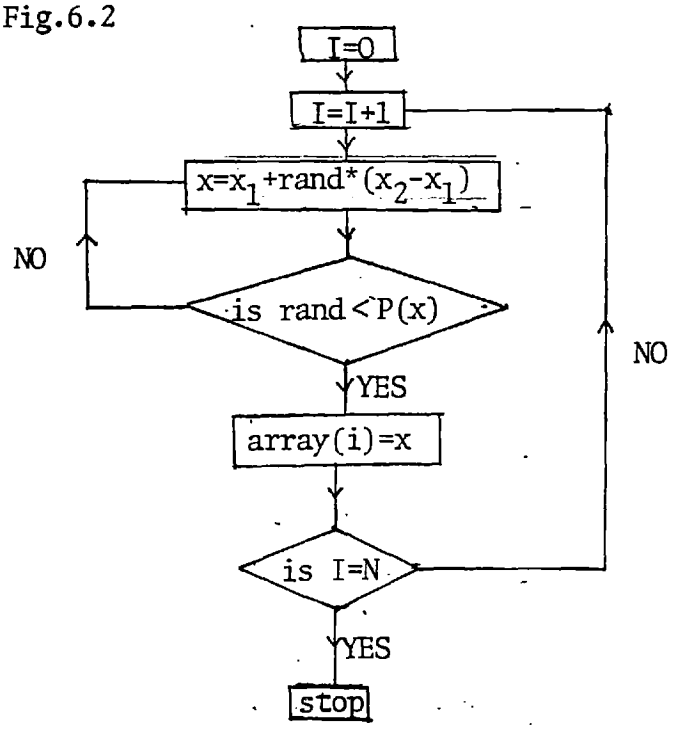

The new polar angle ω' is calculated using:-

$$\omega' = \arccos(\cos\omega \cos\theta + \cos\phi \sin\omega \sin\theta) \qquad (2.2.4)$$

E Field Effects

The deflection due to the E field is calculated using :-

$$\omega'' = \arctan(\sin\omega', \cos\omega' - (eE/m_e)\,\Delta t) \qquad (6.1.3)$$

The E field also changes the speed of the particle. This is calculated using:-

$$\text{speed}' = (\text{speed}^2 \sin^2\omega' + (\text{speed}\cos\omega' - (eE/m_e)\,\Delta t)^2)^{\frac{1}{2}} \qquad (6.1.4)$$

Look up Tables for Trigonometric Functions

In the above equations (2.2.4) and (6.1.4) the sine and cosine functions are frequently used. Great accuracy is not required in calculating these functions so, as a time saving device, look up tables have been used. The range $0 - 2\pi$ was split up into 1000 intervals and arrays were filled with the sines and cosines of these angles $0, \frac{2\pi}{1000}, \ldots \frac{999 \cdot 2\pi}{1000}$. To calculate the approximate sine and cosine of an angle an integer

$$\text{INT} = \text{MOD}(\text{IFIX}(500\pi \cdot \text{angle} + 0.5), 1000) + 1$$

was calculated and the sine and cosine of the angle were equated to the INT^{th} elements of the arrays containing the sines and cosines.

This results in approximately a 40% saving in the time involved in calculating these functions. (On a CDC 6500 using FTN).

6.2 Mason's Method

A method used by Mason (133) will now be described. If Poisson's equation is used to update the electric field, the time step used in the calculation must be less than $(1/\omega_{pe})$. This is usually less than any timescale of interest in a macroscopic simulation. Mason artificially expands the plasma period so that it is comparable to the time step which must be used when moving the Monte Carlo particles.

Poisson's equation:-

$$\nabla \cdot \varepsilon E = \rho$$

gives:- $$\nabla \cdot \frac{\partial}{\partial t}(\varepsilon E) = \frac{\partial \rho}{\partial t} = -\nabla \cdot J$$

This integrates to give:-

$$\frac{\partial}{\partial t}(\varepsilon E) = -J + F(t)$$

In a vacuum $J = 0, E = 0$ so $F(t) = 0$.

Mason uses:- $$\varepsilon_M \frac{\partial E}{\partial t} = -J \qquad (6.2.1)$$

where ε_M is chosen so that the dilated plasma period $(ne^2/\varepsilon_M m_e)^{-1}$ is a few times the computational time step for particle moving.

We have used :-

$$\nabla \cdot \varepsilon_M E = \rho \qquad (6.2.2)$$

This is equivalent to (6.2.1) when ε_M is not a function of time. Two factors lead to prefering this to equation (6.2.1). Firstly we wish to calculate E at the n+1 time level (see equation (6.1.1)) ρ but

not J is defined at this level. Secondly we wish to chose ϵ_M using the local density of the electrons. This will fluctuate, see below, and hence ϵ_M is a function of time.

The E field is calculated as follows. The space charge, ρ, is calculated in each cell. The integral form of equation (6.2.1)

$$E_i = \frac{1}{\epsilon_{m_i}} \sum_{j=1}^{i} \rho_j \qquad (6.2.3)$$

is used to calculate the E field at the cell boundaries. E = 0 is specified at the first (i = 0) boundary. Since particles do not leave the simulation region, E = 0 on the last boundary.

Let us consider the effect of dilating the plasma period. Clearly this results in a dilation of the Debye length ; $\lambda_D = v_{th}/\omega_{pe}$. Consider the case of an isothermal plasma with scale length for density variation, L . The E field which will preserve quasi neutrality is :-

$$E = -\frac{\nabla P_e}{en_e} = -\frac{kT}{eL} \qquad (6.2.4)$$

But we use :-

$$\nabla \cdot (\epsilon_M E) = \rho = -e\delta n$$

where δn is the difference between n_e and n_i. Then :-

$$E = \frac{-e\ \delta n L}{\epsilon_M} \qquad (6.2.5)$$

From (6.2.4) and (6.2.5) :-

$$\frac{\delta n_{sc}}{n} = \left(\frac{\varepsilon_M kT}{n_e e^2}\right)\frac{1}{L^2} = \frac{((\lambda_D)_{mod})^2}{L^2} \qquad (6.2.6)$$

where δn_{sc} is the space charge density which would give the quasi neutral E field.

One also has to consider the effect of shot noise (156). This will give, at best:-

$$\frac{\delta n_{noise}}{n} = \frac{1}{n_D^{\frac{1}{2}}}$$

n_D is a generalisation of the Debye number for finite sizes particles.

$$n_D = n(\lambda_{D_{mod}} + S)$$

where S is the size of the particle. This is equal to the mesh spacing for P.I.C. area weighting. This gives :-

$$\delta n_{noise} = \frac{n}{(n(\lambda_{D_{mod}} + S))^{\frac{1}{2}}}$$

$$\text{as} \quad \delta n_{sc} = n\frac{\lambda_D^2}{L^2}$$

$$\frac{\delta n_{noise}}{\delta n_{sc}} = \frac{L^2}{(n(\lambda_{D_{mod}} + S))^{\frac{1}{2}}\lambda_{D_{mod}}^2} \qquad (6.2.7)$$

For a useful quasi neutral simulation one requires that both :-

$$\frac{\delta n}{n} \ll 1 \qquad (6.2.8)$$

and :- $$\frac{\delta n_{noise}}{\delta n_{sc}} \ll 1 \qquad (6.2.9)$$

Using (6.2.9) put $\delta n = \delta n_{sc}$ in (6.2.6), which gives:-

$$\frac{\delta n}{n} = \frac{\lambda_{D_{mod}}^2}{L^2} \qquad (6.2.10)$$

This is the usual condition for quasi neutrality to apply, but with λ_D replaced by $\lambda_{D_{mod}}$. Then from (6.2.7) :-

$$\frac{\delta n_{noise}}{\delta n_{sc}} = \frac{1}{(n(\lambda_{D_{mod}} + S))^{\frac{1}{2}}} \cdot \frac{n}{\delta n} \qquad (6.2.11)$$

Suppose we wanted $(\delta n_{noise} / \delta n_{sc}) = (\delta n / n) = 0.1$. This would require $n(\lambda_{D_{mod}} + S) = 10^4$. This is an undesirably high number. In the next section we describe an attempt to minimise this problem.

6.3 Modification of Mason's Method

An attempt to reduce the prohibitive requirement on the number of simulation particles needed, if Mason's method is to be used, is described in this section. This attempt was unsuccessful and was abandoned in favour of the the method described in the next section.

The approach to the problem was to reduce the noise level by damping oscillations at the dilated plasma period. In doing this the distortion of phase space should be minimised. This may be achieved by letting "artificial collisions" act only on one component of the particles' velocities. The difference between this and using simple collisions is illustrated below.

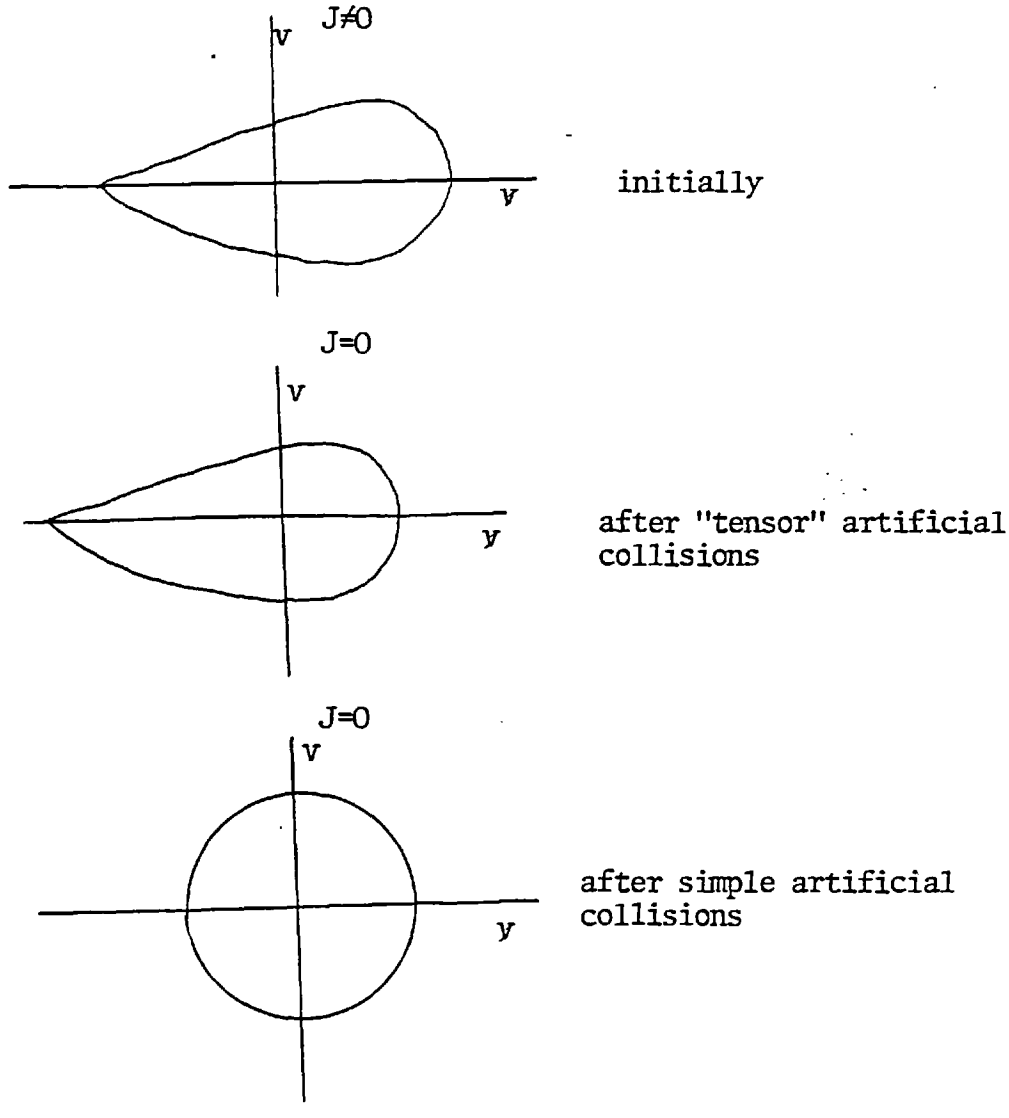

Fig.6.3 Comparison of Tensor and Simple Artificial Collisions

These collisions will remove the energy associated with the centre of mass velocity of the electrons from the system. If energy is to be conserved this energy would have to be added back into the electrons.

The artificial collisions may be effected in two ways:

(1) By acting on each particle so that its component of velocity in the one spatial dimension being considered is changed so that the local electron cantre of mass velocity is reduced. That is

$$(v_\perp, v_\parallel) \qquad (v_\perp, v_\parallel - \alpha \Delta t \bar{v}_\parallel(x)) \tag{6.3.1}$$

(2) By modifying the equation for the E field so that a damping term is introduced. This is prefered to the first method since it requires less computational effort.

Equation (6.2.1) was replaced by :-

$$\nabla \cdot \varepsilon_M E = \rho + \alpha \frac{\partial \rho}{\partial t} \tag{6.3.2}$$

This is equivalent to :-

$$\frac{\partial}{\partial t} \varepsilon_M E = J + \alpha \frac{\partial J}{\partial t} \tag{6.3.3}$$

The motion of the simulation particles may be approximately described by the Ohm's law :-

$$\frac{\partial J}{\partial t} = - \frac{e^2 n}{m_e} (E - \frac{e \nabla P_e}{n}) - \nu_c J \tag{6.3.4}$$

Using equations (6.3.3) and (6.3.4) and neglecting the ∇P_e term we get :-

$$\frac{\partial^2 J}{\partial t^2} = (\frac{-e^2 n_o}{\varepsilon_M m_e})(J + \alpha' \frac{\partial J}{\partial t}) \tag{6.3.5}$$

where $\dot{a}'$ includes the effect of both artificial and real collisions. From equation (6.3.5) it can be seen that the plasma oscillations may be damped. A proper investigation of the stability of such a scheme should involve the analysis of the set of equations (6.3.3), (6.3.4) and

$$\frac{\partial n}{\partial t} + \nabla \cdot (J/-e) = 0 \qquad (6.3.6)$$

Instead of this the stability of the solution of equation (6.3.5) was considered; a far simpler task. At this point it is necessary to consider the analysis of the stability of non-Hermitian finite difference operators.

Stability of Non-Hermitian Schemes

Consider the finite difference scheme :-

$$L_1 \underline{u}^n = \underline{u}^{n+1} \qquad (6.3.7)$$

where u^n is a vector of length (number of variables) $\cdot$ (number of meshpoints). If the spatial dependence of the solution is accounted for by expanding the state vector, u, in Fourier modes, the equation for each mode is :-

$$L_2 \underline{u}^n(k) = \underline{u}^{n+1}(k) \qquad (6.3.8)$$

where $u(k)$ is a vector of length equal to the number of variables. If L_1, L_2 are Hermitian, then the u can be expressed as the sum of eigenvectors of the L. ie :-

$$\underline{u}^n = \sum a_i \underline{c}_i$$

If the c_i are used as a basis then the operator L becomes :-

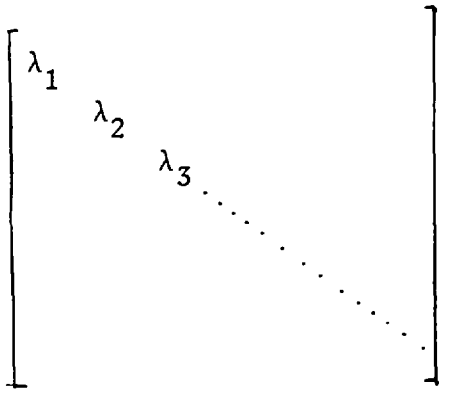

Fig.6.4

where the λ_i are the eigenvalues associated with the c_i .

The magnitudes of the error vectors before and after a time step E^n, E^{n+1} , where $E^n = \Sigma\ c_i a_i$, are given by :-

$$|E^n| = (\Sigma\ a_i^2)^{\frac{1}{2}}$$

$$|E^{n+1}| = (\Sigma\ (\lambda_i a_i)^2)^{\frac{1}{2}}$$

and the stability requirement is :-

$$\lambda_i \leq 1 \quad \text{for all } i \qquad (6.3.9)$$

This is the von Neumann stability condition (157).

This condition is necessary, but not sufficient, for proving the stability of a non-symmetric scheme. A practical method for assesing the stability of such a scheme is given by Buchanan (158,159). This requires that the matrix, L, be transformed into an upper triangular

matrix by a unitary transformation and its eigenvalues nested ie:-

$$|\lambda_r - \lambda_s| \leq k\,|\lambda_i - \lambda_m| \quad \text{if} \quad 1 \leq r \leq s \leq m \quad (k \text{ constant})$$

where the triangular matrix is :-

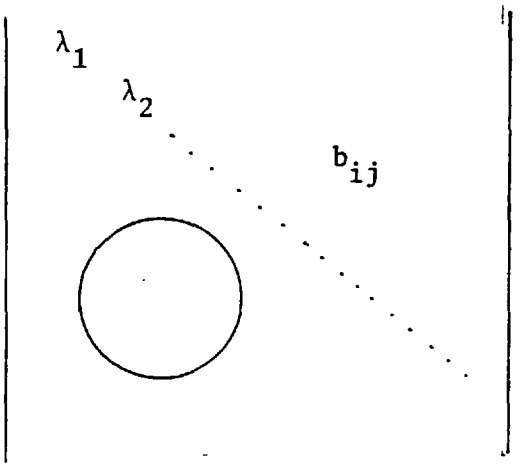

Fig.6.5

A sufficient stability condition is then :-

$$|b_{ij}| \leq k\,\text{Max}(\,|1 - \lambda_i|\,,\,|1 - \lambda_j|\,,\,|\lambda_i - \lambda_j|\,) \qquad (6.3.10)$$

Application to Equation (6.3.5)

The use of leap frog particle moving, and the calculation of the E field by equation (6.2.2), means that the solution of equation (6.3 (6.3.5) is analogous to the solution of:-

$$x_{tt} + \alpha x_t + \omega^2 x = 0 \qquad (6.3.11)$$

by the scheme:-

$$x^{n+1} = x^n + v^{n+1/2}\,\Delta t$$

$$v^{n+3/2} = v^{n+1/2}(1-\alpha\Delta t) - \omega^2\,\Delta t x^{n+1} \qquad (6.3.12)$$

This may be reexpressed as :-

$$\begin{pmatrix} \omega x^{n+1} \\ v^{n+3/2} \end{pmatrix} = \begin{pmatrix} I & \omega\,\Delta t \\ -\omega\,\Delta t & 1-\alpha\,\Delta t - \omega^2\,\Delta t^2 \end{pmatrix} \begin{pmatrix} \omega x^n \\ v^{n+1/2} \end{pmatrix} \qquad (6.3.13)$$

The eigenvalues of the matrix in equation (6.3.13) are given by :-

$$\lambda = 1 - \frac{\omega^2\Delta t^2 + \alpha\Delta t}{2} \pm i(4\omega^2\Delta t^2 - \omega^4\Delta t^4 - 2\omega^2\Delta t^2\alpha\Delta t - \alpha^2\Delta t^2)^{\frac{1}{2}}/2 \qquad (6.3.14)$$

$$\text{if} \quad 4\omega^2\Delta t^2 \quad \omega^4\Delta t^4 + 2\omega^2\Delta t^2\alpha\Delta t + \alpha^2\Delta t^2 \qquad (6.3.15)$$

$$\text{and :-} \quad = 1 - \frac{\omega^2\Delta^2 + \alpha\,\Delta t}{2} \pm (\alpha^2\Delta t^2 + 2\omega^2\Delta t^2\alpha\Delta t + \omega^4\Delta t^4 - 4\omega^2\Delta t^2)^{\frac{1}{2}}/2 \qquad (6.3.16)$$

otherwise .

In the former case $(\lambda\lambda^*)^{\frac{1}{2}}$ is given by $(1-\alpha\Delta t)^{\frac{1}{2}}$.

The inequality (6.3.15) implies that:-

$$\alpha\Delta t < -\omega^2\Delta t^2 + 2\omega\Delta t$$

so that $\alpha\Delta t \leq 1$

For $\omega\Delta t \ll 1$ and degenerate eigenvalues we must have $\alpha = 2\omega$; the condition for critical damping. The choice $\omega\Delta t = \alpha\Delta t = 1$ gives a singular matrix the square of which is a null matrix.

The choice $\omega\Delta t = \alpha\,\Delta t = 1$ gives a matrix which is unitarily similar to :-

$$\begin{pmatrix} 0 & 2 \\ 0 & 0 \end{pmatrix} \qquad (6.3.17)$$

and the choice $\omega\Delta t = 1/4$, $\alpha\Delta t = 1/2$, a matrix which is unitarily similar to :-

$$\begin{pmatrix} (23 - (17)^{\frac{1}{2}})/32 & -0.525 \\ 0 & (23 + (17)^{\frac{1}{2}})/32 \end{pmatrix} \qquad (6.3.18)$$

from which it can be seen that both schemes are stable.

Numerical Experiments

Guided in the choice of α by the analysis of the solution of (6.3.5), numerical experiments using equation (6.3.2) to determine the E field were carried out. The following conclusions were reached.

(1) The energy misconservation (with or without the damping term) is bad for $\omega\Delta t \sim 1$. $\omega\Delta t = 0.25$ gave good results.

(2) For $\bar{v}/\omega = \lambda_{D_{mod}} \ll \Delta x$ (the mesh spacing). The current fluctuation was damped. This however makes it difficult to satisfy equation (6.2.7) and and also places a great limitation on the timestep.

(3) Using $\lambda_{D_{mod}} = \Delta x$, $L = (\text{few}) \cdot \Delta x$ and $\alpha = 2\omega$, it was found that the inclusion of the damping term did not noticeably reduce the level of fluctuation. Some factors which may have caused this are:-

(A) The propagation of the plasma waves

(B) The small damping over a single period included by equation (6.3.16)

(C) The effect of E field interpolation and P.I.C.weighting.

Because of this failure the attempt to use a modified form of Mason's method was abandoned and a new approach was developed. This is described in the next section.

6.4 Iterative Method

An iterative method of finding an E field which gives J = 0 is now described. In general the current which flows through each cell boundary will depend on the E field at all the cell boundaries. However if the timestep is sufficiently short this is not the case.

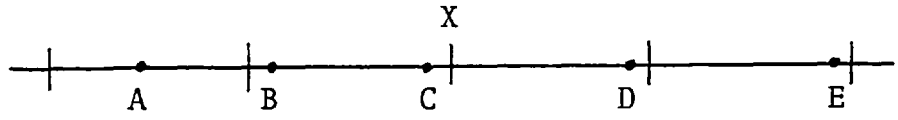

Fig.6.6 Position of Particle Centres

Particles A and E will not affect the current at X. Particle C will have a greater effect than particles B and D because of the P.I.C. weighting. Moreover, because of the interpolation used to calculate the E field acting on a particle, the E field at X will greatly affect particle C, have some effect on particles B and D and none on particles A and E.

Consider the case:-

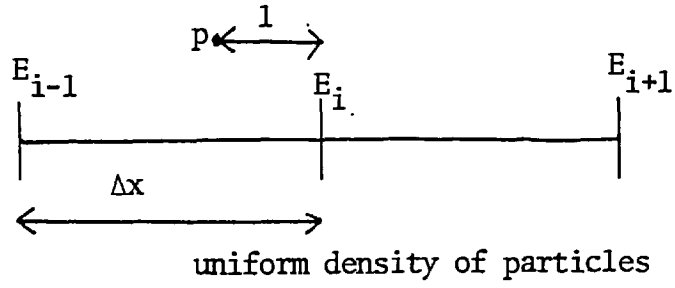

Fig.6.7

with $\Delta t \ll \Delta x/v$

The E field at P is:-

$$E_p = \frac{\Delta x - 1}{\Delta x} E_i + \frac{1}{\Delta x} E_{i-1}$$

The weight of the particle, with respect to the i cell boundary, is :-

$$W_p = \frac{\Delta x - 1}{\Delta x}$$

We wish to calculate the effective E field at i, that is an E field including the effect of weighting and interpolation, which are used to calculate the current (section 6.1) ;

$$E_{eff} = \frac{\int W_p E_p \, dx}{\int W_p \, dx}$$

where the integration is over the cell either side of the i boundary. This gives :-

$$E_{eff} = \frac{1}{6} E_{i-1} + \frac{2}{3} E_i + \frac{1}{6} E_{i+1} \qquad (6.4.1)$$

When the particle density is approximately uniform (ie when $L/\Delta x \gg 1$ $(L = n/\nabla n)$ and $v\Delta t \quad \Delta x$) we would expect $\Delta J/\Delta E_{eff}$ to be approximately independent of ΔE_{eff} , that is :-

ΔJ = constant $\cdot$ ΔE_{eff} + small non-linear part.

We exploit this by using a discrete Newton Raphson iteration to obtain $J_i(\Delta E_{i_{eff}}) = 0$;

$$\Delta E_{eff}^{n+1} = - \frac{J^n}{(\frac{\partial J}{\partial E_{eff}})^n} \qquad (6.4.2)$$

where n denotes number of iterations.

For the first value at the first timestep of $(\partial J/\partial E_{eff})$ we use

$$\frac{\partial J}{\partial t} \simeq \frac{ne^2}{m_e} E \;;$$

$$\Delta J \simeq \Delta t \frac{ne^2}{m_e} \Delta E$$

The first value of E at a timestep is taken as the last value of the previous timestep. Because of the finite Δt which must be used ($v\Delta t = 0.25\,\Delta x$ for instance) there would be some noise associated with calculation of $(\partial J/\partial E_{eff})$. The condition that $(\partial J/\partial E_{eff})$ may not change by more than a given fraction in any step is imposed. Once ΔE_{eff} is known the E field is updated using:-

$$\frac{1}{6}\Delta E_{i-1} + \frac{2}{3}\Delta E_i + \frac{1}{6}\Delta E_{i+1} = \Delta E_{eff_i} \qquad (6.4.3)$$

$$E_i^{n+1} = E_i^n + \Delta E_i \qquad (6.4.4)$$

$E_1 = E_{k+1} = 0$ for a mesh with k cells.

Equation (6.4.3) is solved for the E_i's using a modified version of the subroutine TRIDIAG (written by D.E.Potter).

The iteration for E is terminated when $\sum J_i$ is less than some given value.

Examples

The results of numerical calculations using equations (6.4.2, 6.4.3, 6.4.4) will now be presented. In these examples $\bar{v}\Delta t$ was $\frac{1}{4}\Delta x$ and the ratio of the scale length, L , to Δx varies between ∞ and 2 . Collisions were not included. The convergence of the calculation of the E field and the variation of the electrons' kinetic

energy are illustrated below:

Fig.6.8 Convergence of Iteration for the E Field

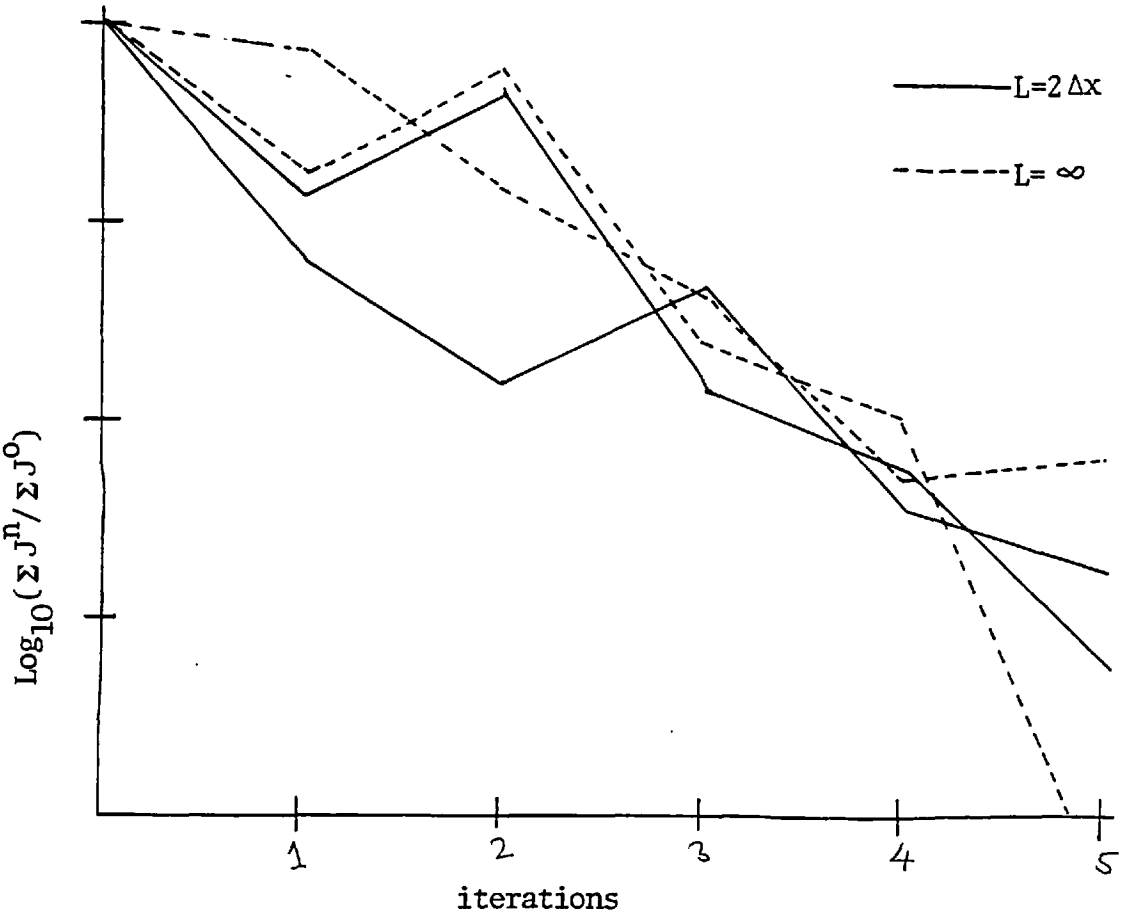

Fig.6.9 Changes in Electron's Kinetic Energy

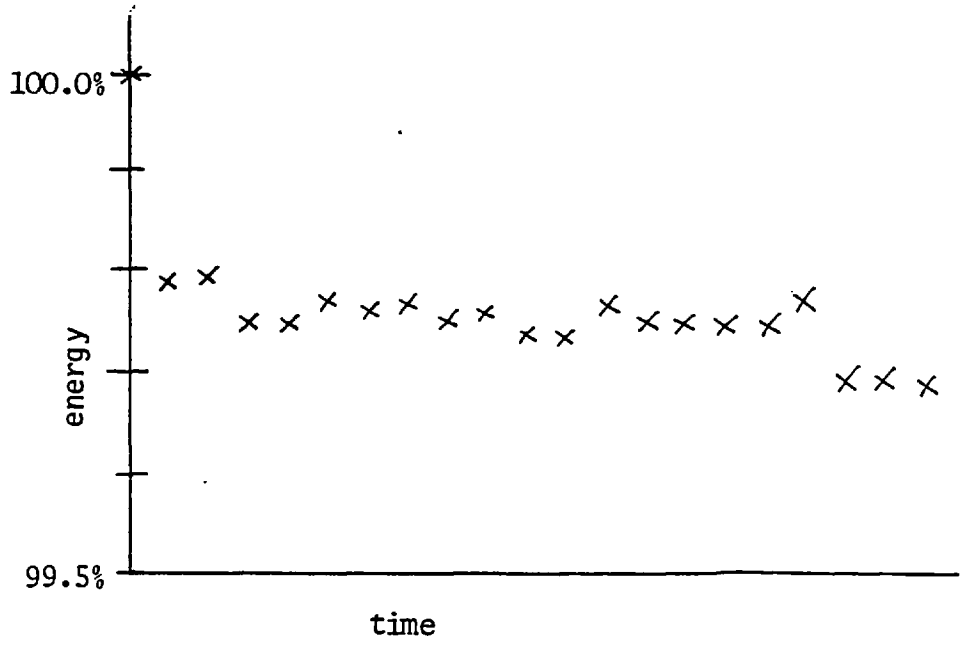

From these examples it can be seen that typically four iterations are required for $\bar{v}\Delta t = (1/4)\,\Delta x$. Thus a total of sixteen moves of each particle are required for a time given by $x/\bar{v}$. There is the additional disadvantage, compared to a non-iterative method, that the coordinates of each particle must be stored before and after an iteration, thus greatly increasing the storage requirement. The value of Δt used by Mason (133) is $\Delta t = 0.2\ (\Delta x/\bar{v})$ so this method would seem to be competitive.

Possible Improvements on the Calculation of E_{eff}

The calculation of E_{eff} described above uses the assumption that the density of adjacent cells is approximately the same. Some improvement could be gained by using :-

$$E_{eff} = \frac{\frac{1}{6}E_{i-1}n_{i-1} + \frac{1}{3}E_i(n_i+n_{i-1}) + \frac{1}{6}E_{i+1}n_i}{\frac{1}{2}(n_{i-1}+n_i)} \qquad (6.4.5)$$

Alternatively one may use a formulation which will give exact results in the limits $t \longrightarrow 0$ and no collisions. That is :-

$$E_{eff_i} = \frac{\Sigma\, E_p W_p}{\Sigma\, W_p}$$

where the sums are over all particles in the two cells next to the i^{th} boundary.

The Method of Calculating the Current

Since the current is not exactly zero after each timestep, departures from neutrality will occur. These may accumulate as the simulation progresses. This is prevented in the following way. The current could be calculated using the continuity equation. The integrated finite difference form of this is :-

$$J_i = \left(\sum_{j=1}^{i} (\rho_j^{n+1} - \rho_j^n)\ \Delta x_j\right)/\ \Delta t \qquad (6.4.6)$$

where n denotes the time level.

If $J_i = 0$ for all i then the space charge density is maintained at its previous value. If at each timestep $J \simeq 0$ is achieved then the ρ_j^n should be small compared to the ρ_j^{n+1} at the start of the iteration. The error in calculating the current using

$$J_i^* = \left(\sum_{j=1}^{i} \rho_j^{n+1}\ \Delta x_j\right)/\ \Delta t \qquad (6.4.7)$$

will be small. The E fields which make J_1^* and J_i zero for all i will be approximately equal. However using J^* instead of J in the calculation of the E field means that achieving $J^* = 0$ restores neutrality. Thus equation (6.4.7) is prefered to equation (6.4.6) in the E field calculation.

6.5 Possible Application

In the previous section the development of a quasi neutral Monte Carlo particle model has been described. In this section the possible applications of such a model will be discussed.

Hybrid Model

A hybrid model has been described by Mason (132) in which the suprathermal electrons are represented by Monte Carlo particles and the thermal electrons by a fluid description. The model has been used to study the effect of the suprathermal current on thermal transport. The method described in the previous section could be used in place of Mason's method for calculating the E field. Since the timestep which may be used for particle moving is restricted, by the range of validity of the multiple scattering distribution, to $\Delta t \lesssim 0.1\ (\lambda_{\pi/2}/v)\ \ (\sim v^2)$, it is desirable to be able to treat the lower energy thermal electrons by a fluid description. However simulations in which both suprathermal and thermal electrons are described by Monte Carlo particles have been described by Mason (133).

Due to the timestep limitation mentioned above and the comparative economy of using a multi group diffusion model, a dual treatment for the suprathermal electrons, in which the less energetic suprathermals are treated by a diffusion model and the more energetic ones, for which flux limited diffusion would be used, by a Monte Carlo model, is attractive. Such an approach seems feasable for solving steady state problems discussed in chapter 4. For the case of a time dependent model there are the disadvantages that:-

(1) The timestep which must be used for the iterative determination of the E field (section 6.4) is very small so that the multi group equations would have to be solved many times in a simulation; this may be prohibitively expensive.

(2) Since the E field can raise the energy of the diffusive suprathermals the coupling between the diffusive and non-diffusive suprathermal classes will be more complicated than when no E field is present.

Energy Loss in the Corona

The method of calculating the E field, described in the previous section, may be used to obtain $J_e \simeq J_i$ if ion motion is included. It may be possible to model energy transfer between the electrons and ions in the corona through the $J \cdot E$ term.

CHAPTER 7

Conclusion

The work described in this thesis has led to three achievements:-

Firstly:the development of a computer programme which can be used to investigate the effect of a resistive E field in inhibiting the flow of suprathermal electrons in a solid target. This programme has been used to design experiments in which the resistive E field plays an important role and has been used in the analysis of these and other experiments.

Secondly:the treatment of E field effects in a multi group diffusion model has been investigated. A multi total energy group model has been implemented. Its superiority over kinetic energy group models for time independent calculations is obvious. Time dependent problems have been treated but in this case it is no longer possible to solve for each group separately.and the direct solution of the equations generated by fully implicit differencing is time consuming. This may preclude the use of this method in a hydro code.

Thirdly:the calculation of the E field in a quasi neutral particle simulation is considered. A method due to Mason has been discussed and has been contrasted with an iterative solution. The latter can be competitive with Mason's method.

Further Work

The work described in chapter 4 is woefully incomplete as the effect of suprathermal energy loss in the corona is omitted. The implementation of a suprathermal transport model which treats E field effects in both the core and the corona is a worthwhile goal. E field calculations in the corona are however plagued with difficulty.

The models for suprathermal transport described in chapters 5 and 6 may also be applicable to the more complicated problems of non-thermal electron energy transport. The inclusion of coupling between one group and a group of both higher and lower energy in the multi group model would allow electron-electron collisions to be modelled. A crude model for electron-electron collisions (160) may be included in a quasi neutral particle simulation.

APPENDIX 1

The incomplete Cholesky conjugate gradient method, ICCG, was developed by Meijerink and van der Vorst (161) and has been investigated and popularised by Kershaw (162). This appendix gives a brief description of the ICCG method and gives the algorithms which can be used with a LDL^T approximate decomposition, which were not explicitly stated by Kershaw.

The conjugate gradient method is described in (163,164). It is an exact method for solving the matrix equation:-

$$M\underline{x} = \underline{y}$$

where M is symmetric and positive definite.
It takes n steps where n is the order of the matrix M. If M has degenerate or clustered eigenvalues, as it will if M is an approximate identity, it is found that $|\underline{x}^i - \underline{x}| \,/\, |\underline{x}|$ can be small for $i \ll n$. $\underline{x}^i$ is the approximation to the solution $\underline{x}$ after i steps.

The matrix, M, may be modified so that it becomes an approximate identity.

Since M is symmetric and positive definite, the most efficient form of elimination is Cholesky decomposition (165). If $M = LL^T$ (where L is a lower triangular matrix) then:-

$$\left.\begin{aligned} L_{ii} &= \left(M_{ii} - \sum_{k=1}^{i-1} L_{ik}^2\right)^{\frac{1}{2}} \\ L_{ji} &= M_{ji} - \sum_{k=1}^{i-1} L_{jk}L_{ik} \,/\, L_{ii} \\ j &= i+1,\ i+2,\ \ldots\ n \end{aligned}\right\} \quad (A1.1)$$

Alternatively if $M = LDL^T$ (where D is a diagonal matrix) then:-

$$\left.\begin{aligned} L_{ji} &= M_{ji} - \sum_{k=1}^{i-1} L_{jk} L_{ij} D_{kk} \\ j &= i,\ i+1,\ \ldots\ n \\ D_{ii} &= L_{ii}^{-1} \end{aligned}\right\} \quad (A1.2)$$

This decomposition avoids the square root. In an incomplete Cholesky decomposition a sparsity pattern is forced on L; ie a set of matrix elements, P, are chosen to be zero and, as (A1.1) or (A1.2) is applied when L_{ij} turns up with (i,j) in P, it is set to zero. The simplest choice of P is:-

$$P = \{(i,j) \mid M_{ij}\} = 0$$

This choice is refered to as ICCG(0) in (162). If $L_{ii} = 0$ the algorithm breaks down and if $L_{ii} < 0$ LDL^T is not positive definite. To avoid this if $L_{ii} \leq 0$ turns up, it is set to a small positive value. This introduces an additional error into the approximate decomposition of M.

Thus one obtains $M \simeq LL^T$ (or LDL^T) so $L^{-1}M(L^T)^{-1}$ (or $(LD)^{-1}M(L^T)^{-1}$) is an approximate identity matrix. For LL^T decomposition the matrix equation can be modified to:-

$$(L^{-1}M(L^T)^{-1})L^T\underline{x} = L^{-1}\underline{y} \qquad (A1.3)$$

The conjugate gradient method would be expected to perform well on this problem. The recursive relations for the conjugate gradient method become:-

$$\underline{r}^o = \underline{y} - M\underline{x}^o \; ; \quad \underline{p}^o = (LL^T)^{-1}\underline{r}^o$$

$$a^i = (\underline{r}^i, (LL^T)^{-1}\underline{r}^i) \; / \; (\underline{p}^i, M\underline{p}^i)$$

$$\left.\begin{aligned} \underline{x}^{i+1} &= \underline{x}^i + a^i \underline{p}^i \\ \underline{r}^{i+1} &= \underline{r}^i - a^i M\underline{p}^i \end{aligned}\right\} \quad \text{(A1.4)}$$

$$b^i = (\underline{r}^{i+1}, (LL^T)^{-1}\underline{r}^{i+1}) \; / \; (\underline{r}^i, (LL^T)^{-1}\underline{r}^i)$$

$$\underline{p}^{i+1} = (LL^T)^{-1}\underline{r}^{i+1} + b^i \underline{p}^i$$

If LDL^T decomposition is used the appropriate relations are:-

$$\underline{r}^o = \underline{y} - M\underline{x}^o \; ; \quad \underline{p}^o = (LL^T)^{-1}\underline{r}^o$$

$$a^i = (r^i, (LL^T)^{-1}r^i) \; / \; (p^i, M(L^{T^{-1}}D^{-1}L^T)p^i)$$

$$\left.\begin{aligned} \underline{x}^{i+1} &= \underline{x}^i + a^i (L^{T^{-1}}D^{-1}L^T)\underline{p}^i \\ \underline{r}^{i+1} &= \underline{r}^i - a^i M(L^{T^{-1}}D^{-1}L^T)\underline{p}^i \end{aligned}\right\} \quad \text{(A1.5)}$$

$$b^i = (\underline{r}^{i+1}, \; (LL^T)^{-1}\underline{r}^{i+1}) \; / \; (\underline{r}^i, \; (LL^T)^{-1}\underline{r}^i)$$

$$\underline{p}^{i+1} = (LL^T)^{-1}\underline{r}^{i+1} + b^i \underline{p}^i$$

(A1.2) and (A1.5) were used to solve problems in which the matrix, M, was quindiagonal.

APPENDIX 2

ILUCG

A generalisation of the ICCG method for arbitrary non-singular sparse matrices has been given by Kershaw (162). The solution of the matrix equation :-

$$A\underline{x} = \underline{y}$$

where $A \simeq LU$

can be achieved using the recursion relations:-

$$\left.\begin{aligned}
\underline{r}_o &= \underline{y} - A\underline{x}_o \\
\underline{p}_o &= (U^TU)^{-1}A^T(LL^T)^{-1}\underline{r}_o \\
a_i &= (\underline{r}_i, (LL^T)^{-1}\underline{r}_i) \,/\, (\underline{p}_i, U^TU\,\underline{p}_i) \\
\underline{x}_{i+1} &= \underline{x}_i + a_i\underline{p}_i \\
b_i &= (\underline{r}_{i+1}, (LL^T)^{-1}\,\underline{r}_{i+1}) \,/\, (\underline{r}_i, (LL^T)^{-1}\,\underline{r}_i) \\
\underline{p}_{i+1} &= (U^TU)^{-1}\,A^T(LL^T)^{-1}\underline{r}_{i+1} + b_i\underline{p}_i
\end{aligned}\right\} \quad (A2.1)$$

The LU decomposition which is used, for quindiagonal matrices, is now described. Let the approximate factorisation of A be as follows:-

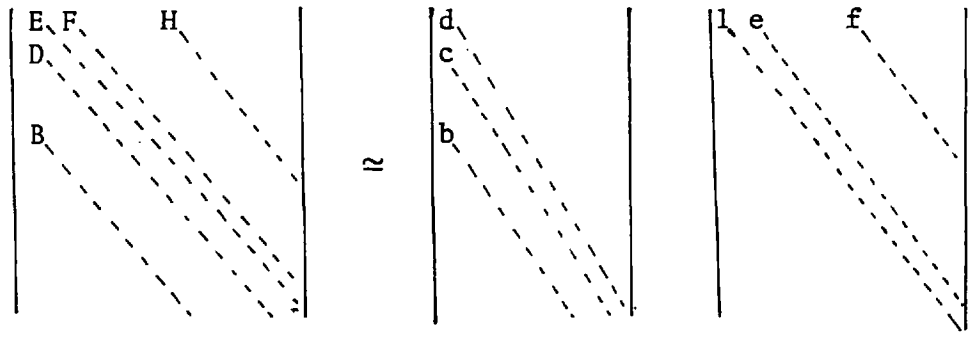

Fig.A2.1

then an approximate factorisation is given by:-

$$\left.\begin{aligned} b_k &= B_k \\ c_k &= D_k \\ d_k + b_k f_{k-N} + c_k e_{k-1} &= E_k \\ d_k e_k &= F_k \\ d_k f_k &= H_k \end{aligned}\right\} \quad \text{(A2.2)}$$

where the subscript labels the row. (A2.2) can be solved to give the quantities on the left hand side. There will be rounding error problems if the diagonal elements of the matrix, A , are very small or very large compared to unity.

(A2.1) and (A2.2) were used in a quindiagonal matrix inversion package. This is been used in the 2-D Eulerian code, LASERB , (166) in place of the strongly implicit procedure (167), for the fully implicit solution of the electron temperature equation. It has also been used to solve the multi group equations encountered in chapter 5 of this thesis.

APPENDIX 3

This appendix gives the Fokker-Planck equation for suprathermal electrons interacting with a thermal background. The equation is given in 1-D plane, cylindrical and spherical coordinates.

Consider first the Vlasov equation :-

$$\frac{\partial f}{\partial t} + \underline{v}\frac{\partial f}{\partial \underline{x}} + \underline{a}\cdot\frac{\partial f}{\partial \underline{v}} = 0 \qquad \text{(A3.1)}$$

Following Wienke (168) (who gave transformations for the force free transport equation in accelerating media) we get the following:-

Slab Geometry

$$\frac{\partial f}{\partial t} + v\mu\frac{\partial f}{\partial x} + a_\mu\left(\mu\frac{\partial f}{\partial v} + \frac{1}{v}(1-\mu^2)\frac{\partial f}{\partial \mu}\right) = 0 \qquad \text{(A3.2a)}$$

where $\mu = \underline{v}\cdot\underline{x}/vx$; $v = (v_x^2 + v_y^2 + v_z^2)^{\frac{1}{2}}$

Cylindrical Geometry

$$\frac{\partial f}{\partial t} + v\mu\frac{\partial f}{\partial r} + \left(\frac{v^2}{vr^*} - \frac{(\underline{v}\cdot\underline{r}^*)^2}{r^{*3}}\right)\frac{\partial f}{\partial \mu} + a_\mu\frac{\partial f}{\partial v} + \frac{a}{v}(1-\mu^2)\frac{\partial f}{\partial \mu} = 0 \qquad \text{(A3.2b)}$$

where $\underline{r}^* = x\underline{e}_x + y\underline{e}_y$; and $\mu = \underline{v}\cdot\underline{r}^*/vr^*$

Spherical Geometry

$$\frac{\partial f}{\partial t} + v\mu\frac{\partial f}{\partial r} + \left(\frac{v}{r} - \frac{v\mu^2}{r}\right)\frac{\partial f}{\partial \mu} + a_\mu\frac{\partial f}{\partial v} + \frac{a}{v}(1-\mu^2)\frac{\partial f}{\partial \mu} = 0 \qquad \text{(A3.2c)}$$

where $\mu = \dfrac{\underline{r}\cdot\underline{v}}{rv}$; and $\underline{r} = x\underline{e}_x + y\underline{e}_y + z\underline{e}_z$

The Fokker-Planck Term

The form of the Fokker-Planck term derived by Rosenbluth, MacDonald and Judd (169) is, for electrons:-

$$\left(\frac{\partial f}{\partial t}\right)_c = \Gamma\left\{ -\frac{\partial}{\partial \underline{v}}\cdot\left(f\frac{H_i}{\underline{v}}\right) + \frac{1}{2}\frac{\partial^2}{\partial \underline{v}\,\partial \underline{v}} : \left(f\frac{\partial^2 G_i}{\partial \underline{v}\,\partial \underline{v}}\right)\right\} \qquad (A3.3)$$

Where $\Gamma = \dfrac{4\pi e^4}{(4\pi\varepsilon_o)^2 m_e^2}\ln\Lambda_j$

$$H_i = \sum_j \frac{m_e + m_j}{m_e} Z_j^2 \int \frac{f_j(\underline{v}_2)\ \ln\Lambda_j}{|\underline{v} - \underline{v}_2|}\, d\underline{v}_2$$

and

$$G_i = \sum_j Z_j^2 \int f(\underline{v}_2)\ |\underline{v} - \underline{v}_2|\ \ln\Lambda_j\ d\underline{v}_2$$

This has been used by Delettrez and Goldman (108) to derive a Fokker-Planck equation for a small number of suprathermal "test particles" which do not interact with each other, but only with a background thermal plasma. Equation (A3.3) then simplifies to :-

$$\left(\frac{\partial f}{\partial t}\right)_c = \Gamma\, n_e \frac{\partial}{\partial \underline{v}}\cdot\left(\ln\Lambda_{sth}\frac{f\underline{v}}{v^3}\right) + \frac{\Gamma}{2}(n_e + Z^2 n_i)\frac{\partial}{\partial \underline{v}}\cdot\left(\ln\Lambda_{sth}\left(\frac{v^2\underline{\underline{I}} - \underline{v}\underline{v}}{v^3}\right) : \frac{\partial f}{\partial \underline{v}}\right) \qquad (A3.4)$$

where $\ln\Lambda_{sth} = \ln\left(\dfrac{\lambda_D}{\lambda_{DeB_{sth}}}\right)$

If v and $\mu = (\underline{v}\cdot\underline{x}/vx)$ are used as coordinates this becomes:-

$$\frac{\Gamma}{2}(n_e + Z^2 n_i)\frac{\ln\Lambda_{sth}}{v^3}\frac{\partial}{\partial \mu}\left((1-\mu^2)\frac{\partial f}{\partial \mu}\right) + \frac{\Gamma\, n_e}{v^2}\frac{\partial}{\partial v}(\ln\Lambda_{sth}\, f) \qquad (A3.5)$$

Acknowledgements

The work described in this thesis was performed while the author was a member of the Plasma Physics group at Imperial College.

He would like to thank Dr. J.D.Kilkenny for his encouragement and guidance and Prof. M.G.Haines (his supervisor) for many discussions and his continued interest in this work.

He would also like to thank :

Dr. D.E.Potter, J.D.Hares, M.G.Brown, C.W.Davies, M.A.Christie, D.E.Everett, Dr. R.W.Lee and Dr. J.Delettrez for their assistance.

The computational work described in this thesis was carried out at Imperial College and University of London Computer Centres. The work described in chapter 4 would not have been possible without the extensive use of free "idle time" computing at the University of London Computer Centre.

REFERENCES

1 J.D.LAWSON. Proc. Phys. Soc. (London) B 70 6 (1957)

2 M.S.CHU. Phys. Fluids 15 413 (1972)

3 J.NUCKOLLS, L.WOOD, A.THIESSEN, G.ZIMMERMAN. Nature 239 139 (1972)

4 W.C.MEAD. U.C.R.L. 82426

5 K.A.BRUECKNER, S.JORNA. Rev. Mod. Phys. 46 325 (1974)

6 D.GREY et. al. Bull. Am. Phys. Soc. 24(8) paper 7D8 (1979)

7 G.GUDERLEY. Luftahrforshung 19 302 (1942)

8 R.E.KIDDER. Nucl. Fusion 14 797 (1974)

9 G.S.FRALEY. Phys. Fluids 19 1495 (1976)

10 R.E.KIDDER. Nucl. Fusion 16 321 (1976)

11 J.EMMETT. invited paper 9th European Conference on Controlled Fusion and Plasma Physics

12 H.MOTZ. "The Physics of Laser Fusion" Academic Press (1979)

13 A.B.LANGDON. U.C.R.L. 82353 (1979)

14 M.D.ROSEN et. al. Phys. Fluids 22 2020 (1979)

15 F.AMIRANOFF et. al. Phys. Rev. Lett. 43 522 (1979)

16 D.G.COLOMBANT, W.M.MANHEIMER. (submitted to Phys. Fluids)

17 J.P.FRIEDBERG, R.W.MITCHELL, R.L.MORSE, L.I.RUDSINSKI Phys. Rev. Lett. 28 795 (1972)

18 K.G.ESTABROOK, E.J.VALEO, W.L.KRUER. Phys. Fluids 18 1151 (1975)

19 D.W.FOSLUND, J.M.KINDEL, K.LEE, E.L.LINDMAN, R.L.MORSE. Phys. Rev. A 11 679 (1975)

20 B.BEZZERIDES, S.J.GITOMER, D.W.FOSLUND. Phys. Rev. Lett. 44 651 (1980)

21 W.L.KRUER, K.ESTABROOK. Phys. Fluids 20 1688 (1977)

22 R.A.CAIRNS. Plasma Physics 20 991 (1978)

23 K.R.MANES et. al. Phys. Rev. Lett. 39 281 (1977)

24 H.DREICER. Phys. Fluids 7 735 (1964)

25 K.NISHIKAWA. J. Phys. Soc. Japan 24 916 (1968)

26 P.F.DU BOIS, M.V.GOLDMAN. Phys. Rev. 162 207 (1967)

27 C.LASHMORE-DAVIES. Plasma Physics 17 251 (1975)

28 C.YAMANAKA et. al. Phys. Rev. Lett. 32 1038 (1974)

29 L.D.LANDAU, E.M.LIFSHITZ. "The Electrodynamics of Continuous Media" Pergamon (1966)

30 H.MOTZ, C.J.H.WATSON. Adv. in Electronics and Electron Phys. 23 153 (1967)

31 F.F.CHEN. "Introduction to Plasma Physics" Plenum p.256

32 J.A.STAMPER. Phys. Fluids 18 735 (1975)

33 W.WOO, J.S.DE GROOT. Phys. Fluids 21 124 (1978)

34 J.VIRMONT, R.PELLET, A.MORA. Phys. Fluids 21 567 (1978)

35 P.MULSER, C.VAN KESSEL. Phys. Rev. Lett. 38 906 (1977)

36 J-L.BOBIN, W.WOO, J.S.DE GROOT. Le Journal de Phisique 38 769 (1977)

37 D.W.FORSLUND, J.M.KINDEL, K.LEE. Phys. Rev. Lett. 39 284 (1977)

38 D.T.ATTWOOD, D.W.SWEENEY, J.M.AUERBACH, P.H.Y.LEE. Phys. Rev. Lett. 40 184 (1978)

39 J.A.STAMPER. N.R.L. Report 7411 (1972)

40 J.A.STAMPER, D.A.TIDMAN. Phys. Fluids 16 2024 (1973)

41 P.MULSER, C.VAN KESSEL. Phys. Lett. 59A 33 (1976)

42 J.A.STAMPER et. al. Phys. Rev. Lett. 26 1012 (1971)

43 D.G.COLOMBANT, N.K.WINSOR. Phys. Rev. Lett. 38 697 (1977)

44 K.MIMA, T.TAJIMA, J.N.LEBOEUF. Phys. Rev. Lett. 41 1715 (1978)

45 R.S.CRAXTON, M.G.HAINES. Phys. Rev. Lett. 35 1336 (1975)

46 G.ZIMMERMAN. U.C.R.L. 50021-72-2 p. 131 (1973)

47 W.P.S.TAN, E.W.LAING. Phys. Lett. 67A 272 (1978)

48 R.S.CRAXTON, M.G.HAINES. Plasma Physics 20 487 (1978)

49 S.I.BRAGINSKII. Rev. Plasma Physics 1 205 p.249 (1965)

50 A.B.LANGDON. Phys. Fluids 21 705 (1978)

51 W.C.MEAD et. al. Phys. Fluids 20 322 (1977)

52 J.J.THOMSON, C.E.MAX, K.ESTABROOK. Phys. Rev. Lett. 35 663 (1975)

53 B.BEZZERIDES, D.F.DU BOIS, D.W.FOSLUUD, E.L.LINDMAN. Phys. Rev. Lett. 38 495 (1977)

54 R.J.MASON. Phys. Rev. Lett. 42 239 (1979)

55 E.J.VALEO. U.C.R.L. 50021-76

56 C.E.MAX, W.M.MANHEIMER, J.J.THOMSON. Phys. Fluids 20 1688 (1977)

57 A.RAVEN, O.WILLI, P.T.RUMSBY. Phys. Rev. Lett. 41 554 (1978)

58 L.SPITZER, R.HARM. Phys. Rev. 89 977 (1953)

59 H.GRAD. Phys. Fluids. 6 147 (1963)

60 H.D.SHAY et. al. Phys. Fluids 21 1115 (1979)

61 W.M.MANHEIMER. Phys. Fluids 20 265 (1977)

62 M.G.HAINES. Private communication (1979)

63 D.R.GREY et. al. Phys. Rev. Lett. 39 1270 (1977)

64 J.A.WESSON, A.SYKES, H.R.LEWIS. Phys. Rev. Lett. 31 449 (1973)

65 K.A.BRUECKNER. Nucl. Fusion 17 1257 (1977)

66 L.M.WICKENS, J.E.ALLEN, P.T.RUMSBY. Phys. Rev. Lett. 41 243 (1978)

67 J.D.HARES, J.D.KILKENNY, M.H.KEY, J.G.LUNNEY. Phys. Rev. Lett. 42 1216 (1979)

68 B.AHLBORN, M.H.KEY. RL-79-033 (1979)

69 M.H.KEY. in 20th Scottish Universities Summer School in Physics - Laser-Plasma Interactions St. Andrews (1979)

70 E.THORSOS et. al. Bull. Am. Phys. Soc. 24(8) paper 2D5 (1979)

71 J.M.AUERBACH et. al. Bull. Am. Phys. Soc. 24(8) paper 5D2 (1979)

72 G.CHARTIS et. al. Plasma Physics and Controlled Fusion Research (I.A.E.A., Vienna, 1975) Vol. II p. 317

73 A.W.EHER. A. J. Appl. Phys. 46 2464 (1975)

74 K.A.BRUECKNER, R.S.JANDA. Nucl. Fusion 17 451 (1977)

75 E.J.VALEO, I.B.BERNSTEIN. Phys. Fluids 10 1348 (1975)

76 R.C.MALONE, R.L.MC CRORY, R.L.MORSE. Phys. Rev. Lett. 34 721 (1975)

77 J.E.CROW, P.L.AUER, J.E.ALLEN. J. Plasma Phys. 14 65 (1975)

78 B.BEZZERIDES, D.W.FOSLUND, E.L.LINDMAN. Phys. Fluids 21 2179 (1978)

79 K.NISHIHARA. Private communication (1978)

80 K.A.BRUECKNER, Y.T.LEE. Nucl. Fusion 19 1431 (1979)

81 D.SHVARTS et. al. Nucl. Fusion 19 1457 (1979)

82 K.A.BRUECKNER, S.JORNA, R.JANDA. Phys. Fluids 17 1554 (1974)

83 J.D.LINDL, W.C.MEAD. Phys. Rev. Lett. 31 1273 (1975)

84 P.J.MOFFE, J.P.BORIS. Bull. Am. Phys. Soc. 24(8) paper 2D12

85 M.H.KEY, J.G.LUNNEY, J.D.KILKENNY, R.W.LEE. Appl. Phys. Lett. 36 269 (1980)

86 Annual Report of Laser Facility Committee 1979, RL-79-036 section 8.4.7

87 G.S.FRALEY, E.J.LINNEBUR, R.J.MASON, R.L.MORSE. Phys. Fluids 17 47 474 (1974)

88 G.B.ZIMMERMAN, W.L.KRUER. Commun. Plasma Phys. 2 85 (1975)

89 R.S.CRAXTON, R.L.MC CRORY. Bull. Am. Phys. Soc. 24(8) paper 2D8 (1979)

90 Laboratory of Laser Energetics Annual Report 1977 Vol. I p.118

91 H.A.BETHE. Ann. Phys. 5 325 (1930)

92 D.A.BROWN. in Handbook of Spectroscopy C.R.C. Press (1974)

93 M.J.BERGER, S.M.SELTZER. "Tables of Energy Losses and Ranges of Electrons and Positrons" N.A.S.A. SP-3012 (1964)

94 L.V.SPENCER, U.FANO. Phys. Rev. 93 1172 (1954)

95 D.PINES, D.BOHM. Phys. Rev. 85 338 (1952)

96 S.GOLDSMIT, J.L.SAUNDERSON. Phys. Rev. 57 24 (1940)

97 G.MOLLIERE. Z. Naturforsch. 3a 78 (1948)

98 E.J.WILLIAMS. Proc.Roy. Soc. 169 531 (1939)

99 J.D.JACKSON. "Classical Electrodynamics" p. 456,463 J.Wiley & Sons (1962)

100 L.SPITZER. "Physics of Fully Ionized Gases" Interscience Publishers (1962)

101 I.P.SHKAROFSKY, T.W.JOHNSON, M.P.BACHYNSKI. "The Particle Kinetics of Plasmas" Addison-Wesley (1966)

102 H.W.LEWIS. Phys. Rev. 85 20 (1952)

103 L.V.SPENCER. Phys.Rev. 98 1597 (1955)

104 C.D.ZERBY, F.L.KELLER. Nuc. Sci. and Eng. 27 190 (1967)

105 M.J.BERGER. in "Methods in Computational Physics Vol 1" B.ALDER S.FERNBACH and M.ROTENBERG Eds. (1963)

106 L.LANDAU. J. Phys. U.S.S.R. 8 201 (1944)

107 O.BLUNCK, K.WESTPHAL. Z. Physik 130 641 (1951)

108 J.DELETTREZ, E.B.GOLDMAN. L.L.E. Report 36 (1976)

109 D.S.KERSHAW. U.C.R.L. 77047 (1975)

110 G.ZIMMERMAN. U.C.R.L. 75173

111 E.GREENSPAN, D.SHVARTS. Nucl. Fusion 16 295 (1976)

112 R.D.RICHTMYER, K.W.MORTON. "Difference Methods for Initial Value Problems" Interscience Publishers 2nd Edition p.224 (1969)

113 K.H.CASE, P.F.ZWEIFEL. "Linear Transport Theory" Addison-Wesley p. 195 (1967)

114 D.S.KERSHAW. L.L.L. Annual Report 1976

115 T.YABE. Private Communication (1979)

116 B.G.CARLSON. in "Methods in Computational Physics Vol. 1" B.ALDER S.FERNBACH and M.ROTENBERG Eds. (1963)

117 B.R.WIENKE. J.Q.S.R.T. 22 301 (1979)

118 K.H.CASE, P.F.ZWIEFEL. op. cit. p.229

119 M.J.ANTAL, C.E.LEE. J. Comp. Phys. 20 298 (1976)

120 I.B.BERNSTEIN, J.M.GREENR, M.D.KRUSKAL. Phys. Rev. 108 546 (1957)

121 P.MORA, R.PELLET. submitted to Phys. Fluids

122 D.S.KERSHAW. U.C.R.L.83494 (1979)

123 Ya B.ZEL'DOVICH, Yu P.RAIZER. "Physics of Shock Waves and High Temperature Hydrodynamics" Academic Press p. 149

124 J.DELETTREZ. Private communication (1979)

125 D.MOSHER. Phys. Fluids 18 846 (1975)

126 J.S.CHANG, G.COOPER. J. Comp. Phys. 1 (1970)

127 D.SHVARTS, C.JABLON. Universite de Paris-Sud internal report (1977)

128 T.YABE et.al. paper E1 9th European Conference on Controlled Fusion and Plasma Physics

129 Annual Report of Laser Facility Committee 1979, RL-79-036 section 8.4.1

130 P.M.CAMPBELL, D.J.TANNER. 1977 Annual Report K.M.S.F. KMSF-U762

131 P.M.CAMPBELL, D.J.TANNER. Bull. Am. Phys. Soc. 24(8) paper 3G6 (1979)

132 R.J.MASON. LA-UR-78-2776

133 R.J.MASON. Bull. Am. Phys. Soc. 24(8) paper 4E1 (1979)

134 E.G.CORMAN, W.E.LOEWE, G.E.COOPER, A.M.WINSLOW. Nucl. Fusion 15 377 (1975)

135 J.R.ALBRITTON, I.B.BERNSTEIN, E.J.VALEO, E.A.WILLIAMS. Phys. Rev. Lett. 39 1536 (1977)

136 I.P.SHKAROFSKY. Phys. Rev. Lett. 42 1342 (1979)

137 D.J.BOND, J.D.HARES, J.D.KILKENNY. Bull. Am. Phys. Soc. paper 4E9 (1979)

138 P.CHOI. Imperial College Internal Report

139 J.D.HARES. Ph.D Thesis University of London (to be submitted)

140 Handbook of Spectroscopy Vol. I C.R.C. Press (1974)

141 Annual Report of Laser Facility Committee 1979, RL-79-036 section 4.4

142 H.R.GRIEM. "Plasma Spectroscopy" McGraw Hill (1964)

143 R.S.COHEN, L.SPITZER, P.MCR ROUTLY. Phys. Rev. 80 230 (1950)

144 J.D.JACKSON. op. cit. p.453

145 Ya B.ZEL'DOVICH, Yu P.RAIZER. op. cit. p.201

146 B.I.BENNET, J.D.JOHNSON, G.I.KERLEY, G.T.ROOD. LA-7130 (1978)

147 R.L.MORSE, C.W.NEILSON. Phys. Fluids 16 909 (1973)

148 K.LEE, D.W.FOSLUND, J.M.KINDEL, E.L.LINDMAN. Nucl. Fusion 19 1447 (1979)

149 D.A.TIDMAN. Phys. Rev. Lett. 35 1228 (1975)

150 J.D.HARES. Private communication (1979)

151 R.D.RICHTMYER, K.W.MORTON. op. cit. p.292

152 J.DELETTREZ. Private communication (1979)

153 R.M.BEAM, R.F.WARMING. AIAA Journal 16 393 (1978)

154 R.W.HOCKNEY. J. Comp. Phys. 8 19 (1971)

155 R.L.MORSE. in "Methods in Computational Physics Vol. 9, Plasma Physics" B.ALDER, S.FERNBACH, M.ROTENBERG. Eds.

156 C.K.BIRDSALL, A.B.LALGDON, H.OKUDA. ibid.

157 R.D.RICHTMYER, K.W.MORTON. op. cit. p.70

158 M.L.BUCHANAN. J. Soc. Indust. Appl. Math. 11 474 (1963)

159 M.L.BUCHANAN. J. Soc. Indust. Appl. Math. 11 919 (1963)

160 P.L.BHATNAGER, E.P.GROSS, M.KROOK. Phys. Rev. 94 511 (1954)

161 J.A.MEIJERINK, H.A.VAN DER VORST. Math. Comp. 31 148 (1977)

162 D.S.KERSHAW. J. Comp. Phys. 26 43 (1978)

163 L.FOX. "An Introduction to Numerical Linear Algebra" Clarendon Press (1964)

164 J.K.REID. in "Large Sparse Sets of Linear Equations" Ed J.K.REID Academic Press (1971)

165 F.S.ACTON. "Numerical methods That Work" Harper and Row

166 R.S.CRAXTON. Ph.D Thesis University of London (1976)

167 H.L.STONE. SIAM J. Numer. Anal. 5 530 (1968)

168 B.R.WIENKE. Phys. Fluids. 17 1135 (1974)

169 M.N.ROSENBLUTH, W.M.MAC DONALD, D.L.JUDD. Phys. Rev. 107 1 (1957)